Technology Collaboration Programme
by IEA

International Energy Agency
Photovoltaic Power Systems Programme

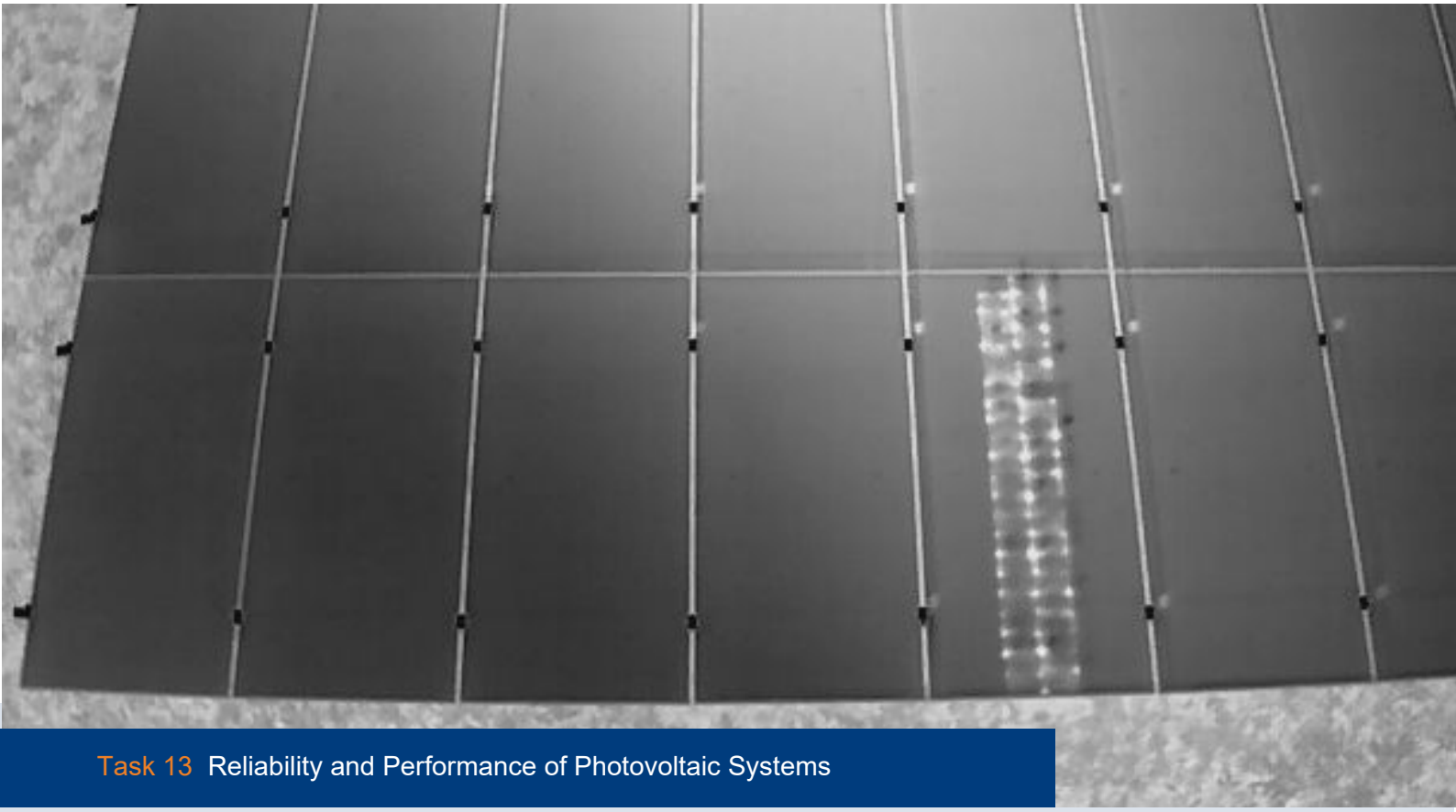

Task 13 Reliability and Performance of Photovoltaic Systems

PVPS

Degradation and Failure Modes in New Photovoltaic Cell and Module Technologies

2025

Report IEA-PVPS T13-30:2025

What is IEA PVPS TCP?

The International Energy Agency (IEA), founded in 1974, is an autonomous body within the framework of the Organization for Economic Cooperation and Development (OECD). The Technology Collaboration Programme (TCP) was created with a belief that the future of energy security and sustainability starts with global collaboration. The programme is made up of 6.000 experts across government, academia, and industry dedicated to advancing common research and the application of specific energy technologies.

The IEA Photovoltaic Power Systems Programme (IEA PVPS) is one of the TCP's within the IEA and was established in 1993. The mission of the programme is to 'enhance the international collaborative efforts which facilitate the role of photovoltaic solar energy as a cornerstone in the transition to sustainable energy systems'. In order to achieve this, the Programme's participants have undertaken a variety of joint research projects in PV power systems applications. The overall programme is headed by an Executive Committee, comprised of one delegate from each country or organisation member, which designates distinct 'Tasks', that may be research projects or activity areas.

The IEA PVPS participating countries are Australia, Austria, Belgium, Canada, China, Denmark, Finland, France, Germany, India, Israel, Italy, Japan, Korea, Malaysia, Morocco, the Netherlands, Norway, Portugal, South Africa, Spain, Sweden, Switzerland, Thailand, Turkiye, and the United States of America. The European Commission, Solar Power Europe and the Solar Energy Research Institute of Singapore are also members.

Visit us at: www.iea-pvps.org

What is IEA PVPS Task 13?

Within the framework of IEA PVPS, Task 13 aims to provide support to market actors working to improve the operation, the reliability and the quality of PV components and systems. Operational data from PV systems in different climate zones compiled within the project will help provide the basis for estimates of the current situation regarding PV reliability and performance.

The general setting of Task 13 provides a common platform to summarize and report on technical aspects affecting the quality, performance, reliability and lifetime of PV systems in a wide variety of environments and applications. By working together across national boundaries, we can all take advantage of research and experience from each member country and combine and integrate this knowledge into valuable summaries of best practices and methods for ensuring PV systems perform at their optimum and continue to provide competitive return on investment.

Task 13 has so far managed to create the right framework for the calculations of various parameters that can give an indication of the quality of PV components and systems. The framework is now there and can be used by the industry who has expressed appreciation towards the results included in the high-quality reports.

The IEA PVPS countries participating in Task 13 are Australia, Austria, Belgium, Canada, Chile, China, Denmark, Finland, France, Germany, Israel, Italy, Japan, the Netherlands, Norway, Spain, Sweden, Switzerland, Thailand, the United States of America, and the Solar Energy Research Institute of Singapore.

COVER PICTURE

Infrared image of an energised module string at night. One module has a not connected bypass diode. Thanks to photovoltaikbuero Ternus & Diehl GbR for the permission to use the image.

ISBN 978-3-907281-71-0: Task 13 Report: Degradation modes and Failure in New PV Cell and Module Technology

INTERNATIONAL ENERGY AGENCY

PHOTOVOLTAIC POWER SYSTEMS PROGRAMME

IEA PVPS Task 13

Reliability and Performance
of Photovoltaic Systems

Degradation and Failure Modes in New Photovoltaic Cell and Module Technologies

Report IEA-PVPS T13-30:2025

February 2025

ISBN 978-3-907281-71-0

AUTHORS

Main Authors

Marc Köntges, ISFH, Germany
Jay Lin, PV Guider
Alessandro Virtuani, CSEM, Switzerland
Gabriele C. Eder, OFI, Austria
Junjie Zhu, IFE, Norway
Gernot Oreski, PCCL, Austria
Peter Hacke, NREL, USA
Joshua S. Stein, SNL, USA
Laura Bruckman, CWRU, USA
Paul Gebhardt, Fraunhofer ISE, Germany
Dounya Barrit, Total Energies, France
Mirra Rasmussen, CWRU, USA
Ina Martin, CWRU, USA
Kristopher O. Davis, UCF, USA
Gianluca Cattaneo, CSEM, Switzerland
Bram Hoex, UNSW Sydney, Australia
Ziv Hameiri, UNSW Sydney, Australia
Ebrar Özkalay, SUPSI, Switzerland

Contributing Author

Sara Baumann, ISFH, Emmerthal, Germany

Editors

Marc Köntges, ISFH, Germany
Jay Lin, PV Guider
Ulrike Jahn, Fraunhofer CSP, Germany

TABLE OF CONTENTS

ACKNOWLEDGEMENTS

This report received valuable contributions from several IEA PVPS Task 13 members and other international experts. Many thanks to:

Eckhard Fleiss from Ingenieurbüro Fleiß for giving the permission to use his drawing as template for Figure 14 and Matthias Diehl from photovoltaikbuero Ternus & Diehl GbR for allowing us to use the cover image.

This report is supported by the German Federal Ministry for Economic Affairs and Climate Action (BMWK) under contract no. 03EE1120A, 03EE1120B and 03EE1120C, the Swiss Federal Office of Energy (SFOE) under the contract no. SI/502398-01, the Austrian Federal Ministry for Climate Action, Environment, Energy and Mobility (BMK), the Danish Energy Technology Development and Demonstration Programme (EUDP), project number 134-22016, "IEA PVPS Task13 - Reliability and performance of photovoltaic systems", and the Austrian Research Agency (FFG) under contract no. FO999908094_05102023_160512119.

This work was authored in part by the National Renewable Energy Laboratory, operated by Alliance for Sustainable Energy, LLC, for the U.S. Department of Energy (DOE) under Contract No. DE-AC36-08GO28308 in the project 38263 "R&D to Ensure a Scientific Basis of Qualification Tests and Standards," funded by the U.S. Department of Energy, Office of Energy Efficiency and Renewable Energy, Solar Energy Technologies Office. The views expressed in the article do not necessarily represent the views of the DOE or the U.S. Government.

Sandia National Laboratories is a multi-mission laboratory managed and operated by National Technology and Engineering Solutions of Sandia, LLC, a wholly owned subsidiary of Honeywell International Inc., for the U.S. Department of Energy's National Nuclear Security Administration under contract DE-NA0003525.

Supported by:

Federal Ministry
for Economic Affairs
and Climate Action

on the basis of a decision
by the German Bundestag

LIST OF ABBREVIATIONS

Al-BSF	Aluminium back surface field	MHP	Metal halide perovskite
ARC	Anti-reflective coating	OC	Open-circuit
a-Si	Hydrogenated amorphous Si	PA	Polyamide
BOM	Bill of materials	PERC	Passivated emitter and rear cell
BPD	Bypass diode	PERT	Passivated Emitter and Rear Totally Diffused
c-Si	Crystalline Si	PET	Polyethylene terephthalate
CTE	Coefficient of thermal expansion	PID	Potential-induced degradation
CTL	Charge transport layer	PID-p	PID-Polarisation
DH	Damp heat	PMMA	Poly (methyl methacrylate) polymer
EL	Electroluminescence	P_{MPP}/P_{max}	Maximum power
EPE	EVA-POE-EVA	PO	Polyolefin
EVA	Ethylene-Vinyl-Acetate	POE	Polyolefin elastomer
FA	Formamidine	PSC	Perovskite solar cell
FF	Fill factor	PV	Photovoltaic
HF	Humidity freeze	PVDF	Polyvinylidene fluoride
IBC	Integrated-Back Contact	PVF	Polyvinyl fluoride
IEA	International Energy Agency	PVFS	Photovoltaic Failure Fact Sheets
IEA PVPS	IEA Photovoltaic Power Systems Programme	RH	Relative humidity
IEC	International Electrotechnical Commission	SEM	Scanning electron microscopy
IRT	Infrared thermography	SHJ	Silicon Hetero-Junction
I_{SC} (J_{SC})	Short Circuit Current (density)	TC	Thermal cycling
ITO	Indium tin oxide	TCO	Transparent Conductive Oxide
ITRPV	International Technology Roadmap for Photovoltaic	TCP	Technology Collaboration Programme
IV	Current-Voltage	TOPCon	Tunnel Oxide Passivated Contact
LCOE	Levelized cost of electricity	UV	Ultraviolet
LeTID	Light and elevated temperature -induced degradation	UVID	UV induced degradation
LID	Light-induced degradation	V_{OC}	Open-circuit voltage

EXECUTIVE SUMMARY

The levelized cost of electricity (LCOE) of photovoltaic applications depends on, among other things, the performance, price and durability of the photovoltaic (PV) module. Performance and price can be determined with little effort. Durability is the least known of these three factors. In this report, we evaluate the impact of degradation/failure modes of innovations in the market.

The reliability situation of Tunnel Oxide Passivated Contact (TOPCon) and Silicon Hetero-Junction (SHJ) is shown in Figure 1 for selected degradation and failure modes. Especially semiconductor-related degradation modes show degradation and recovery paths: light (and elevated temperature)-induced degradation (LeTID/LID), UV-induced degradation (UVID), and potential-induced degradation (PID). Their impact can only be assessed if the degradation and recovery paths are understood, and a test method is available. Common degradation modes or failures related to embedment, glass and junction box are shown in Figure 1 on the right. Current standard tests, especially of the IEC 61215 standard, cannot reveal these degradation or failure modes. As these modes are safety relevant, it is important to understand the causes and develop standardized tests to identify these reliability problems.

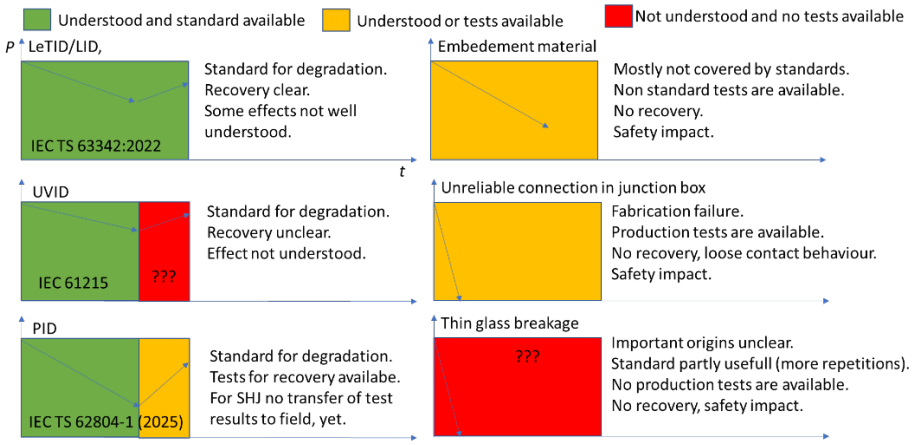

Figure 1: Overview of test availability and impact of currently relevant degradation modes of TOPCon and SHJ module designs.

In the following we go through degradation modes which changed with new innovation. We find that the impact of cell cracking has been mostly overcome by the innovation of multi-wire technology. Also, LID/LeTID has been well understood and solved by switching from Boron to Gallium as a dopant for Si-wafers, by using adjusted processes in the cell production together with the use of thin wafers, and lowering the number of impurities in the wafer production. Furthermore, standard test procedures are available, so that the LID/LeTID impact on long-term performance can be tested even for innovation. The degradation mechanisms which lay behind PID can be triggered and mitigated at cell, module and system level. These degradation mechanisms are caused by high system voltage and may be influenced by light, in particular UV irradiation. PID tests for modules with Passivated Emitter and Rear Totally diffused (PERT) cells have shown that additional light during a PID test can effectively prevent degradation. It has been shown in one case that an UV irradiance equivalent to the UV content in the standard AM1.5 spectrum at 1000 Wm^{-2} can reduce the PID effect for a module with TOPCon cells to below 3%. In contrast, in this case no UV irradiation during the PID test leads to a degradation of 28%. For PV modules with SHJ cells a new potential PID degradation mechanism is identified. However, no PID affected modules are found in the field corresponding to this mode, yet.

To assess the irradiation impact on real installations, the upcoming PID standard IEC TS 62804-1 (2025) offers a combined potential and light test procedure.

In some solar modules with TOPCon and SHJ cells, UVID is pronounced after accelerated aging tests. It is still unclear whether the degradation can be reversed by outdoor exposure and how the test can be transferred from laboratory to field, since many interacting mechanisms influence UV degradation and recovery. It must be emphasized that the UVID is a solvable problem, since some modules in accelerated tests are UV-stable. The reflection or absorption of UV radiation before it reaches the c-Si/passivation interfaces (e.g. by the encapsulation material) can mitigate the UVID.

For encapsulant materials standardized PV module tests (e.g., of the IEC 61215 series or other PV safety standards) often do not reveal relevant degradation paths as their focus is on the electrical performance of the PV modules and not on the polymer materials stability. Therefore, many PV modules are found in the field with damaged lamination material. Combined stresses with e.g. temperature change, humidity and UV radiation can reveal these polymer-related degradation paths. Especially for these degradation modes, new combined aging tests are required as discussed in detail in the IEA PVPS TASK 13 sister report “Accelerated testing - combined stress vs. sequential stress testing methods and inclusion of specific load situations”. As degradation of encapsulation material is not recoverable and often leads to safety issues, these additional tests are recommended for new encapsulant materials.

In practice, thin glass (thickness ≤ 2 mm) used in new glass/glass modules sometimes results in unpredictable high glass breakage rates. In documented cases 5% to 10% of the module rear glasses broke in the first two years after installation. The mechanical load test in IEC 61215 cannot reveal this vulnerability, as it would need parallel tests on tens of modules, instead of only one, to assess the failure rate. Currently, only a high number of tests in the final mounting position can reveal the stability of thin glass modules.

More frequently than before, it happens that electrical contacts in the junction boxes are not soldered correctly. This may mean that the bypass diodes (BPDs) are not properly contacted. Faults in the junction box can lead to fires and power losses in entire module strings. However, unconnected BPDs are difficult to detect in PV systems that have already been installed. It is therefore recommended to check the function of 100% of the BPDs during production. A PV system installation should be 100% tested if there are indications that this type of failure is occurring in the selected modules.

This report also includes a concise summary on the reliability of metal halide perovskite (MHP)-based PV modules according to the current scientific literature. There are many known degradation paths for which remedies exist at the conceptual or laboratory level. For example, protective encapsulation against UV radiation, moisture and oxygen basically helps to stabilize the perovskite solar cells (PSCs). However, besides others, two prominent challenges are the temperature and the ion migration stability. The limited temperature stability and the high ion mobility lead to unsolved degradation paths under normal operation conditions like shading and high system voltage. There are new degradation modes in tandem solar cells with MHPs. For example, the reverse voltage states occurring in the top and bottom cells during shaded conditions depend on the irradiation spectrum and cannot yet be reproduced by standard qualification tests. New tests addressing this shading condition are important to evaluate new degradation pathways that do not occur in single junction PV modules.

To produce reliable PV modules, all degradation pathways must be understood and mitigated in one solution. There are currently no comprehensive solutions in the literature to address the multiple reliability issues of PSCs.

1 INTRODUCTION

The previous IEA PVPS reports on PV module failures [1], their assessment [2] and quantification of technical risks [3] are still relevant documents for assessing and mitigating of degradations and failures in PV modules. A degradation mode is an observable specific change mechanism of a PV module like it is defined by Jordan et al. [4] that can (but does not have to) lead to a failure mode. For the word “failure” we use the definition from Köntges et al. [1] where a failure in a PV module means that the power warranty of a module is no longer fulfilled or the safety of a PV system is affected. A failure mode is a specific type of failure. With this document we like to target a broad audience starting from cell and module manufactures up to PV system owners. As in the former reports, we strongly focus on Si-wafer-based solar modules here. However, the PV module technology has developed fast. This document aims to give an update of degradation mechanisms and currently important failures in current PV cell and module technologies.

Chapter 2 therefore presents in-depth information on degradation mechanisms and potential mitigation strategies on production level. We start with degradation mechanisms (cell cracks, LID, LeTID) which had been important in the former review but lost importance within current (2023) PV module products. Thereafter, we present degradation modes which are still relevant for PV module technologies (PID, substring protection and module embedment) and which show specific differences to former reviews mentioned above. At the end of chapter 2 we analyse degradation modes which are specifically relevant for the current cell technologies TOPCon and SHJ. This breaks the strict sorting along degradation and failure modes but allows the reader to quickly read about all special degradation modes for TOPCon and SHJ. All chapters contain an explanation of the degradation mode, its impact on module/system level, how to identify it, how to test it, and if possible, how to mitigate the degradation mode. All sections contain numerous up-to-date references to the most relevant publications, if additional information is needed.

Due to the rapidly growing development of MHP-based solar cells and modules, we report in chapter 3 on their known degradation modes and existing mitigation strategies. Chapter 3 is addressed to the scientific interested reader as all available data is extracted from scientific publications. We have no information on degradation modes of market available MHP-based modules.

In the previous IEA PVPS Task 13 report by Herz et al. [3] PV-related failures have been collected and systematised in Photovoltaic Failure Fact Sheets (PVFS) for the first time. For the application related reader these PVFS have been updated with the content of this work and can be downloaded as a separate document from the IEA PVPS website area [5]. These fact sheets explain all needed information for the application, such as how to detect a failure or degradation, information on safety and power production, and how to mitigate the problem if possible. Unfortunately, not all degradation and failure modes have been transferred to the PVFS, as there is not always enough material available to visualise the failure and provide clear recommendations for action. Especially for MHP-based solar cells and modules no PVFS exists, yet.

2 DEGRADATION AND FAILURE MODES IN RECENT TECHNOLOGIES ENTERED THE MARKET

Photovoltaic module technologies and their application profiles evolve with time. As the degradation modes are always related to technologies and their application profile they also change with time. The testing sequences defined by the International Electrotechnical Commission (IEC) in the IEC 61215 series standard [6] are a good way to assess that new technologies degrade slow enough in the application. However, testing is always a compromise between finding failures and test simplification. The test simplification may lead to false positive or false negative results for new technologies. One prominent example is the PID of PERT cells which may degrade in a PID test under dark conditions, but under realistic conditions the sunlight compensates for the PID effect, so the degradation is not relevant in the application.

In the following, we discuss if the most relevant degradation mechanisms already described in previous PVPS TASK 13 reports [1], [2] which are changed due to new innovations. Afterwards, we discuss new technologies, the knowledge about their degradation modes, and their relevance for the application.

2.1 Cut Si wafer-based cell cracking and multi-wire design

The cutting of Si wafer-based cells in half cells or 1/3rd cells increases the risk of cracking at the cutting cell edge when preparing modules from the cells. Cutting of Si cells into half or even in one third by a laser ablation process introduces small micro cracks into the groove area of the laser ablation process. Hwang et al. shows that with increasing crack opening width in the laser groove surface, the break force needed to break the cells in a 4-point bending test decreases [7]. They also show that the number of broken cells in a module increases with increasing micro crack opening in the laser groove surface. Module power measurements after a mechanical load test show that the number of cracked cells and the power loss increases with the crack opening in the laser groove. For multi-wire solar modules, the power loss due to cell cracks is reduced compared to former ribbon-based modules. Hwang et al. show 0.2% power loss per dendritic-like cracked half-cell for a multi-wire Passivated Emitter and Rear Cell (PERC) cell in the module [7]. For a relevant power loss of 5% one needs about 25 dendritic-like cracked cells. So, cell cracks still influence the module power for multi-wire connected halved cells, but the final impact on the module power is low. Thermal laser separation method can be used to reduce cell cracking in cut solar cells compared to laser ablation method [8].

Figure 2 a) shows that small cracks induced at the cut edge may already exist after production. They are ignored at this stage but frequently grow into dendritic cracks during transportation and installation, as well as mechanical loads and temperature variations that may occur in the field. Figure 2 b) shows the electroluminescence (EL) image of one of these glass/backsheet modules tested on arrival at the installation site.

The same batch of modules was delivered to two different sites and an EL inspection of 50 modules was performed on arrival at each site. The defects are categorised as major defects when dendritic cracks are found, simple branch cracks are categorised as minor defects, and few single cracks are categorised as normal.

At one site the defect rate was 78% major, 18% minor and 4% normal, whereas at the other site the defect rate was 70% major, 30% minor, and no normal modules. Dendritic cracks per cell result only in ~0.2% of power loss in the module. However, this kind of cracks can occur

with a high proportion of cells in the module and the total power loss could be noticeable, but very small for PV systems.

For glass/glass modules the cell crack occurrence is typically very low. To our best knowledge, all papers on PV module degradation caused by cell cracks are based on 2 to 4 cell interconnect ribbons per cell with full cell module design. In this way, according to our present knowledge, no field degradation data on cut cell and multi-wire designs are available.

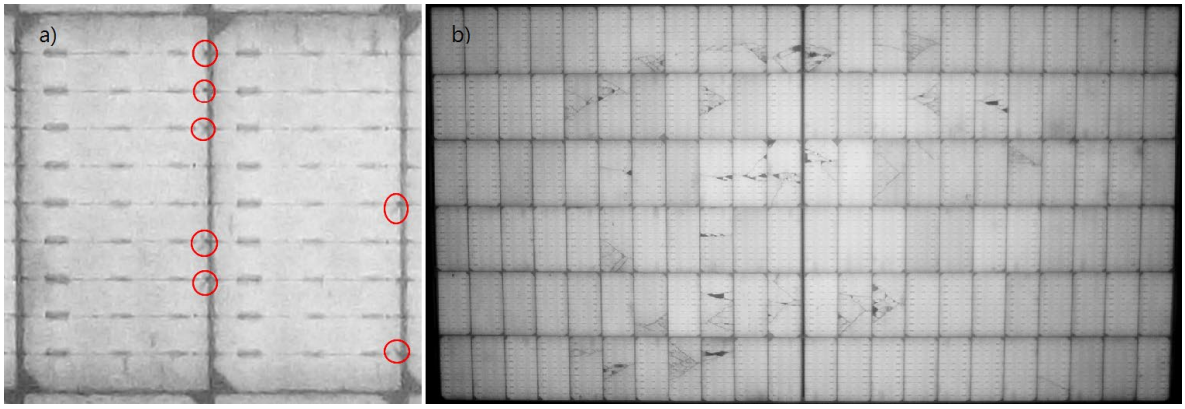

Figure 2: a) Cracks induced at the edge of laser cutting during module production. b) The cell cracks appeared after transportation while they were not seen in the final EL inspection in the module production line. The current inactive cell areas are below 5% per cell.

2.2 Light-induced degradation

In recent times, light-induced degradation phenomena had been a large effect on some multi-crystalline and PERC-based solar cell types. Therefore, through this chapter we discuss the relevance of new developments in wafer and cell technology regarding to the light-induced degradation modes.

2.2.1 Boron related light-induced degradation

Light-induced degradation is the phenomenon of cell and module power degradation due to incident light. The main degradation mechanism is based on the formation of Boron-Oxygen complexes (B-O LID) and was particularly strong in Czochralski-grown Si mono-crystalline cells, in part due to its high oxygen concentration [9]. The maximum degradation of LID typically happens within the first few hours of light exposure and it may amount to several percent relative to the initial module performance. After the degradation phase, a slow recovery can sometimes be observed upon further operation, which is often difficult to quantify in the field, because it is superimposed by other degradation or weather effects.

In recent years, the prevalence and severity of LID in PV modules has dropped significantly due to the usage of Ga instead of B as dopant in p-type cells. In theory this exchange removes the possibility to form B-O complexes due to the absence of B atoms. Nevertheless, LID may still be observed in Ga-doped p-type [10] and even in n-type cells [11], due to B impurities present in the wafers. Due to the generally low number of impurities (B and Fe) in today's Si wafer the relevance of LID is low for nearly all current PV modules based on Ga p-type and n-type doping.

2.2.2 Light and elevated temperature-induced degradation

Light and elevated temperature-induced degradation (LeTID) is a degradation mechanism that mainly affects p-type PERC modules. The exact mechanism is linked to hydrogen-related defects, which become active under the combined thermal and light stress conditions, causing minority charge carrier recombination and therewith reduced power output. Regeneration occurs when the defects responsible for degradation are gradually passivated under controlled thermal or electrical conditions. This process typically involves the redistribution and reactivation of hydrogen, leading to the recovery of cell efficiency over time. Due to its degradation-regeneration behaviour through the first years of operation, it can lead to significant yield loss in field operation (sometime reaching values over 10%). Similarly to LID, a regeneration phase, that is largely influenced by weather and seasonal effects, can be observed in the years after the maximum degradation has been reached [12], [13].

Based on a mechanistic understanding of the underlying phenomena, involving hydrogen diffusion from the cell surface and defect formation in the bulk, mitigation strategies for cell production, such as adapting temperature profiles in the firing process [14], [15] or using thinner wafers [16], have been developed in recent years. Furthermore, the transition from Boron- to Gallium doping in p-type solar cells led to a decrease in LeTID [17].

According to current experience, modules containing n-type TOPCon cells are substantially less susceptible to LeTID than early p-doped PERC cells.

The above-explained reasonings for LID and LeTID have been demonstrated in the following experiment, where a large selection of commercial TOPCon modules was subjected to 322 hours of LeTID tests (IEC TS 63342:2022 for 2 × 162 h at I_{SC} – I_{MPP}) after LID preconditioning (IEC 61215-2:2021 gate 1), see Figure 3. The results show minor effects on the PV module performance.

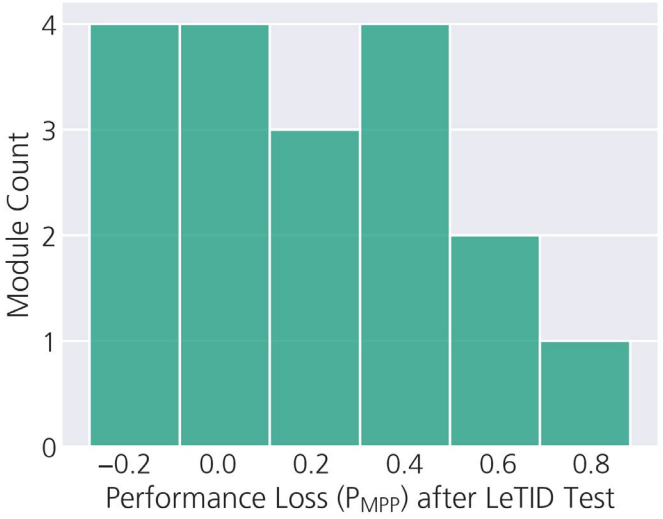

Figure 3: Performance loss (P_{MPP}) of commercial TOPCon modules after 322 hours of LeTID tests [18].

At PV module and PV system level we expect no detectable degradation from the LeTID effect in current TOPCon modules based on Ga doped p-type wafers.

2.3 Potential-induced degradation

System voltage potential-induced degradation (PID) involves electric charge transfer through the encapsulation of PV modules to or from the cell. Depending on the module type, the polarity and level of the voltage potential, which develops according to voltage difference between the cells in the module and ground, and environmental factors, a number of different PID modes may manifest.

The known and documented PID modes are summarised by Molto et al. [19] and listed in the following:

PID-Corrosion involves electrochemical reactions at the cell surface, including the metallization, the dielectric, and the Si itself. Chemical species within the cell and encapsulation dissociate and drift under the applied electric field.

PID-Delamination involves electrochemical reactions at the cell surface which produce gaseous products leading to delamination of encapsulants. The process may also involve the precipitation of ions at interfaces that promote delamination.

PID-Penetration involves drift of Na^+ or other ions that migrate to the cell circuit, penetrating the passivating dielectric, including at pinholes, depositing on the Si surface, and leading to degrading surface passivation which reduces photocurrent and voltage.

PID-Polarisation (PID-p) involves motion of charge into or out of the dielectric passivation layers in such a manner that more minority carriers are attracted to the interface of the Si with the passivating dielectric. This leads to reduced photocurrent and voltage. There may be several mechanisms responsible for PID-p. The charged species may be a static charge, which can be dissipated by UV irradiation due to photoconductivity in the dielectric, or, speculatively, an elemental ion with a charge that is not dissipated by UV irradiation.

PID-Shunting involves migration of ions, particularly Na^+ from the glass and encapsulant, but also from cell production handling, drifting to the cell surface and dielectric, and then diffusing through defects through the emitter of the cell, leading to junction recombination and shunting.

PID-Shunting has already been addressed in former PVPS TASK 13 reports and has not been observed in current cell types. PID-Delamination occurs very rare in the field and is usually mitigated when other PID-mechanisms are solved with higher resistivity encapsulation and there is little information in the literature. PID-Corrosion is no new degradation mechanism and no field-related cases for current crystalline silicon solar modules are reported in literature. PID-Penetration is a process appearing after or together with other PID mechanism or it occurs at harsh test conditions. Among all these PID modes, PID-p is the most relevant, emerging, degradation mode for current cell types [19]. Therefore, we focus on this mode in the next chapters.

2.3.1 Potential-induced degradation by polarisation on cell rear of bifacial PERC solar cells

The rear side of bifacial PERC solar cells, which have a structure from front to back consisting of anti-reflective coating (ARC)/n^+/p/ARC, is particularly susceptible to PID-p because there is no diffused surface field repelling minority carrier electrons there, except at the localised cell contacts. The rear ARC dielectric may consist of a stack including AlO_x, SiO_x, or SiN_x. AlO_x deposited in the dielectric is preferably deposited to contain a negative charge that serves to repel the minority carrier electrons in the p-doped cell base. However, when the cell circuit is negatively biased, positively charged species can drift through the rear encapsulation towards

the dielectric stack. That net positive charge developing in the rear increasingly attracts minority carrier electrons in the p-type base towards the rear dielectric, resulting in an increased effective surface recombination velocity, see Figure 4. This mechanism results in a loss of photogenerated carriers, which reduces the photocurrent and the voltage of the cell, especially if the power is measured by light-current-voltage (light-*IV*) characteristics from the rear.

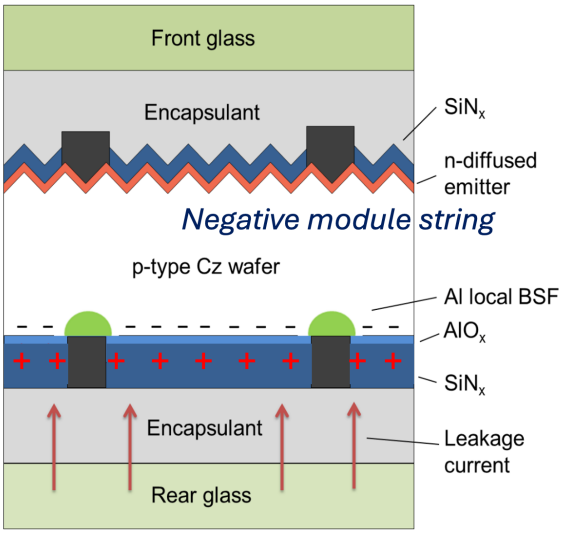

Figure 4: Schematic of the PID-p process in the PERC module rear. The red arrows indicate the motion of current (positive charge) through the encapsulation.

In recent times, there has been a migration to higher sheet resistance of the n-type emitter on the front face of the cell. This transition has been achieved using methods such as selective emitters or Ag grid finger metallization, which enable contact with higher sheet resistance front emitters. While front ARC usually is based on some combination of SiO_2 and SiN_x layers, where SiN_x has a built-in positive charge, placing the cells in a positive bias which can lead to transport phenomena resulting in more negative charge in the front. This process increasingly attracts minority carrier holes in the front emitter and more front surface recombination. Further, PID-shunting becomes more probable if the junction depth of that emitter is shallower. Since the rear side is weakly doped and usually receives less light, it has less photoconductivity in the SiN_x layer to counteract PID-causing charge. As a result, the rear side is more sensitive to PID-p than the front side, although the front side also has a certain sensitivity.

Several studies have demonstrated PID-p degradation under laboratory conditions. Since the rear side of the cell has weak doping and is therefore more sensitive, it has received greater attention in research studies. An example of the degradation magnitude of PID-p when effectuated on the module rear is shown in Figure 5. It can be seen that the degradation magnitude of PID-p is much greater for light I-V testing from the rear than such testing with illumination incident on the front of the module, because the photogenerated carriers are largely generated close to the rear surface where increased recombination takes place. As the stress testing duration increases, a recovery in power output is observed. This is attributed to inversion at the rear surface, where the silicon base effectively becomes n-type [20], [21].

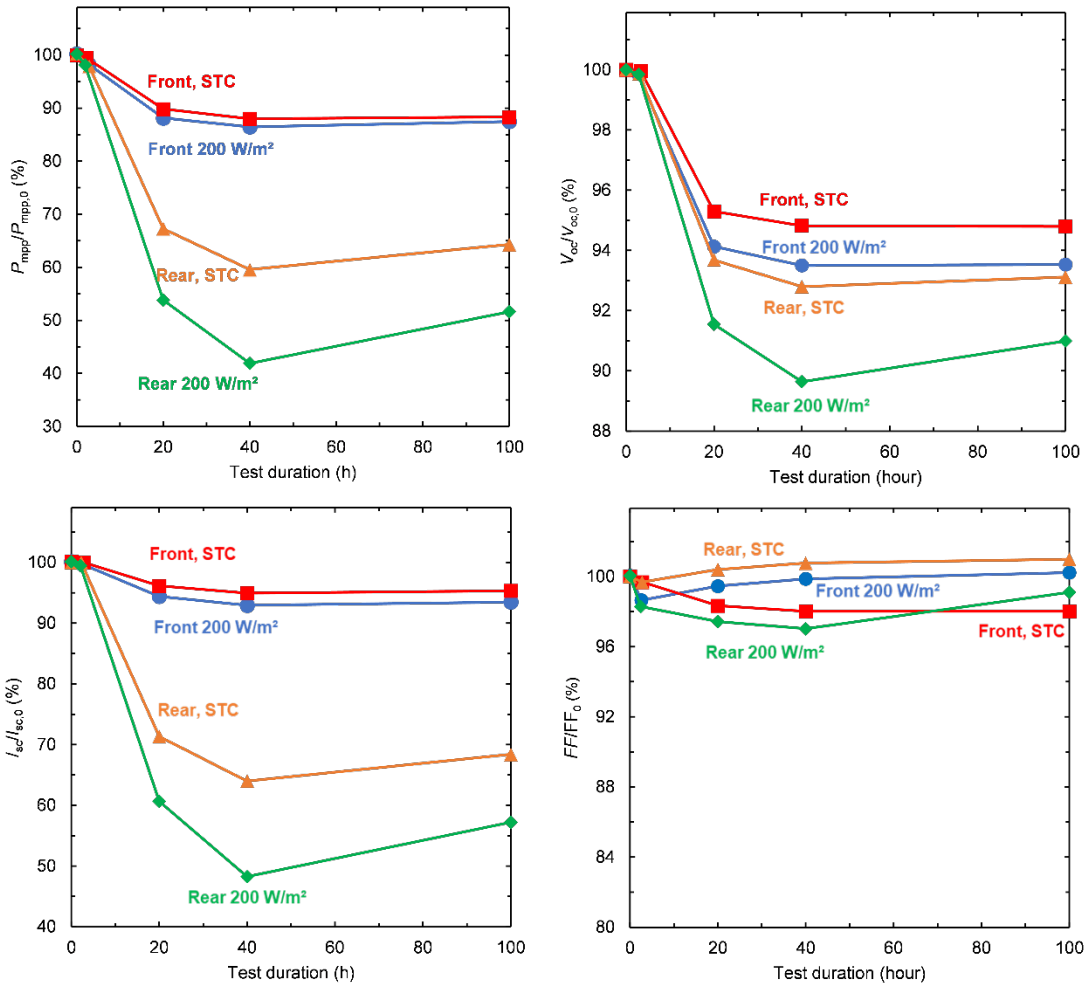

Figure 5: Normalized *IV* curve parameter of bifacial PERC modules with Ethylene-Vinyl-Acetate (EVA) encapsulant as function of test duration when biased with -1000 V applied to the cells and the rear glass face grounded. The values are obtained by flash testing under standard test conditions (25°C, 1000 W/m²) and under 200 W/m² from the front and rear as indicated in the figures. Values are from the averages of 3 samples. The solid lines are visual guides. The figure is redrawn from Luo et al. [20].

Several studies point to the existence of PID-p in PERC modules under field stress conditions. Combined-accelerated stress testing using the extremes of the natural environment (temperature cycles, irradiation and at the same time system voltage, dynamic and static load, low and high humid conditions together with water spray), indicated that PERC cells in glass/glass modules with EVA encapsulation on the front and rear side exhibited PID-p [22]. Although there was convolution with a much lesser amount of LID, with -1200 V bias voltage applied between the cell circuit and the module frame during periods of illumination (including about 7.5% albedo in the UV range), there was almost 10% relative degradation when flash tested from the front and more than 50% degradation when flash tested from the rear at standard test conditions associated with PID-p on the rear [22].

For testing PID-p in the field, commercial bifacial glass/glass PERC modules with EVA encapsulant were put in two different mounting configurations. One mounting is near (0.3 m) ground with small insolation and one is an open rack (2 m) above ground with higher rear insulation

and with their maximum rated system voltage of -1500 V or +1500 V bias during the day. Modules in open racks, either close to ground or elevated in open racks with -1500 V exhibited PID-p within several weeks whereas modules with +1500 V did not exhibit such degradation, see Figure 6.

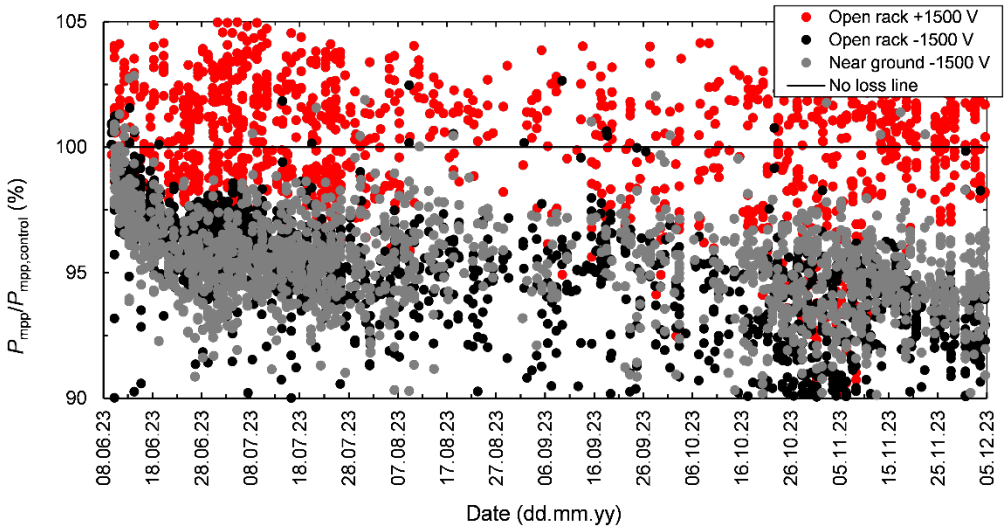

Figure 6: Normalized power to control sample for outdoor PID stress testing of PERC modules on two different racks with +1500 V and -1500 V system voltage between cells and rack in Cocoa, Florida USA (Cfa climate in Köppen Geiger classification 2006). Measured points are assembled from three samples per rack type. The figure is redrawn from Hacke et al. [23].

PID-p may be partially mitigated by inclusion of SiO_x in the rear dielectric stack (i.e. $AlO_x/SiO_x/SiN_x$) [24]. The use of a more resistive encapsulant such as a polyolefin (PO)-containing encapsulant rather than EVA and/or a polymeric backsheet instead of glass are more certain mitigations [20]. Ultimately, testing the module simultaneously with voltage bias and light with UV content, is helpful to understand whether PID-p will be a problem in the field [25].

Testing for PID in crystalline Si (c-Si)-based modules has been done with the two methods described in the standard IEC 62804-1 (2015) [26]. Stress method (a), testing in an environmental chamber, employs a non-condensing humidity level to serve as a conductive pathway to electrical ground. It frequently applies less stress toward the centre of the module face and the PID effect is concentrated toward the module edges, as is often observed for PID in PV systems. The testing conditions are module temperature of 60°C or, for further acceleration, 65°C and 85°C which is most commonly used and adopted in IEC 61215 series (2021) [6], the design qualification and type approval test. Further test conditions are the chamber relative humidity (RH) of 85%, the duration of 96 hours, the module rated system voltage, and polarity applied during the test.

Stress method (b) consists of contacting the surfaces with a grounded conductive electrode. It evaluates cell sensitivity and some effects of the component embedment materials such as glass and encapsulant resistivity, but does not differentiate the effects of some construction methods of mitigating PID, such as the use of rear rail mounts, edge clips, and insulating frames. Severities prescribed are test temperature of 25°C or, if further acceleration is desired, 50°C or 60°C, RH less than 60%, a dwell duration of 168 hours, module rated system voltage, and the polarities applied during the test period.

For testing PID-p, illumination of the sample is recommended. In IEC 62804-1 (2025) [27], two methods are given to provide a transparent conductive electrode for the module face with which an electric field is applied while allowing the transmission of UV irradiation. Method (c) uses an electrolyte gel serving as an electrode for the module face that is covered by a UV-transparent polymeric film, to reduce evaporation of the gel. The alternative method (d) uses a fine metal mesh weighed down by a UV transparent sheet on the module face to transmit UV irradiation and serve as an electrode for the module face. The test temperature is 60°C, the duration 20 hours, with the module rated system voltage and polarities. For testing on the superstrate side, 3.0 W/m^2 in the range of 290 nm to 400 nm irradiation level is prescribed. For testing on the substrate side, the measured UV irradiance level incident on the module rear, or by default if not measured, 0.3 W/m^2 in the range of 290 nm to 400 nm is prescribed. The UV light irradiation spectrum is defined in IEC 61215-2 MQT 10 [28], in the UV preconditioning test.

As a diagnostic measure of extent of possible PID-p recoverability under a standard level of irradiance, an additional test is included in IEC TS 62804-1 (2025) [27] with a level of irradiance for front surfaces of modules of 100 W/m^2 in the range of 290 nm to 400 nm with irradiance source specified in IEC 61215-2 MQT 10 [28] and a module temperature of 60°C.

The test procedures described here may be used for the cell types described below, but the relationships between the PID test and field behaviour for SHJ-based modules have not been explored.

2.3.2 Potential-induced degradation by polarisation on PERT and TOPCon front and rear side

PERT and TOPCon solar cells are grouped together based on their common structure of p$^+$/n cell doping on the cell front, see Figure 7. Due to the relatively lower solubilities of the boron forming the p$^+$ emitter region of the cell and the relatively reduced front surface field provided by that doping compared to the n$^+$/p fronts of PERC and Al-back surface field cells, the sensitivity to the polarisation is elevated. When the cells experience negative voltage potential, positive charge drifts through the encapsulation to the front cell dielectric. In turn, minority carrier electrons in the front p$^+$ emitter tend to recombine more actively at the front surface, attracted by that developing positive charge in the front dielectric. Rear sides of PERT and TOPCon have significant phosphorus n$^+$ doping, also in polysilicon the case of TOPCon, so the rear of these devices is correspondingly found to be less sensitive to polarisation [25], [29], although it is important to check as each module type shows different PID behaviour.

These cell types have significantly evolved over time. For example, the PERT type which came on the market earlier in time, tended to have SiN_x/SiO_2 front passivation stacks. Later module types added AlOx films to the stack, which have a built-in negative charge. This charge repels minority carrier electrons in the emitter, reducing sensitivity to PID-p [30].

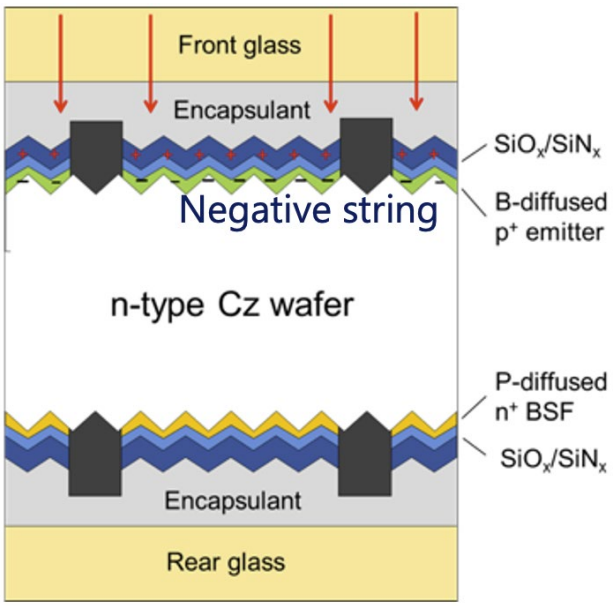

Figure 7: Schematic of the PID-p process in one manifestation of the PERT module front (the front ARC stack may differ, including with the use of AlO_x). The red arrows indicate the motion of current (positive charge) through the encapsulation. The mechanism is the same for the TOPCon front (which has an SiO_x/n-type polysilicon/SiN_x rear side instead of what is shown here for a PERT module).

For PERT cell modules, there are several studies where extremely rapid degradation has been measured; for example, in the dark [31], and while varying the level of full spectrum illumination and encapsulant resistivity [32]. Figure 8 shows the relative degradation in cell parameters as PID-p occurs. PID-p in the case of a single cell consists of the loss in open-circuit voltage (V_{OC}) and short circuit current (I_{SC}), but a negligible change in fill factor (FF). Overall, this results in the loss of maximum power (P_{mpp}).

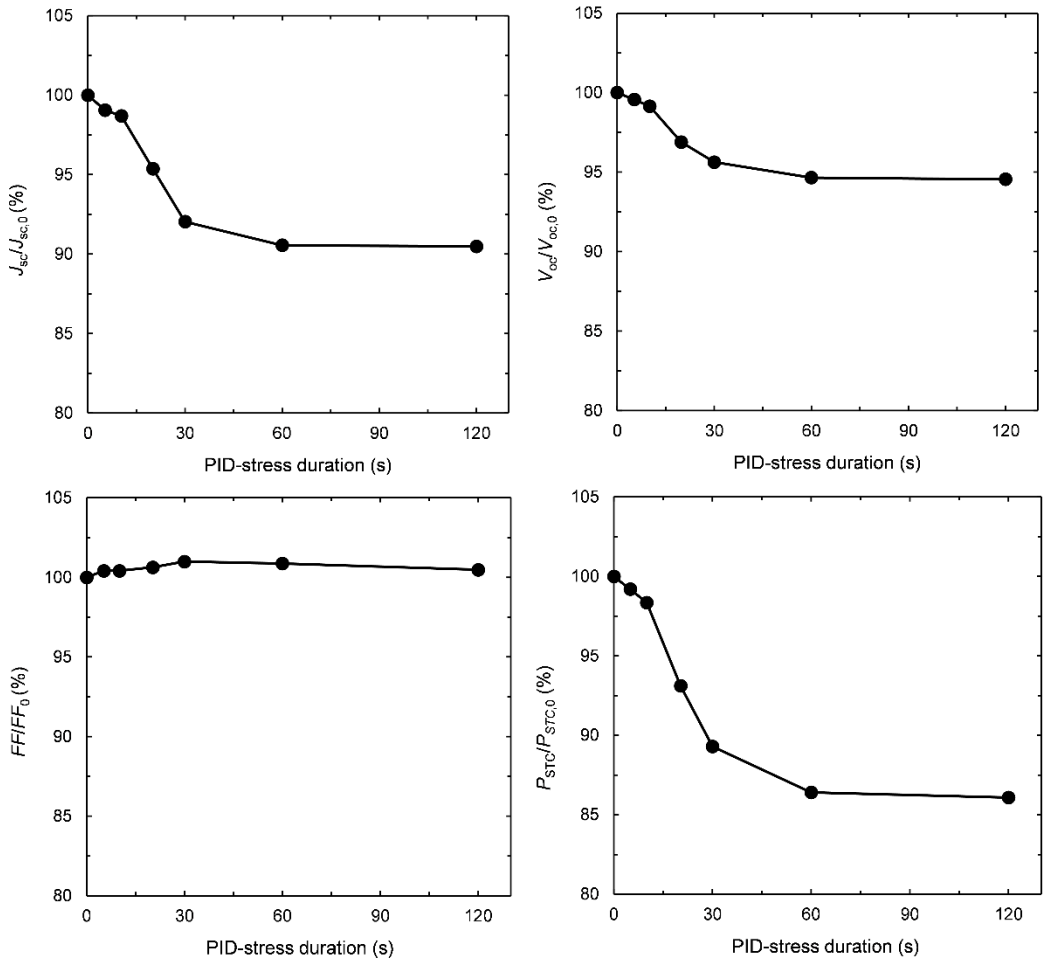

Figure 8: Change of $J_{SC}/J_{SC,0}$, $V_{OC}/V_{OC,0}$, FF/FF_0, and $P_{mpp}/P_{mpp,0}$ of n-type c-Si PERT single cell modules as function of the duration of PID stress. The voltage bias and temperature in the PID tests are set to −1000 V and 85°C, respectively. The data points represent the mean values of three identical single cell modules and the solid lines are visual guides. The figure is redrawn from Yamaguchi et al. [31].

High resistivity encapsulants and the generally high level of front side radiation reduce PID-p effects for PERT and TOPCon solar modules. Figure 9 shows how increased levels of the encapsulant resistivity and illumination with the module surface maintained wet lead to a reduction of PID-p. In these modules the degradation occurs regardless of the irradiation using this low resistivity EVA encapsulant. Conversely, even the most resistant encapsulations will exhibit PID-p if they are kept under voltage stress in the dark for long enough.

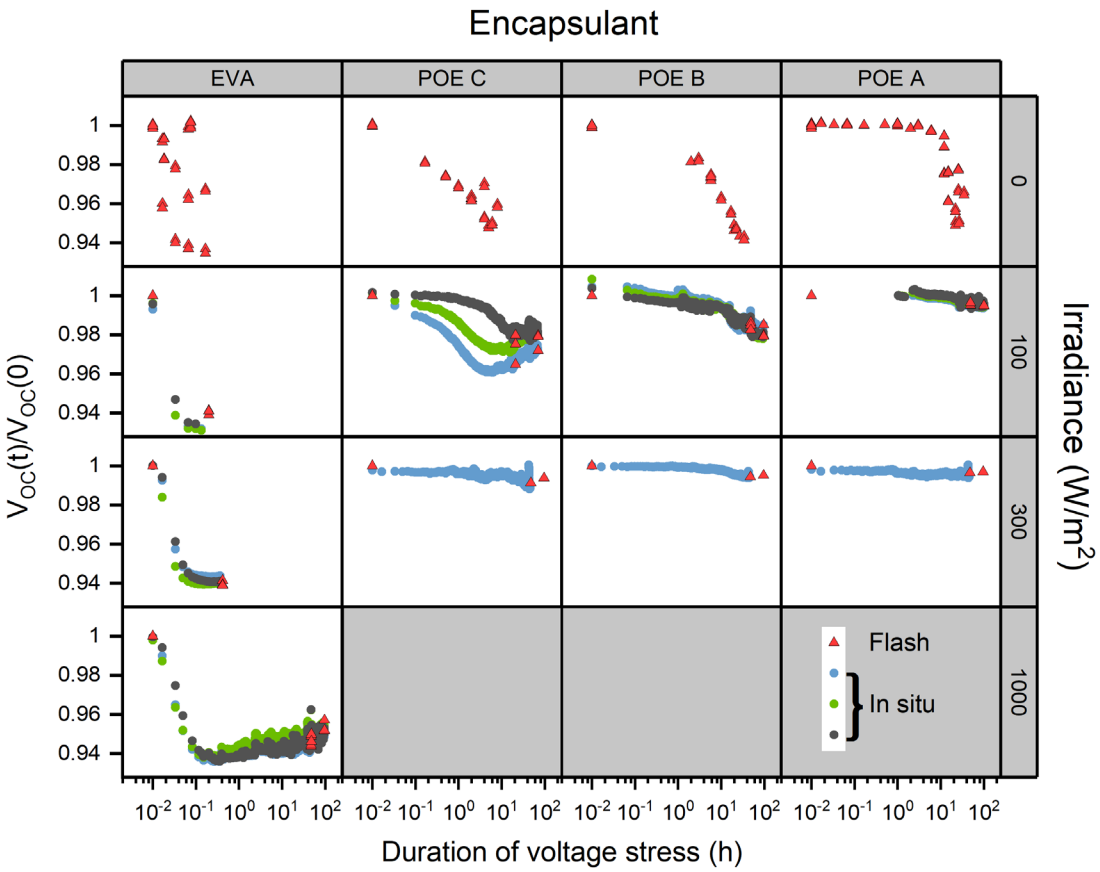

Figure 9: Normalised VOC of PERT single cell mini modules, measured via flash testing (triangles) and in situ (circles) during PID testing. Different coloured circles mark in situ measurements that were taken on each of three samples running at the respective illumination level. Thereby, 60°C and -1000 V were applied to the cells and the front glass face grounded. Resistivity in Ω·cm for the encapsulant Polyolefin elastomer (POE) A $1.2x10^{16}$, POE B $3.8x10^{14}$, POE C $8.5x10^{13}$, and EVA $1.1x10^{13}$ [32].

For PERT modules tested outdoors, it has been reported that degradation occurs during periods of wet weather, when the module surface becomes conductive and facilitates coulombic charge transfer across the glass between the cell circuit and the ground, while there is a lack of full sunlight. However, after periods of sunny weather, the power of the modules is at least partially restored, see Figure 10.

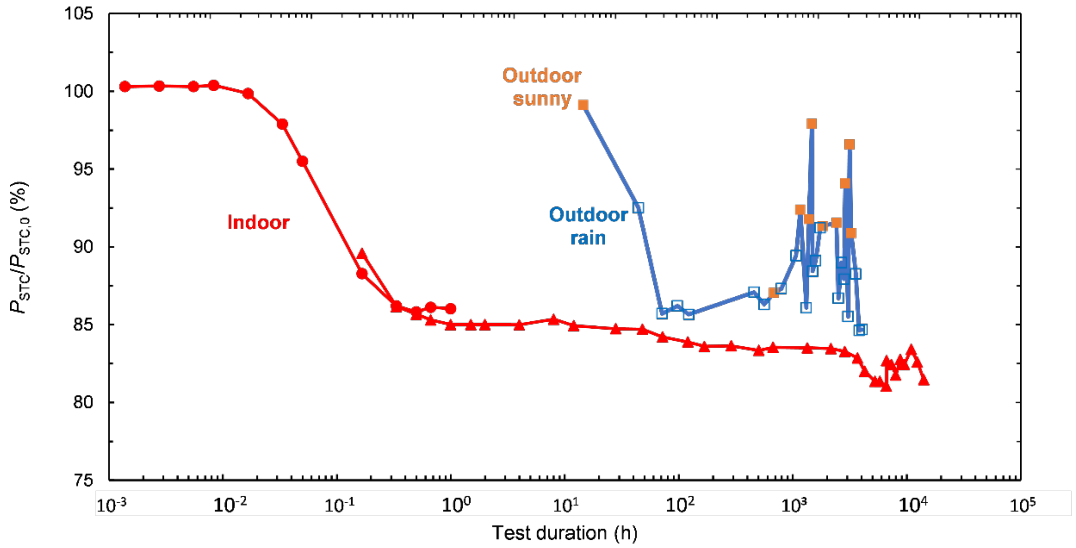

Figure 10: Normalized STC power to initial values of PERT PV modules as a function of the indoor (red) and outdoor (blue/orange) PID test duration at a voltage of −115 V. At the 10 h point indoor testing the slope slidely changes indicating a shift from PID-p mode to PID-shunting mode. The open blue and filled orange square data points indicate the results for the outdoor PID test in or just after rainy and sunny days, respectively. The figure is redrawn from Ohdaira et al. [33].

TOPCon modules with EVA encapsulation show a maximum of ~3% PID p-front degradation with -1000 V applied to the solar cells and the glass rear face with the front glass face grounded in a test setup for the polarisation of the p+/n front structure over 96 hours in humid and cloudy (~0.1 sun) weather. However, under 0.1-sun-equivalent level with UVA illumination corresponding to 0.051 $W \cdot m^{-2}$ nm^{-1} at 340 nm, they show progressively less degradation, see Figure 11. The cell rear side did not show any PID effect in that study [25].

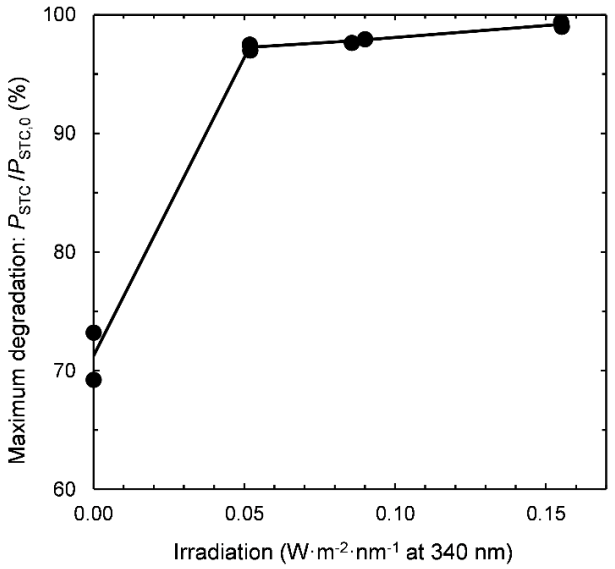

Figure 11: Normalized STC power PSTC relative to initial STC power PSTC,0, observed with −1000 V applied at 60°C over a period of 96 h versus simultaneously applied UVA irradiance level at 340 nm. For reference, Air Mass 1.5 global spectrum according to ASTM G173-03 contains 0.502 W·m^{-2}·nm^{-1} at 340 nm. Two repetitions were performed per irradiance level shown with markers (●). The figure is redrawn from Hacke et al. [25].

In the case of the TOPCon module tested, the PID-p rapidly and repeatedly recovers under sunlight when the voltage potential across the front glass is removed. Such properties suggest that PID-p will rapidly recover in the field and that it may not even occur to any significant extent because solar irradiation is accompanied by the development of system voltage stress in the module string. However, the relative sensitivity to PID-p under the factors of system voltage and solar irradiation must be checked for each module type.

2.4 Protection of substrings in the modules

The protection of the module's substrings against acting as a power load is one of the most important safety features of a solar module. A module can act as a power load if it is partially shaded or if there is high resistive interruption due to a failure in the electric current path (substring). There are two widely used options to protect a module's substring against high power dissipation during shading. The cheapest and most commonly used option is to protect a substring against overheating by a bypass diode (BPD). The second option is to avoid overheating during shading is by using solar cells with a low, not localised breakthrough, voltage which acts similar as a cell-wise BPD. Even in the second case, an additional BPD per string, is used to reduce the power loss during excessive shading, and to achieve an additional safety feature in the event of a high resistive interruption in the module's substring. With current module types (1500 V and 600 W_p) 10 kW and more can be generated in a single module string. The higher the string power, the more harmful a failure of the substring protection can be.

2.4.1 Hot cells

Cell cracking or shading of PV modules can cause current mismatch and reverse bias voltages in underperforming solar cells, causing the cells to dissipate power and generate heat. The difference between the well-known hot spot and the hot cell effect is that the hot spot is mainly associated with multicrystalline silicon solar cells and causes localised heat generation (local junction breakdown), whereas the hot cell is associated with monocrystalline silicon solar cells and causes a homogeneous temperature rise throughout the cell area [34]–[36], see Figure 12. The most important junction breakdown mechanism in monocrystalline silicon solar cells is avalanche breakdown, which occurs at reverse bias voltages below -20 V for PERC cells [37] and even more negative for TOPCon, SHJ, and possibly for MHP/Si tandem [36]. A hot cell can cause heating above the typical module operating temperature of 50°C - 70°C, reaching temperatures above the highest module's lamination temperature of 150°C.

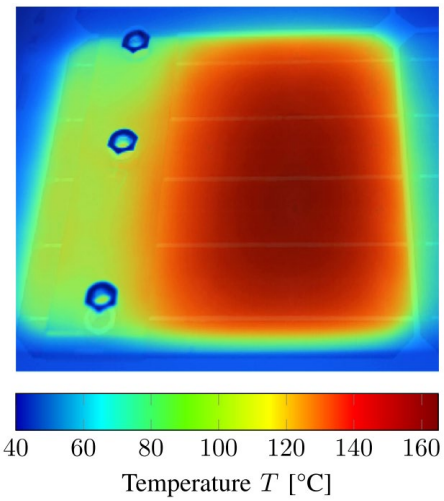

Figure 12: Temperature distribution of a partially shaded cell during the IEC 61215-2 MQT 09 Hot-spot endurance test [28], [35]. The shadow mask is shading the cell with a 4 cm wide cover strip.

The occurrence of a hot cell may lead to the generation of other failure modes, including discolouration, interconnection failures, cell cracks, delamination, loss of electrical insulation, and a permanent change in the reverse bias characteristics of a shaded cell [38]–[40]. The standard

hot-spot endurance test (IEC 61215-2:2021 MQT 09 [28]) assesses the ability of the solar cell and module materials to withstand localised point heating at a module temperature of 55°C ± 15°C under worst-case partial shading.

PV manufacturers are taking measures to minimise the impact of hot cells on the reliability and durability of PV modules. These measures include sorting cells into bins based on the cell current rating and the screening of individual cells for low shunt resistance [41], [42]. In addition, manufacturers insert BPDs into PV modules to minimise the formation of hot cells and mitigate their harmful consequences. The incorporation of the BPDs ensures that the power dissipated by the shaded cell is at most the power generated by the rest of the cells in the same sub-string. This way, although BPDs can reduce the power losses caused by shadows, they do not eliminate the negative effects of hot cells, which can still lead to significant performance losses and safety risks [43]. The market now offers a variety of shade-resistant PV modules, such as half-cell modules, shingled modules, and modules with built-in diodes for each cell [44]–[46]. However, the term "shade resistance" is poorly defined, and there is no reliable way to compare different PV products. Researchers are working to standardise this, focusing primarily on minimising yield loss, but often neglecting improved reliability [47]. In addition, decreasing the number of solar cells per BPD lowers the hot cell temperature, as it operates at less negative reverse voltages [35], [36], [48].

In Interdigitated Back Contact (IBC) solar cells, the p^+ and n^+ regions can be designed to be in direct contact with each other, resulting in the formation of a Zener diode that functions as a built-in BPD and significantly lowers the breakdown voltage (> -5 V) of the cell [49], [50]. As shown in [48], during the indoor hot-spot test, the hot cell temperature of the IBC module was at most 25°C higher than the module temperature. Moreover, it was significantly lower than the temperature of the PERC and SHJ module technologies under the same conditions, see Figure 13.

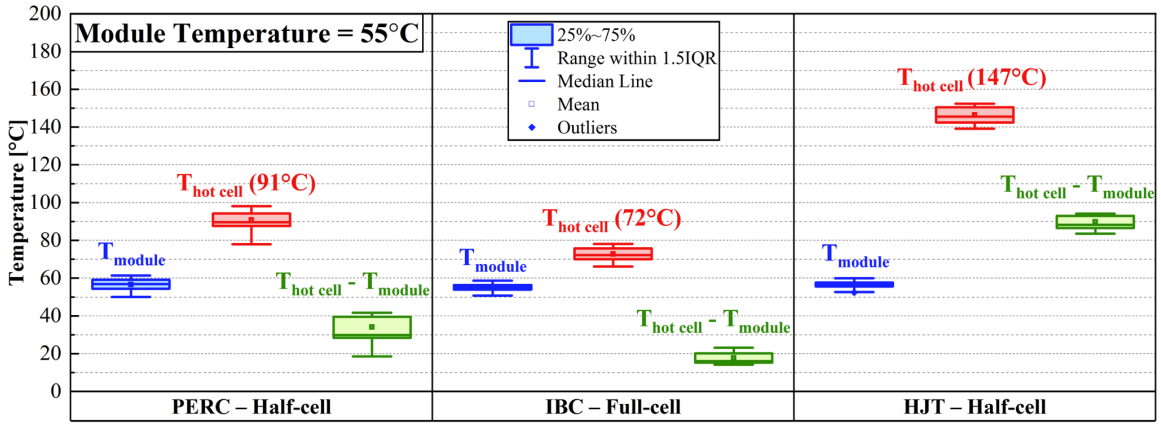

Figure 13: Module and hot cell temperatures of PERC - half-cell 365 Wp, IBC - half-cell 400 W_p and SHJ - half-cell 375 W_p modules from indoor hot spot tests performed at 55°C module temperature by following IEC 61215-2:2021 [28], [48].

High temperatures above 150°C can have significant implications for polymeric materials (i.e. discolouration, delamination, embrittlement [38], [51]), which are designed to operate below this temperature. Furthermore, temperatures above 170°C can lead to bubbles and deformation of the backsheet material, and in extreme cases, the junction box may even detach [51]. It is also crucial to ensure that the temperature of the hot cell does not exceed the solder melting temperature, which leads to solder joint failures [52]. The liquidus temperature of $Sn_{63}Pb_{37}$ solder is 183°C and for lead-free solders around 220°C [35]. In addition, high cell

temperatures can also put the glass at risk of breaking. IEC 61730-2 MST 21 temperature test exposes the module to 1000 W/m^2 sunlight until the temperature stabilized and the pass criteria of the standard is that no measured temperature exceeds the limits of the surface materials. This limit is given in the standard as “TI/RTE/RTI”, which is the maximum service temperature at which the critical properties of a material will remain within acceptable limits over a long period of time. The duration spent at these high temperatures is as important as the temperature itself, as degradation mechanisms require time to occur. Thermoplastic materials require a certain exposure duration to undergo material changes due to elevated temperatures.

Nowadays there is a clear trend towards bifacial modules, but their ability to receive light from both sides can cause non-uniform illumination patterns at the rear side [53]. In the event of current mismatch, the higher current produced by bifacial modules can result in higher hot cell temperatures compared to monofacial modules [54]. Another current trend is the adoption of half-cells, which are advantageous in terms of heat dissipation due to the larger perimeter-to-area ratio. However, larger Si wafer dimensions decrease this ratio, resulting in higher hot cell temperatures for modules using larger wafer formats [35]. Up to now, the hot cell effect occurs in the standard hot spot test, but not as severely in the field. Nevertheless, increasing the substring length and increasing cell efficiency raises the risk of encountering modules with laminate defects caused by regular shading in the field.

2.4.2 Unreliable connection in junction box

A reliable connection between the inner parts of a PV module and the BPD is mandatory. A working BPD and a reliable connection of the inner cell strings is responsible to avoid high power dissipation on shaded cells in a PV module. A defect in the BPD or in the connection process can often lead to arcs in the module laminate, which may cause a fire. This can result in the loss of both the mechanical and electrical integrity of the module. In addition, power losses can occur in the entire string, either while the module is shaded or after the disintegration of the affected module. Therefore, this kind of failure type is one of the worst possible. The half-cell module type, introduced around 2020 as a mainstream module layout, is accompanied by changes in the interconnection of inner parts and the diode box. Compared to former full-cell modules, the substring interconnects of half-cell modules are very short at the point where they lead into the junction box. This may cause an unwanted surface contamination onto the ends of the short substring interconnect from the lamination material during the lamination process. Furthermore, it is more difficult to reach the interconnect ends by factory workers/robots as they are now in the middle of the module and not near the frame. Additionally, the diode boxes are quite small. In the past, most connections were made by reliable clamping in the junction box. Nowadays soldering is used as the space in the boxes is too small for clamping. Furthermore, since then the diode boxes are filled with a filler material as a standard. With all these modifications lamination material contamination on the interconnection wires can cause a bad electric contact in the junction box, the difficult handling could cause a poor quality/bad visual quality control of the soldering process, and the filler material can cause the loosening of a weak connection in the diode box by shrinkage or by chemical changes.

If there are unreliable connections in the junction box, modules show connection failures in the junction box within one and two years of installation in the field. The experience is that the rate of new failures per year drops down fast in the second year for one installation. Figure 14 shows an overview which failure modes (A, B, C) are possible, how to detect them, and what consequences the failure mode provokes for the safety risk and the power loss. In Figure 14, the consequences are given for the extreme case that the cold solder joints are fully disconnected. All shown failure modes can happen in all thinkable combinations. Failing BPD [55] cannot be differentiated from failure mode A without a destructive analysis of the junction box.

However, having a mixture of failure modes A and B in a fleet of modules indicates that a cold solder joint is the cause of the defect.

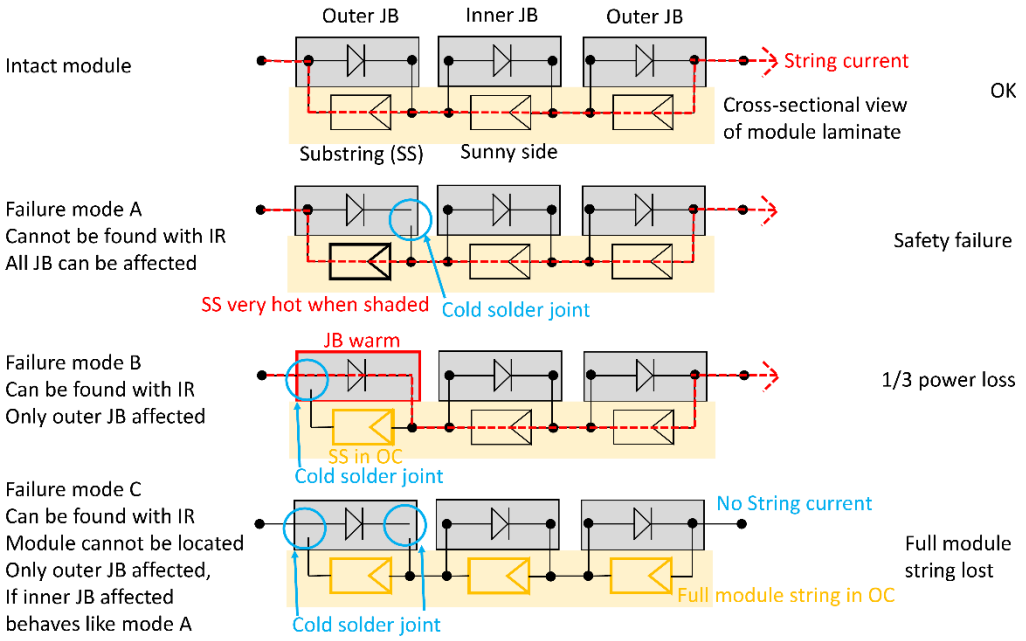

Figure 14: Failure modes of unreliable connections in separated junction boxes. Open-circuit (OC) substrings or module strings appear 5-10 K hotter in IRT inspection compared to active strings.

However, as long as the likelihood of a cold solder joint is low, a combination of different failures in the same module is very unlikely. Failure mode A can occur at four different solder joints. Two of four solder joints are in the middle substring. Failure mode B can occur at two possible joints, whereas failure mode C needs two joints failing in parallel. Therefore, failure mode A occurs at least double as likely as failure mode B. Failure mode A cannot be detected by infrared thermography (IRT) inspection, but failure mode B and C can. This means that if failure mode B or even C is present, failure mode A is very likely to occur at a rate at least twice as high as that of failure mode B. However, without shade on the modules failure mode A will stay without notice. A shaded module with failure mode A can heat up very quickly (within seconds) and may char or even burn. The danger rises if the module is shaded at high irradiation level or if the shade is applied for many seconds. Figure 15 shows a high power TOPCon module with failure mode A after being shaded in a long module string. To find mode A failure or open BPD, a string wise BPD test at night is useful. Measure the reverse bias voltage achieved in the string when 3% to 5% of rated I_{SC} is applied. If a string with extraordinarily high reverse voltage is found, search for some Kelvin warmed up substring with night infra inspection to locate PV modules with mode A failure or open BPD, see Figure 16.

Figure 15: Rear side of TOPCon PV module with failure mode A being shaded by natural obstacles. Module has already been dismantled from the mounting rack.

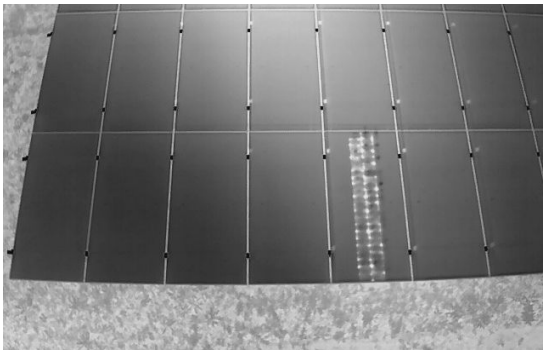

Figure 16: Not connected BPDs found by night IRT inspection while applying string wise reverse voltage with 3%-5% of rated I_{SC}. Image: photovoltaikbuero Ternus & Diehl GbR.

All failure modes can occur also with arbitrary contact resistance at the cold solder joint. This means that a junction box which is hotter than the other boxes can be an indication for a cold solder joint. However, resistive heating at a cold solder joint for failure mode A can only be observed during shading or with greater safety for the inspecting person within the BPD test.

A cold solder joint usually appears in a certain percentage of modules in the production because the problem is typically the same for the whole batch of modules. Figure 17 shows the IRT image of multiple modules with failure mode B, with OC substrings resulting from cold solder joints in the outer junction box. It is frequently observed that this unstable connection appears for a small percentage of modules from the same production batch.

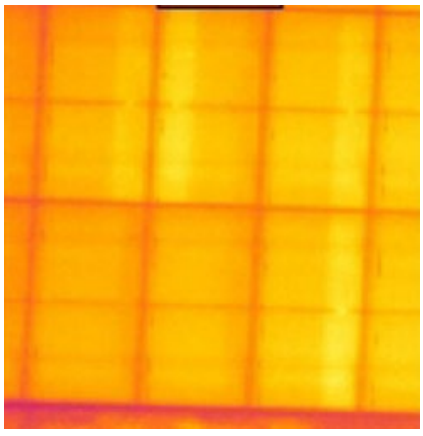

Figure 17: IRT of OC substrings resulting from an unstable connection of the outer junction box. Failure mode B can happen only in the outer junction boxes. Current flows through diode of outer junction box.

Figure 18: Module with burnt junction box resulting from unstable connection in the junction box.

Even if the inspection at the end of the production was inconspicuous, unstable connections could be found in one batch of modules during pre-shipment inspection. The voltage and power of the defective modules are only 2/3 of the normal value, while they had normal power during the measurement at the end of production. It is a typical unstable connection where the performance is sometimes OK and sometimes not. The modules from the same batch showed more open substrings in the IRT inspection. Figure 18 shows a module with burnt junction box probably resulting from failure mode C with some contact resistance still present.

To avoid this failure type during production, we recommend a reverse voltage sweep in the dark in series with the flash, EL, or high potential test of the PV module, as specified in IEC 61730-2:2023 Annex A5 a) or b) but not c). A reverse voltage sweep in the dark would show unconnected diodes (no current flowing through them) and would also reveal high contact resistances within the junction box (define max. allowed resistance in the BPD *IV* curve). However, some not fully operational contacts may be overseen, as these contacts are low resistive at this stage. To detect these cases, an automated visual inspection test is recommended after soldering the leads into the junction box. At system level, a reverse voltage sweep should be done for each module string to detect non-connected or high resistive BPDs in failure mode A, and a thermal inspection is recommended to detect failure mode B and C. In case of a single failure, all modules should be tested due to the high risk of fire.

2.5 Encapsulation degradation and failure modes

The basic module design of standard PV modules has changed dramatically in the last few years. The entry of bifacial solar cells into the market triggered a transition from the prevailing standard glass/backsheet module architecture to increased use of glass or transparent backsheets as the backside layer of the PV modules. EVA has been the most commonly used polymer encapsulating material, and polyvinyl fluoride (PVF) films in combination with polyethylene terephthalate (PET) core (PVF-PET-PVF known as Tedlar) have been commonly used for backsheets in PV modules for more than 30 years [56]. Although their technical, environmental and economic characteristics were satisfactory, there was still room for improvement. Around 2010 polyvinylidene fluoride (PVDF)-PET-PVDF and polyamide (PA)-based backsheets entered the market; followed by pure PET-backsheets [56]–[58]. More recently, new encapsulation and backsheet films based on PO were developed, and after intensive testing, some of them were also commercially launched within the last years [59]–[63]. Furthermore, silicone-based encapsulants are also promoted and tested [64] .

Looking at the distribution of reported PV module failures [38], [65], [66], defects of the backsheet such as discoloration, delamination and backsheet cracking represent a significant group [67], [68]. Jordan et al. developed a rating system to classify the severity of failure/degradation modes by ranking them from 1 to 10, where 1 indicates that the observed degradation mode has no effect on performance, meanwhile 10 indicates both, a major effect on power and safety [38]. Degradation related to the backsheet layer was divided into two categories:

(i) backsheet insulation compromise (e.g. adhesion issues and cracking) has a significant effect on power and/or yield and also represents a safety hazard = severity 10,

(ii) backsheet other (e.g. bubbles, discoloration, and chalking) do not affect module performance immediately = severity 1.

There have been reports of an increased occurrence of failures of PV modules with cracked PA back films [69], [70], especially since 2016. In addition, cracks and insulation problems in PVDF-PET-PVDF and PET-based backsheets [68], [71], [72] have been increasingly reported in recent years. Based on extensive field measurements, Buerhop et al. report yield losses if

the inverters fail to start in the morning because dewy, torn backsheets cause an insulation fault [71]–[73].

In the following, the major chemical and physical degradation mechanisms for these failure modes will be compiled.

As backsheet cracks are typically revealed after several years of field ageing, and they have never been observed in previous qualification and reliability tests according to standard IEC 61215-2:2021 [28], the probable origin is suggested to be the result of a combination of multiple stresses and might also include unexpected material interactions as drivers. Similar PA backsheet cracks could be reproduced by a newly designed indoor accelerated ageing test, by utilising simultaneous combined or sequential stresses (UV, humidity, temperature and thermo-mechanical load) [22], [56], [68], [74], [75]. These newly developed ageing tests can now be used to test the crack susceptibility of new backsheets during the product development phase. If cracks occur in the backsheet of a PV system, a repair coating or tape/foil can be applied to restore the insulation resistance as shown in chapter 2.2 of the PVPS Task 13 report "Performance and Reliability of Second Life PV" [76].

Various types of backsheet cracking can be distinguished [69], [77], [78] and are described in sections 2.5.1.- 2.5.3.

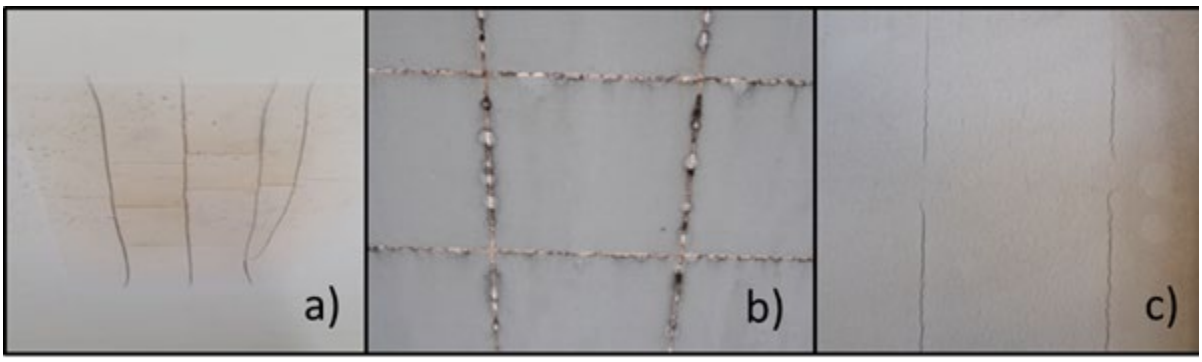

Figure 19: Backsheet crack types. a) cracked backsheet beneath a hot cell/temperature induced crack. b) squared cracks beneath cell interspaces; thermo-mechanical induced crack combined with photo-oxidative degradation. c) longitudinal cracks located beneath busbars; thermo-mechanical stress induced crack [69].

In addition, when new materials were introduced, incompatibilities between the encapsulating and backsheet films were observed in some cases. These were partly caused by undesirable additive migration within the polymer laminate and led to adhesion problems/delamination and/or discoloration [56], [70], see chapter 2.5.4. Furthermore, specific failure modes were also observed with new PO-based encapsulant films, see chapter 2.5.5, and innovative polymeric front sheets [79], [80], [81].

Such material incompatibilities can be mitigated by selecting appropriate materials and thoroughly testing their compatibility by applying tests suggested in chapter 4.1 of the PVPS Task 13 report "Accelerated testing - combined stress vs. sequential stress testing methods and inclusion of specific load situations" [79].

The different backsheet failure modes are described in the following. Finally, chapter 2.5.8. will deal with the frequent breakage problem which has emerged in new large-format thin glass modules.

2.5.1 Backsheet cracking type I: micro-cracking and chalking

UV photons can open chemical bonds at a surface and the open bonds subsequently react with oxygen leading to degradation and discoloration of the material. This process is called photo-oxidative degradation. Surface weathering can lead to photo-oxidative degradation of the outer backsheet layer, resulting in decomposition of the polymer and release of the inorganic filler (=chalking), see Figure 20 b). The root cause for cracking type I is insufficient weathering stability of the individual outer layer of the backsheet, e.g. missing or lack of UV-stabilisation, which can happen with different types of backsheets which have polymeric outer layers prone to photo-oxidative degradation, e.g. PA or PO. Chalking of the backsheet has no direct impact on module reliability or the performance of the PV system. However, in some cases, chalking can be an initial indication of later microcracking which in the long term could evolve on deep cracking, see Figure 20 a) and b).

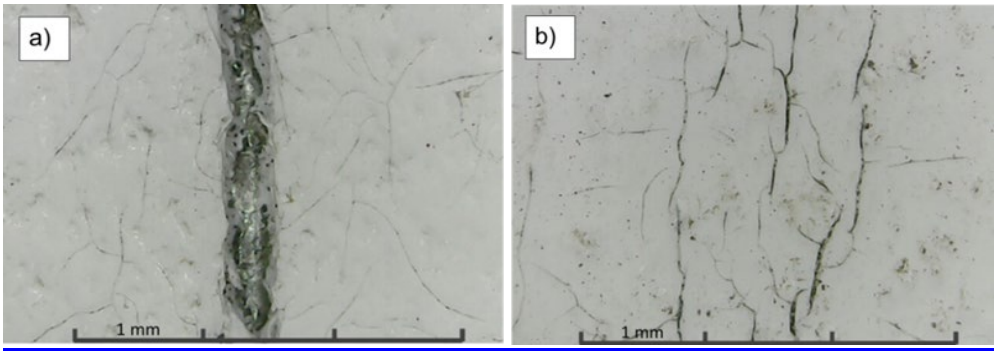

Figure 20: Light microscopic images of (a) longitudinal cracks (whole backsheet is disrupted) and (b) surface near microcracks [69].

Chalking is the result of photo-oxidative degradation of the polymer in the outer backsheet layer which leads to the release of filler. A simple wipe test can be carried out to check this phenomenon in the PV system. Preventatively, the backsheet can be subjected to accelerated weathering tests, and then these wipe tests can be applied. Chalking is a superficial phenomenon and not directly related to the insulation resistance of the backsheet. Unfortunately, there is no possibility to predict if chalking is a precursor for future cracking or potential changes in other backsheet properties like electrical insulation, as there are no systematic studies on the topic and its effect on long-term stability of the backsheet and the module. For example, cracking was observed with and without chalking for PA backsheets [69]. Another example is cracking of PVDF-based backsheets, where chalking is usually is not observed [82].

2.5.2 Backsheet cracking II: temperature-induced

Hot cells or hot spots lead to local overheating (200°C or higher) of the backsheet and the encapsulant layers, resulting in strong chemical degradation, followed by locally cracking of the backsheet. This reaction is often accompanied with browning phenomenon or even gas formation within the encapsulant and backsheet, like shown in Figure 19 a). The main reason for cracking II is the extreme thermo-oxidative stress impact from the overheated cell or interconnection, caused by heat generating electrical defects like isolated cell parts caused by cell cracking, insufficient solder contacts on cells or other wiring parts, or excessive local shading of cells in a module. This failure mode can occur with all the different types of backsheets and typically occurs with only some individual PV modules in a PV plant. Thus, low impact on the performance of the PV plant is expected, but the defective modules should be replaced.

2.5.3 Backsheet cracking III: thermo-mechanical stress induced

The phenomenon of backsheet cracking type III occurs with increasing operational time and seems to depend on the local weathering conditions. If backsheet cracking type III occurs mostly all modules of a PV plant with identical module design in terms of bill of materials (BOM) are affected [69]. Backsheet cracking III can have two appearances, see Figure 19 b) for squared cracks and Figure 19 c) for longitudinal cracks. Drivers for these cracking modes are:

i) mechanical stress within the backsheet at the positions of the busbars, which is originated already from the lamination process;

ii) unbalanced thermo-mechanical properties of the backsheet e.g. caused by mismatches in the coefficients of thermal expansion (CTE).

With co-extruded backsheet types, e.g. a 3-layer PA backsheet, a high direction dependence of the mechanical properties has been measured [58], [69]. Physical cracking starts at the outer surface of the backsheet and propagates towards the core and the inner layer. No chemical degradation is observed in the case of longitudinal cracks [69]. However, since the backsheet film is damaged across the entire cross-section, the insulation requirements for the backsheet are no longer met and the insulation resistance collapses especially under wet conditions, leading to a significant safety risk [38]. Since all modules with the same backsheet type are usually affected, either the entire system must be repowered, or the modules must be repaired using a suitable coating or film.

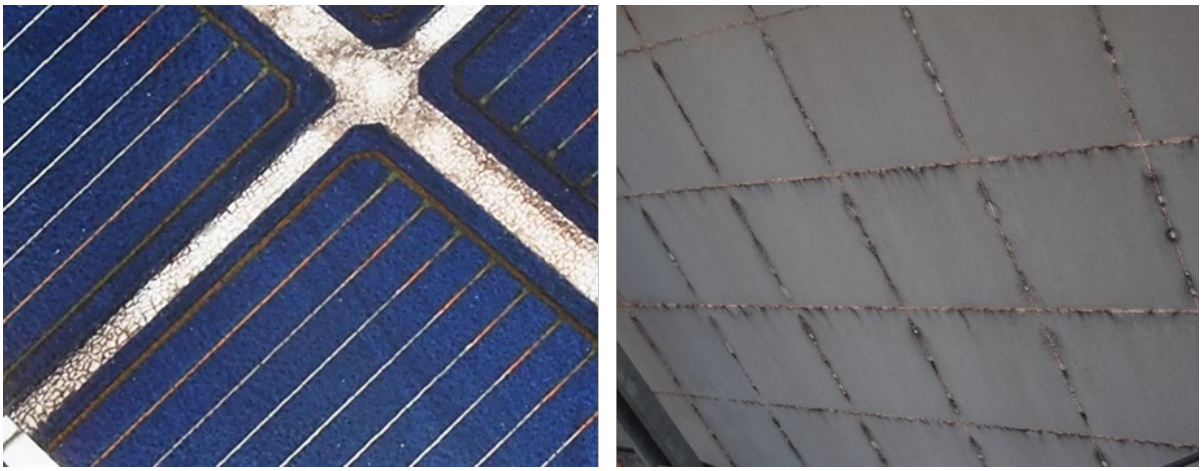

Figure 21: PV module with squared cracks from the front (left) and rear side (right).

In the case of squared cracks, on the contrary, an additional driver is the insufficient UV-stabilisation of the encapsulant. In a first step photo-chemical degradation in between the cell gaps creates acetic acid with a high local concentration at the interface EVA encapsulant/inner layer of the backsheet. A chemical degradation between acetic acid and the backsheet weakens the mechanical strengths of the backsheet, followed by a physical cracking of the backsheet from the encapsulant side to the air side [69], see Figure 21. Serious safety problems [38] are the consequence of this type of degradation, which can only be remedied by replacing all modules of this BOM. A repair is not possible in this case.

Similarly, as for PA, two distinct types of PVDF backsheet cracking have been observed in the field. The PVDF cracking type III i) involves cracks along the busbars that penetrate the entire thickness of the backsheet, while the PVDF cracking type III ii) involves randomly distributed longitudinal cracks that only affect the outer PVDF layer. The outer layer of the PVDF-based backsheet can have a mono or multi-layer structure, and the PVDF is often mixed with a

poly(methyl methacrylate)polymer (PMMA) and TiO_2 [74], [83], [84]. Apart from cracking, the PVDF layer undergoes physical ageing processes, leading to changes in crystallinity, crystalline phase, and shrinkage when it is exposed to elevated temperature [85], [86] as well as depletion of PMMA under exposure to sunlight [85], [86]. Due to the often undisclosed variations in the composition of the PVDF layer in the backsheet, no clear correlation between the structural parameters of the PVDF layer and backsheet cracking has been established yet.

2.5.4 New backsheet types: degradation modes

With the increasing use of bifacial solar cells, the need for transparent backsheets is increasing. The trend is strongly towards glass-glass modules, but transparent polymer backsheet films are also used if double-glass modules represent a too high weight load. However, polymer films without fillers are more difficult to stabilise, thus, the emergence of new failure modes related to transparent backsheets are to be expected. Compared to traditional filled backsheets, transparent backsheets can be more susceptible to UV-degradation, as light transmits through the transparent outer layer into the backsheet core and the inner layers [87]. A change in the type of backsheet may also require a change in the encapsulation material. One option is to use different encapsulations sheets on the front and back side. In this scenario the danger of material incompatibilities described above come back into play. Thus, in the product development phase accelerated ageing tests as described in chapter 2.5 of the Task 13 report “Accelerated testing - combined stress vs. sequential stress testing methods and inclusion of specific load situations” [79] have to be performed to prove the material compatibility between backsheet and encapsulant.

Conductive backsheets are used for interconnection of back contacted cells. These backsheets typically have a thin metal inner layer (Cu or Al) laminated onto the PET core layer [88]. Potential new backsheet degradation modes include delamination or corrosion of the metallic layer. In this case accelerated ageing tests of the conductive backsheets in a laminate with the encapsulant to be used along with the cells and connectors must be applied as well. Test procedures as described in the IEC 61215-2 should be used, especially MQT 11 thermal cycling (TC), MQT 12 humidity freeze (HF) and MQT 13 damp heat (DH) [28].

Currently, due to lack of long-term field experience with these types of backsheets, no critical failures after field exposure have been reported so far. Therefore, at the current state (as of September 2024), no statements can be made about relevance and potential mitigation measures.

2.5.5 Encapsulant-backsheet incompatibility

If new polymer films are going to be developed or used to encapsulate the active solar cells and connections, it is strongly recommended to test the compatibility of the materials with the adjacent layers during the product development phase. For example, it must be verified whether undesirable reactions or additive migration occur at the polymer interface between the encapsulation material and the backsheet under stress, such as increased temperature. Furthermore, the adhesion of the encapsulant to the glass panes and/or backsheet has to be evaluated after stress impact, such as high irradiation, temperature, or humidity in accelerated ageing tests.

PO encapsulants can be incompatible with PO-based backsheets, because additive-migration upon DH testing can lead to strong discoloration [89]. The yellowing effect results from an undesired interaction of oxidised additives of the encapsulants with additives of the PO-backsheet. These chromophoric compounds, with conjugated double bonds, formed under the influence of temperature and humidity and decomposed upon irradiation (photo-bleaching).

Since PV modules are always simultaneously exposed to sunlight, temperature, and humidity under operating conditions, this yellowing effect does not occur in real life. Furthermore, encapsulant discolouration has only a minor impact in the order of several percent on the PV module's electrical performance [56].

Also, PV modules with PO encapsulants and Tedlar backsheets may show adhesion problems, since the adhesion of the encapsulant to the glass may deteriorate under accelerated aging, especially in areas without cells underneath (e.g., edge areas and cell gaps). Furthermore, light microscopy images show deposition of substances at the glass/polymer interface, see Figure 22. Na^+-ions were detected at the depositions on the detached surface of the encapsulant by X-ray diffraction (XRD) and carboxylic groups were found by Infrared-spectroscopy. Thus, migration of an unwanted carbon acid or ester from the backsheet to the encapsulant/glass interface took place, weakening the adhesion.

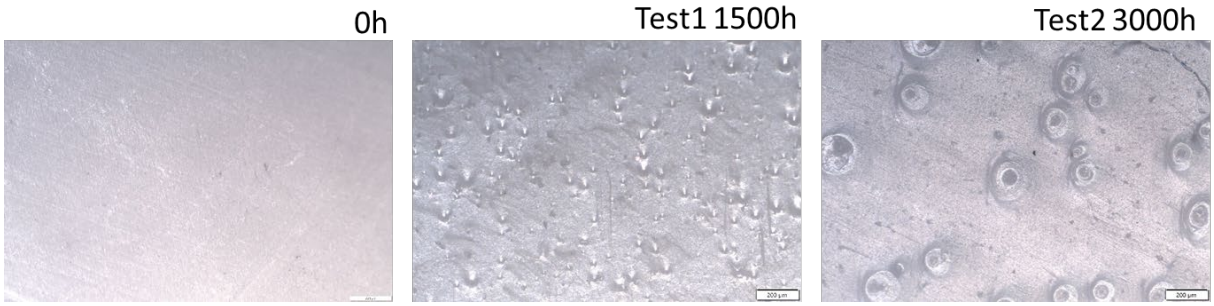

Figure 22: Detached surface of the PO encapsulant from the glass in the original state 0 hours and after two types of accelerated ageing tests. Test1: constant Xe-irradiation at 1000 W/m² at elevated temperature (chamber 65°C, PV module 96°C) and humidity (80%r.H.). Test2: sequential (i) 500 hours DH, (ii) 50 temperature cycles and (iii) 200 hours Xe-irradiation at 1000 W/m², 3 sequences.

2.5.6 New polyolefin-encapsulants with EVA: degradation modes

The development of new materials, based on ethylene copolymers in particular, has driven the replacement of EVA. Various types of next-generation encapsulation films have been introduced in the last years under the label "polyolefin encapsulants" that could attract significant market share in the future [59], [63], [90]–[95].

However, there is no comprehensive knowledge on outdoor behaviour of PV modules using these materials available. The new materials caught the attention of the academic and industrial sectors, but additional studies are necessary, especially long-term indoor and outdoor exposure investigations, to discover new degradation modes that might appear [96]. Additionally, the effects of the long-term interaction between the new encapsulant materials and the other module components are still an open question.

These material innovations tend to be classified as cross-linked POE and TPO encapsulants. The new materials do not contain vinyl acetate moieties, and consequently, do not produce acetic acid upon degradation. Therefore, PV degradation mechanisms mainly associated with acetic acid [59] does not take place. Hence, the following positive effects of the use of alternative PO encapsulants have been reported:

- Reduced corrosion (no acetic acid, lower vapour transmission rate (WVTR)) [59], [61], [97], [98]
- Reduced PID [32]
- Reduced yellowing [98].

Unfortunately, the terms POE or TPO are used in a manner that implies that all POE or TPO encapsulants are the same. Additionally, the term “polyolefin” or PO is understood differently in the PV industry. Elsewhere, a PO is any class of polymers produced from a simple olefin (i.e., an alkene with the general formula C_nH_{2n}) as a monomer. That includes TPOs like polyethylene and polypropylene, but also POEs such as polyisobutylene or ethylene propylene rubbers. The PV industry uses the term PO for all non-EVA encapsulants based on polyethylene or polyethylene copolymers, which also contain other functional groups such as acrylates or acrylic acids [99].

The most recent developments resulted in the market introduction of so-called EPE films, which are co-extruded films combining the benefits of EVA (E) and POE (P). The outer EVA layers provide better adhesion to glass and the solar cells, whereas the POE core layer provides lower WVTR values. However, as of September 2024, only one publication about the properties of modules using EPE films [100] and no publications on long-term outdoor behaviour are available. Yang et al. reported excellent stability of the EPE film after exposure to different accelerated test conditions [100].

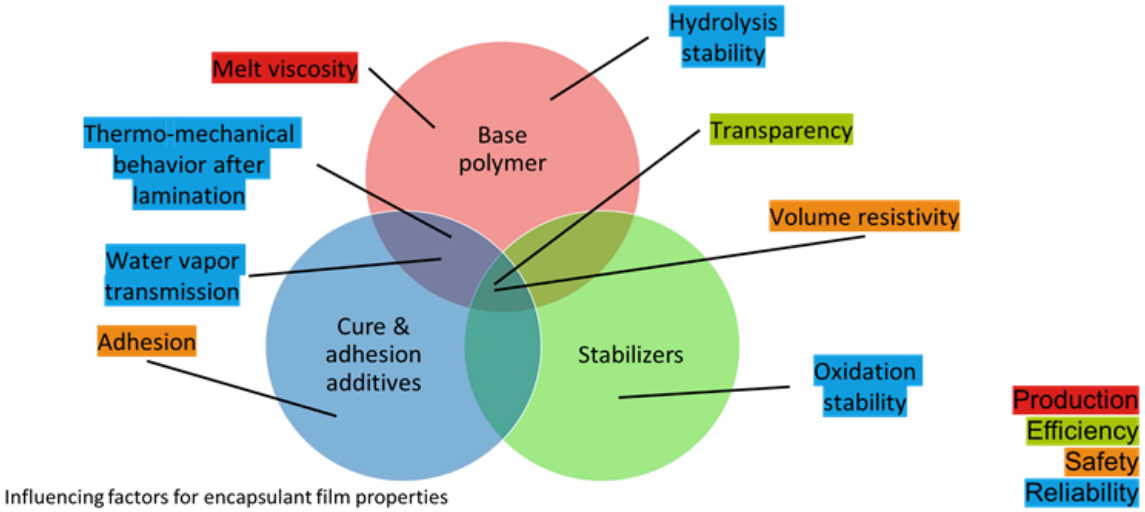

Figure 23: Influencing factors for encapsulant film properties [99].

Apart from the base polymers, it has to be emphasised that encapsulant additive formulation has a greater influence on durability than the type of polymer resin [56], [59], [83], [99], see Figure 23.

For PO encapsulants, the following new degradation modes have been reported:

- Reduced optical transmittance due to physical ageing: Exposure to elevated temperature leads to an increase of crystallinity of the polyethylene chain sections and consequently higher scattering of incident light [83]
- Interdiffusion of additives at front-encapsulant (UV transparent) - back-encapsulant (UV blocking) interface leads to ring patterns visible in UV fluorescence imaging [101]

With growing diversification in encapsulant and backsheet materials, material incompatibilities could also become a relevant issue [66], [102], e.g. encapsulant - backsheet delamination. Therefore, the materials must be tested both individually and in combination in the complete PV laminate in specific accelerated ageing tests (irradiation, temperature and humidity impact, isolated and combined). However, we are still lacking long-term outdoor experience with

polyolefin-based encapsulants. Most degradation and reliability studies including PE encapsulants were done based on accelerated ageing tests. As of September 2024, no cases of damage or failure of EPE-based PV modules following outdoor exposure have been reported.

2.5.7 Coloured components: degradation modes

For coloured PV modules white or black rear encapsulation or special backsheet films are required to achieve the requested colour effect. Furthermore, the ribbons might be blackened with ink or black tapes. Similarly to other additives, colourants and/or pigments can migrate within the polymer stack causing unwanted colour changes [103]. Although aesthetically unwanted, these effects have no impact on the electrical output. In a comparative study of white EVA back encapsulants, it was shown that there are stable and non-stable white EVA grades, depending on the type of white pigment [104].

To ensure that the materials used in the modules are stable and compatible with the adjacent layers, the manufacturer must carry out certain accelerated ageing tests. With tests suggested in chapter 4.1 of Task 13 report “Accelerated testing - combined stress vs. sequential stress testing methods and inclusion of specific load situations” [79], the decomposition and migration of pigmented lamination materials can be assessed. Although aesthetically unwanted, these effects have no impact on the electrical output.

2.5.8 Breakage of thin glass

In the year 2023, mainstream bifacial glass/glass PV modules have a glass thickness of 2 mm to 1.6 mm (thin glass). Up to 10% breakage rates are reported for recently built PV power plants with 2 mm glass/glass modules [105]. In a published case bifacial modules with 2 mm/2 mm glasses have been mounted on a rack and on a tracker mount system [106]. For 50% of the modules, the glass broke within 9 months of exposure. About 32% of the modules cracked on the rack and 57% on the tracker. This indicates that the mounting system has a clear influence, but it is not the only cause behind the glass breakage phenomenon. The modules cracked at a practically constant rate within the tested 9 months period. No special weather event or module internal failure (hot spots) could be identified as the root cause. In 59% of all cracked modules the rear-side glass broke. The front side cracked in 28% of all cases and in 13% both front and rear glass were broken. There are many confidential cases in the field involving 2 mm/2 mm bifacial modules with a similar characteristic and an unknown root cause. In many cases, the manufacturers have certified the sub construction for the use together with the modules. It is important to emphasise that by far most PV systems in the field with thin glass/glass modules are without conspicuous glass breakage.

The glass resistance against stress, impact and scratches depends on the preparation of the cutting edges and on the prestress of the glass surface. A high compressive stress at the glass surface protects the glass against opening of microcracks in the surface. The maximum compressive stress induced to thin glass surface with current glass tempering techniques is well below the producible compressive stress of 3 mm thick glass. Furthermore, there is no existing standardised technique to measure the compressive stress for thin glass (≤ 2 mm). Moreover, standardised breakage tests are not applicable for thin glass [107]. At the time of writing, there is no standardised way to check the delivered glass quality for thin glass for PV module applications. The lack of quality control may be the reason that glass breakage occurs more frequently in certain cases. Another reason may be the continuous increase of module size and gradual decrease in frame height, which both increase the stress in the glass [108].

Broken PV module glass is a catastrophic failure because it violates the mechanical and electrical safety of a PV module. Typically, the module power is not affected immediately after glass

breakage occurs. Isolation failure may be a first fault signal at the PV inverter. Very often the cracking of thin glass starts on the rear glass, so a visual inspection of the modules' rear side is required to detect the failure. Theoretically, internal arcing and fire may be a secondary failure after some time of outdoor exposure.

As the root cause of the glass cracking is not known yet, new measurement/testing techniques for characterising the compressive stress of the glass surface are needed. One attempt to measure this characteristic is to use a SCALP-05 [109]. This device couples a laser into the glass, where the present stress causes a rotation of the polarization plane. This, in turn, reduces the scattering intensity orthogonal to the initial polarization plane, which can be detected perpendicularly to the initial beam. As a result, the surface stress of the glass in the module compound can be measured. Figure 24 shows results of PV modules with different glass thicknesses, where significantly different glass surface stress levels are detected.

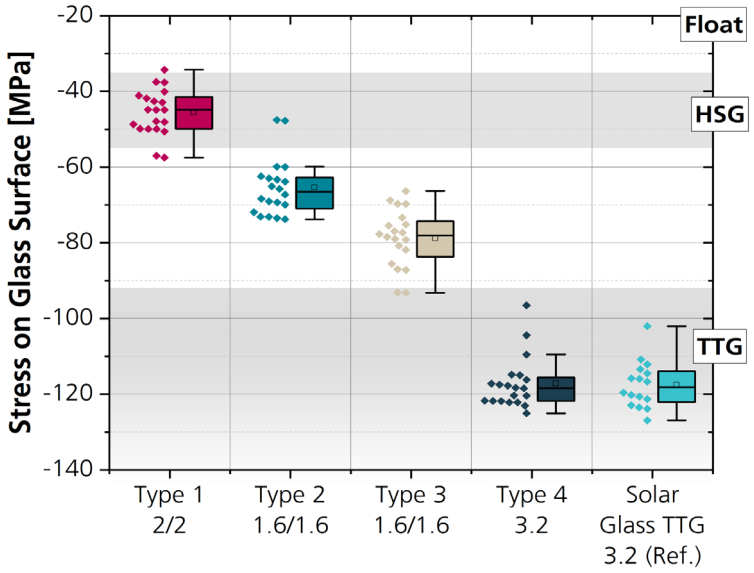

Figure 24: Results of SCALP measurements on the front glass of PV modules, revealing the surface stress [110]. The grey shaded areas characterise the typical compressive stress level for production methods of Heat Strengthened Glass (HSG) and Thermally Toughened safety Glass (TTG).

Since glass follows a Weibull distribution in its cracking behaviour, no specific threshold for its breaking resistance can be defined. As the cracking resistance for thin glass is typically much lower than 3 mm glass, the Weibull distribution moves to lower stresses. Therefore, the stress resistance of thinner glass must be known even more precisely, to withstand typical stress in PV applications.

Even though hail impact is not the cause of the cases discussed here, hail impacts show the challenge we face if thin glass is used in a PV module. The hail impact test on PV modules with 2 mm glass/glass and 3 mm glass/backsheet shows the mechanical resistance difference between these two module types. Kedir et al. measured the Weibull distribution of that two module types for a wide variety of hail kinetic energy [111]. They showed that, compared to a 3 mm glass/backsheet structure, modules with a 2 mm glass/glass structure experience 50% less kinetic impact energy from the ice balls at a 50% glass breakage probability. However, both structures perfectly survive hail impacts at the kinetic energy level required for IEC 61215-2:2021 MQT 17 hail test with 25 mm ice ball diameter [28].

As mentioned earlier, thin glass cannot be fully tempered like 3 mm thick glass. Therefore, the surface resistance against stress, impacts and scratches is much less than for fully tempered glass. The current mechanical load test MQT16 in IEC 61215 [28] focuses on frame deformation, cell breakage, and all other non-glass related features. Testing the breakage of brittle materials, such as glass, which is characterised by a probability of breakage, requires a larger number of samples. As we know from the field, the rear glass is most affected by the breakage. A mechanical pressure load is therefore effective for testing this failure. One current practical option to test the reliability of a thin glass-based module is to test about 20 modules of one type in the final mounting position to roughly estimate breakage rates down to 5%.

2.6 New material degradation modes specific to TOPCon and SHJ

According to industry experts and the 2024 International Technology Roadmap for Photovoltaics (ITRPV), in the next decade TOPCon on *n*-type wafers will grow from 29% to 53% market share, and *n*-type SHJs will grow from 5% to 19% [112]. TOPCon is expected to be the dominating cell technology after 2025 [112]. Cell design is evolving rapidly, driven by manufacturing needs such as reducing silver consumption, in addition to the need for higher device efficiency and lower LCOE. TOPCon and SHJ cell architectures are evolving rapidly with new cell designs being implemented and deployed in commercial PV modules in ~6-month time frames. Therefore, the small amount of field data from TOPCon and SHJ cells may not be necessarily representative for the modules currently or in the future being produced.

These advanced c-Si cell architectures mitigate the energy conversion losses present in traditional architectures. Both achieve higher V_{OC} by minimising contact recombination, without reducing the *FF* [113]. The introduction of new materials and processes introduces the potential for new failure modes. Furthermore, there are broad parameter spaces available for materials and designs that can affect both performance and long-term durability (e.g., the composition of the paste used in metallization for TOPCon and SHJ, the a-Si:H layer and transparent conductive oxid (TCO) in SHJs, the number and composition of passivation layers). Thus, there is significant variability within a device technology, both as the composition of the layers evolve towards improved efficiencies and as different manufacturers follow different paths towards optimization. While field studies of degradation are the gold standard for understanding longevity, the findings become less transferable when critical materials change practically every six months.

2.6.1 Degradation of the front metal contacts of TOPCon

Metal pastes featuring glass frit are used across cell architectures to contact the front side of PV cells, typically where the homojunction (i.e., emitter) is located. The glass frit enables the metal paste to etch through the dielectric passivation and the antireflection coating on the front side when fired at high temperatures. This approach is used for aluminium back surface field (Al-BSF), PERC, nPERT, and now for TOPCon cells. When these cells are encapsulated with EVA in the presence of moisture, the front metallization and cell-to-cell interconnects become susceptible to corrosion at the interface between the metal and the Si [114], [115], caused by acetic acid, a decomposition product of EVA [116]. This has been observed in modules installed in the field [117]–[119], encapsulated modules exposed to accelerated DH testing [120]–[123], and bare cells directly exposed to acetic acid [124], [125].

Recent reports have shown that TOPCon cells and modules can be even more susceptible to this type of metal corrosion than Al-BSF and PERC [125]–[128]. Evidence of this corrosion in the metal oxide glass frit has been observed in cross-sectional scanning electron microscopy (SEM) images of TOPCon cells exposed directly to acetic acid, as shown in Figure 25 [125].

In this study, TOPCon cells experienced a significantly higher increase in the contact resistivity over two hours of acetic acid exposure compared to the PERC and SHJ groups. DH testing on unencapsulated PERC, SHJ, and TOPCon cells exposed to sodium chloride resulted in TOPCon exhibiting the highest level of power loss [126]. A similar study featuring TOPCon cells with different pastes and a laser-assisted firing process used on some cells showed the corrosion sensitivity is likely related to a high aluminium content in the front paste [129]. Accelerated damp-heat testing on encapsulated TOPCon has also shown substantial power loss. Sen et al. evaluated seven combinations of encapsulation material and backsheet with TOPCon cells, as well as three combinations with PERC cells. After 1000 hours of DH test, they found that the maximum power loss in TOPCon modules varied significantly, ranging from $4\%_{rel}$ to $65\%_{rel}$, depending strongly on the encapsulation material. In contrast, PERC modules showed only a $1\%_{rel}$ to $2\%_{rel}$ power loss [128]. Sommeling and Kroon showed that the use of TPOs can mitigate power loss in 1000 h DH [127]. Unfortunately, there are limited reports on this form of degradation in field exposed TOPCon modules, because it has only recently been adopted in high-volume production.

a) Cross-sectional SEM

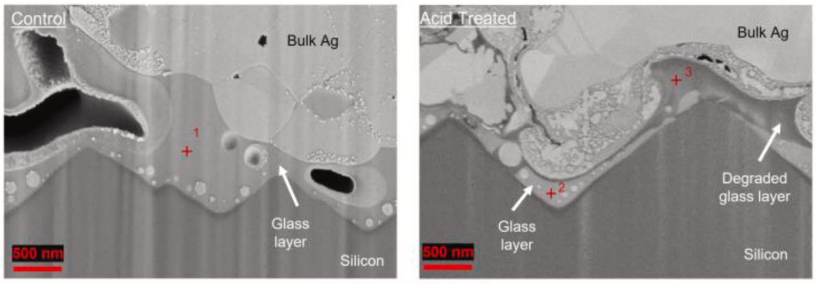

TOPCon G1 (Front)

b) EDS quantification

	TOPCon G1 (Front)		
	Control (Wt. %)	Acid Treated (Wt. %)	
Elements	P1	P2	P3
Ag	33.5	42.7	35.2
Si	24.9	28.2	38.4
O	9.7	7.7	17.8
C	2.8	2.7	3.6
Al	0.6	0.5	0.4
Pb	26.2	17.1	4.1
Zn	2.3	1.1	0.5

Figure 25: a) SEM cross-sectional images and b) quantification of the energy-dispersive X-ray spectroscopy for the front side of the control and acetic acid treated bifacial TOPCon metal paste contact interface to poly-Si emitter [125].

2.6.2 SHJ: ITO and a-Si:H degradation modes

The SHJ cell architecture limits contact recombination by decoupling the absorber from the metal contact, by including a passivating, carrier selective contact layer stack. This stack comprises an intrinsic a-Si:H layer to passivate dangling bonds at the *n*-type c-Si wafer surface, a doped a-Si:H layer provides carrier selectivity, and an appropriate TCO provides lateral transport and ensures good contact quality with the metal. Typically, ITO is used as TCO. It serves as an ARC and assists in light trapping at the cell's rear.

SHJ cells are sensitive to stressors such as moisture, heat, and irradiance, and the resulting degradation varies from manufacturer to manufacturer. A recent literature review [130] found average performance loss rates for SHJ modules of 0.83%/year. These values fall between the loss rates of c-Si and thin-film modules reported in 2016 [131].

A possible route of performance change specific to SHJ is the increase of ITO resistance or deterioration of the a-Si:H/ITO or ITO/contact interfaces. Jordan et al. found that increased ITO resistance has not been observed in fielded SHJ cells as compared to cells of a control module kept indoors [132]. In degradation studies of non-encapsulated SHJ solar cells, X-ray photoelectron spectroscopy (XPS) data of DH-exposed samples showed signatures of surface degradation of the ITO and the surface gridlines. However, there was no corresponding change in the device performance [133].

Another degradation mode related only to SHJ is studied by Arruti et al. [134]. Arruti et al. have shown that bifacial rear-emitter SHJ solar cells encapsulated in EVA in glass/glass laminates degraded in damp heat (DH) tests. However, DH tests with negative bias applied show a slightly accelerated degradation compared to no voltage applied, see Figure 26. The degradation of the cell under negative bias is shown in the EL images in Figure 27. Modules in positive bias voltage or positive bias voltage with periods of illumination [22] consistently exhibit no degradation during the DH test. The prerequisite for degradation is explained by molecular NaOH from the glass either diffusing through the EVA, which has absorbed moisture, or by Na^+ ions drifting due to the electric field when a negative bias is applied to the cell circuit. Furthermore, with positive bias applied to the cell circuit, apparently Na^+ ions are driven away from the cell and therefore no degradation is observed. In the study by Aruti et al., the sensitivity to migrating Na^+ seemed to be greater on cell fronts than on the rear side [134].

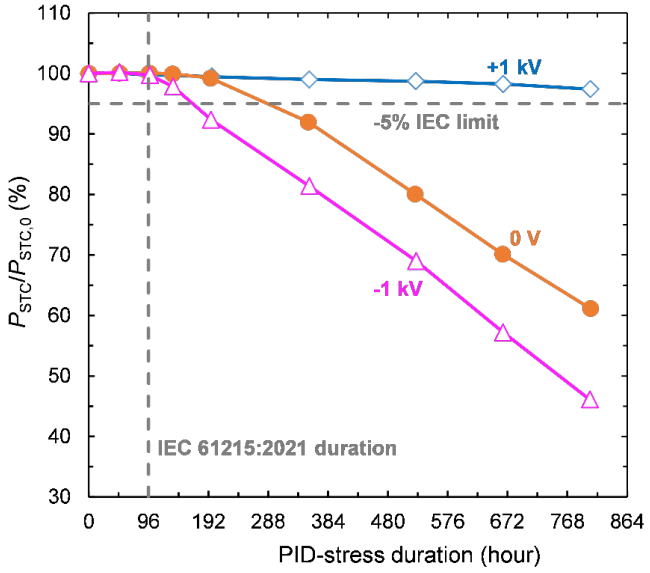

Figure 26: Normalised STC power to initial power of the front-side of SHJ 1-cell glass/glass laminates with EVA, after 800 h of PID testing at 85°C/85% RH for the bias conditions -1 kV, 0 V, and +1 kV. Figure is redrawn from Arruti et al. [134].

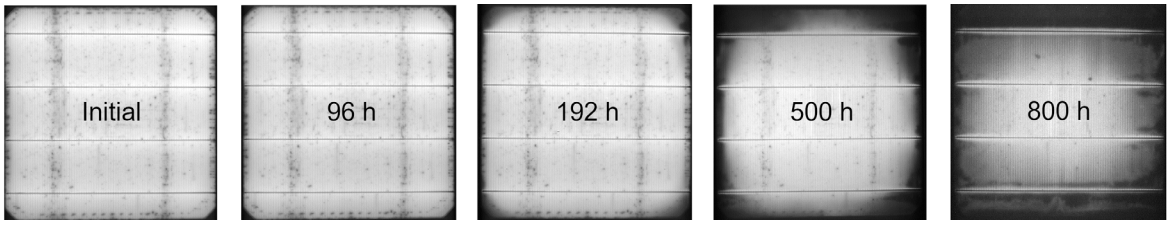

Figure 27: EL images of SHJ glass/glass mini-modules with EVA subjected to PID testing at 85°C, 85% RH and -1 kV bias for up to 800 h. EL images show that degradation starts at the edges of the cell, gradually expanding inward, associated with moisture ingress facilitating Na^+ transport [134].

The mechanisms of moisture damage are multifaceted, and have recently been explained by a corrosion mechanism, see Figure 28 [135]. The adoption of encapsulants with a relatively high water-uptake, such as EVA, favours a corrosion reaction of the glass cover(s) releasing Na^+ ions that, in combination with water, form molecular NaOH. Na^+ ions can diffuse through the grain boundaries of the indium tin oxide (ITO), reaching either the front or rear hydrogenated amorphous silicon (a-Si:H)/c-Si interface creating recombination centres for charge carriers, see Figure 29.

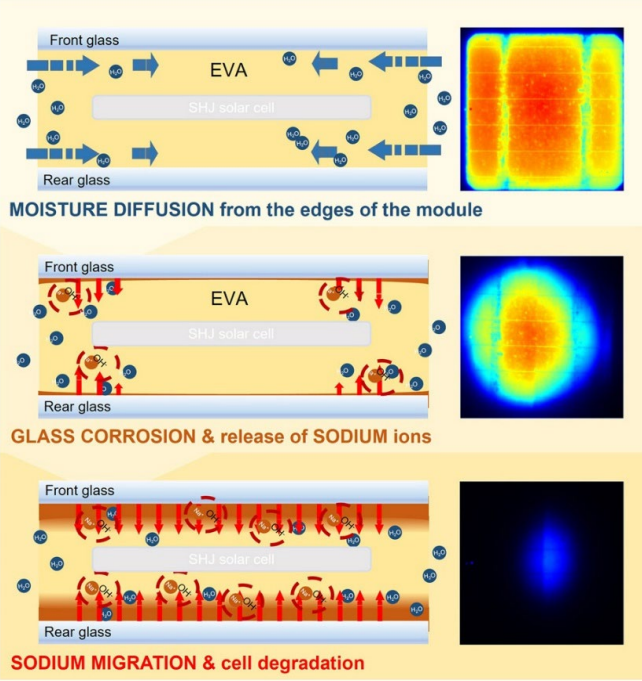

Figure 28: Left: physical model explaining the sensitivity of SHJ to water. The observed degradation mechanism is specific to the SHJ technology [135]. Right: Photoluminescence image of one SHJ cell glass/glass laminate taken at 0 h, 500 h and 1000 h of DH testing.

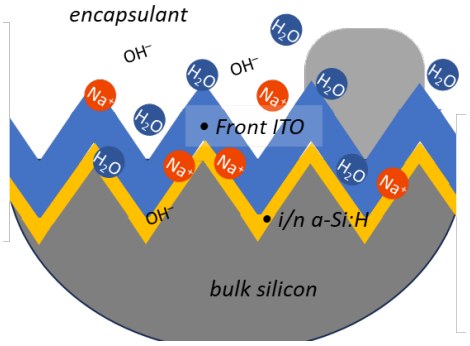

Figure 29: Schematic of the microscopic model proposed to explain the sensitivity to water of SHJ cells encapsulated in a glass/glass structure with EVA encapsulant. Na+ and OH- ions cross the ITO and degrade the passivation layer at the a-Si:H/bulk Si interface. Adapted from [135].

However, to our knowledge, there are no studies in which SHJ modules installed outdoors exhibit PID. The humidity levels of the 85°C/85% RH condition leads to an unnaturally high level of humidity in the module, entering from the module edges, as can be seen in Figure 27 and Figure 28. This accelerates Na^+ migration considerably.

In the past, EVA alternatives such as thermoplastic polyolefin (TPO), ionomer [31] and backsheets containing Al foil [136], which do not allow moisture to pass through as easily as EVA, have been used for SHJ modules manufactured by Sanyo [137]. Efforts are being made to reduce the costs by use of EVA and other module encapsulants [137]. These authors found

dual issues of degradation by Na^+ diffusing from the glass due to water content in 85°C and 85% RH DH and damage from acetic acid formation of the EVA. They found good success in glass/glass modules using POE in the front and rear of the cells and with POE on the front and EVA on the rear of the cells with glass/backsheet constructions. Presumably in the later configuration, the primary sensitivity to Na^+ is on the front side with these cells and the PID is mitigated by use of the lower moisture transmission of the POE and use of backsheet allows any acetic acid to diffuse out, thus mitigating acetic acid-based damage.

More recently, humidity induced degradation in SHJ was observed related to soldering flux and contamination introduced onto the cell prior to module fabrication [126], [138], [135]. These contaminations must be avoided during production.

The water-sensitivity and PID in SHJ modules can be mitigated at module level by using a high-volume resistivity encapsulant with a low WVTR and low water uptake (i.e., POE lamination material), appropriate edge sealants, proper rear and front covers, and/or the use of barrier layers (glass/glass, glass/aluminium foil) [139].

2.6.3 UV degradation of current c-Si cell structures

Modern TOPCon, HJT, PERT, and PERC solar cells frequently show high degradation rates in accelerated UV degradation tests [140], [18], [141].

Gebhardt et al. examined 14 different TOPCon types in UV tests showing severe power loss ranging from 0.5% to 8% with a median of 3% after 60 kWh/m² UV dose [18]. Shina conducted similar tests with 28 TOPCon and 2 SHJ module types and found a degradation range from 0% to 10% and for SHJ from 1% to 2.5% after applying also 60 kWh/m² UV dose [140]. Depending on the location, 60 kWh/m² UV dose corresponds to 1 to 2 years of outdoor exposure. Both authors applied short-circuit conditions to the PV modules during the UV test.

Gebhardt et al. demonstrated that the power degradation of TOPCon modules in accelerated UV tests and outdoor exposure is roughly halved when switching from short-circuit to open-circuit conditions. This was observed for a small number of indoor tested samples and for a single outdoor tested sample [18]. Sinha et al. found similar results for UV tests with short-circuit and open-circuit conditions of bare SHJ, n-PERT and p-PERC cells [142].

Dark storage strongly accelerates the degradation of TOPCon modules after UVID testing [18],[143]. Heat storage conditions (85°C) can partly or completely reverse the dark storage effect [18], [143].

The fundamental origin of the UVID are UV triggered changes in the passivation efficiency of the passivation stack/silicon interface [144], [142] or possibly a defect rich silicon surface for the PERC cell front side [143]. The deposition methods and the process parameters of the passivation layers have a great impact on the UV stability of the solar cells [141],[145]. Passivation layers which prevent the silicon wafer surface from UV radiation below 360 nm, like the rear passivation of TOPCon cells, by a UV blocking polysilicon layer, can be very UV stable. No detailed outdoor studies on UVID are available for TOPCon modules. SHJ specific UV degradation shows a reduction of V_{OC} over time. It is attributed to a partial loss of the front passivating layers properties by UV irradiation. This problem was historically solved by moving from front to rear-emitter SHJ solar cells. Jordan et al. compared the degradation of fielded SHJ and PERC modules. While the observed degradation rates of the SHJ modules (-0.51%/a) [144] are on par with conventional Si cell-technologies (-0.69% to -0.91%), the loss mechanisms differ [146], [147]. PERC and Al-BSF cells primarily show performance losses due to a reduction of I_{SC}, whereas SHJ devices also experienced reductions in *FF*, but the degradation was dominated by voltage loss. The loss was correlated with an increase in midgap trap

densities near the c-Si/a-Si:H interface due to weathering-related defects. This results in an increased recombination current towards the interface between the bulk Si wafer and the junction-forming a-Si:H passivation layers. Sinha et al. compared the effect of UV exposure on the performance of different non-encapsulated silicon architectures. Overall, they found that degradation was more pronounced in emerging cell technologies, including SHJ devices, compared to classic Al-BSF devices [142]. The authors concluded that the damage to the SHJ cells originates from hydrogen effusion near the surface, followed by its migration into the bulk Si, leading to increased recombination current loss. Furthermore, Bertoni's work [148], [149] with surface recombination velocity measurements of c-Si/a-Si:H stacks supports the degradation of the surface passivation layer as a root cause of the observed loss performance over time.

Even if the root causes differ for all cell types and passivation stacks, the main UVID accelerating factor is the amount of UV photons reaching the passivation layer/silicon interface. Any means of reducing this amount, like UV reflecting ARC, UV-absorbing glass, lamination material, or passivation layer can mitigate the UVID impact [142].

As the operating point in a PV generator is the maximum power point and not the short-circuit conditions as used in the UV tests, the field degradation rate may be lower than the UV dose in the accelerated aging test suggests. Light soaking may recover UVID for HJT modules [150]. The strong dark storage degradation reported after UVID tests of TOPCon modules may accelerate the field degradation during nighttime. However, the reported UVID tests also show that there are some UV stable TOPCon and HJT modules on the market. We can expect manufacturers to mitigate the high UVID rates found in standard UV tests.

UVID testing can induce LeTID/LID effects in addition to chemical changes at the irradiated semiconductor layers and interfaces of a solar cell. To separate both effects, it is important to keep the cell and module temperature below 60°C during UV degradation tests [151]. Additionally, a light soaking procedure IEC 61215 MQT 01 and a LeTID test IEC 61215 MQT 23 should be done before UVID testing. So far, we recommend an extended UV degradation test for PV modules with 60 kWh/m² UV irradiation dose under short-circuit conditions to assess the module quality between different module products.

3 PEROVSKITE-BASED FUTURE TECHNOLOGIES

Metal halide perovskite PV cells have attracted considerable research and development interest as an alternative to c-Si PV absorber material and as an addition to c-Si in tandem structures. This excitement is due to their meteoric rise in record cell efficiencies [152] since their discovery in 2009 [153], their potential for very low production costs, and their bandgap tunability [154]. While record efficiencies have reached parity with c-Si, the ability of perovskite solar cells (PSCs) and in particular larger area modules to survive outdoor operating conditions is still uncertain with a wide variability in reported lifetimes for laboratory samples. This chapter provides a summary of degradation mechanisms of MHP-based PV cells and modules and their mitigation based on the work of Baumann et al. [155].

There are several known degradation modes for MHP PV cells and modules. These include **intrinsic** (pertaining to material properties), **cell-device-specific** (pertaining to device design and manufacturing), **extrinsic** (pertaining to environmental stressors), and **module-device-specific** (pertaining to the interconnection of cells into modules and embedment). In the following sections, we introduce degradation models for each type and highlight mitigation strategies that are under investigation.

3.1 Intrinsic degradation causes

Phase instability and impurity – The perovskite structure of typical MHP PV has a cubic unit cell with a molecular formula of ABX_3, where A is either an organic molecule (e.g., Formamidinium (FA)), or an inorganic element (e.g., Cs) or a mixture of both; B is a metal (Pb or Sn), and X is a halide (Cl, Br, or I). If any of the A, B, or X components has an effective ionic radius that is too large or too small compared to the other constituents, the cubic structure cannot form, due to physical space constraints, leading to the formation of undesired phases. In addition, the stability of the structure can change with temperature leading to phase instability during operation. For example, both $FAPbI_3$ and $CsPbI_3$ are not stable in the cubic phase at typical operating temperatures (-45°C to 85°C). However, a common practice to mitigate phase instability is to alloy these two constituents to create a stable cubic formulation over a range of operating temperatures. Phase instability can also be caused by leftover MHP precursor and phase impurities. MHP layers are typically deposited as liquid inks and then annealed to create solid thin films. A common instability occurs when the mixing and solubility of the MHP ink is not optimal or the ink has degraded. PbI_2 can photolyze under illumination where it absorbs light, i.e. blue or UV light, breaking down into I_2 and metallic Pb among other by-products [156]–[159]. This can lead to phase segregation and degradation at nucleation sites. Mitigation options include optimization of composition, stoichiometry [158], [160], and processing to, for example, minimise PbI_2 residues or, if possible, to avoid them completely. Post-treatments to remove unwanted phases may also be possible.

Phase segregation (cation/halide) – Mixed cation/mixed halide MHP compositions are favoured for high efficiency and a band gap ideally suited for MHP/Si tandem cells. Such alloyed compositions may be energetically prone to de-mixing, leading to the formation of non-cubic phases or even the coexistence of different phases simultaneously. To test if a given composition will phase-segregate under operating conditions, crystallographic studies as a function of time under realistic conditions are needed. Using a spatial/structural analysis technique, such as nano-XRD or time-of-flight secondary ion mass spectroscopy (ToF-SIMS), can detect the scale, morphology, and composition of segregated phases [161]. To prevent phase segregation energetic calculations should be carried out on a given composition to determine which are more or less likely to de-mix. Segregation can be suppressed by keeping Br <20% in the

case of halide segregation, reducing defect densities, growing single crystal MHPs [162], [163], and adding Cs^+, Rb^+, or K^+ in the case of cation segregation [164].

Ion Migration - MHP materials are mixed electronic/ionic conductors with a low activation energy for the formation of mobile ions [165], [166]. Mobile ion concentrations in MHP are several orders of magnitude higher than in conventional semiconductors (Si, CdTe, III-V) and this can lead to *IV* hysteresis [167], [168], photoinduced low-frequency capacitance [169], photoluminescent quantum yield changes, halide segregation, and various other irreversible degradation modes [170], [171]. When exposed to light, a PV device generates an electric field that can move (drift) ions. At night, these ions can move according to concentration gradients. To mitigate ion migration, researchers are investigating a variety of solutions [172], including compositional engineering (e.g., adding large A site cations [173], [174]), 2D and 1D MHPs [175], [176], increasing grain size and modifying grain boundaries [177], [178], additives (e.g., ionic fluids [179], polymers [180], potassium salts [181], [182]), passivation, and blocking layers (e.g., diethylammonium formate (DMAFo), thermotropic liquid crystals like 3,4,5- trifluoro-4'-(trans-4-propylcyclohexyl)biphenyl, $CsPbI_{1.85}Br_{1.15}$ quantum dots, tri-s-triazine-based graphitic carbon nitride).

Thermal Degradation - When exposed to high temperatures, MHP PV absorbers decompose into gaseous carbon and nitrogen compounds and solid PbI_2, depending on composition and temperature. In order for MHP PV modules to be commercialised, they must be able withstand temperatures at least up to ~85°C, over a complete diurnal (light/dark) cycle [6]. Mitigation strategies include reducing ion migration with blocking layers, thermotropic liquid crystals [183] or quantum dots [184], adding thermally conductive materials to remove heat, and/or avoiding extreme climates.

Mechanical Degradation - MHP PV materials are very weak/soft, resulting in possible damage during fabrication (soldering, finger screen printing, lamination) and operation. 2D MHPs are even weaker than 3D [185]. Mitigation strategies include material selection and, in the case of 2D MHPs, engineering to increase the strength of the MHP layer, increasing the number of inorganic layers, and adding a strong insulating layer between the electrode and the interconnector [186].

3.2 Cell-device-specific degradation modes

Charge transport and passivation layer reactions - Charge transport layers (CTLs) should remain connected to the MHP layer and be stable under operational conditions. Instability can be caused by both chemical and mechanical processes and has proven to be a particularly significant challenge for MHP devices. Most of the materials used for CTLs have stability issues when exposed to light and UV radiation [187]–[190]. Mitigation options include choosing an intrinsically stable inorganic material such as metal oxides [191] or sulphides [192], minimising CTL reactivity with MHP by choosing a CTL that is neither acidic nor basic, and also screening for light + heat sensitivity in the final device.

Electrode-induced degradation – Strong chemical gradients across the interfaces of electrode, CTL and MHP materials drive reactions and ion migration that negatively impact performance and stability [193]. Most metals chosen as electrodes for PSCs react with the MHP [157], [170], [194]. To mitigate these reactions, electrode interlayers made of Ti [195] or metal oxides (e.g., ZnO [196], Cr-Cr_2O_3 [197], g-C_3N_4 [198], MoO_x [199], [200]) are proposed. Despite advances, electrode-induced degradation remains a major challenge. One approach is to replace the metal with either carbon as the electrode [201]–[203] or transparent conducting oxides [204], [205]. However, to date, devices with non-metallic electrodes exhibit high resistive losses and lower efficiencies.

Degradation related to scribe processing – Scribing is used to separate and interconnect individual cells into modules. Ultrafast pulse width laser scribing is favoured, as it does not transfer high heat loads to the material [206], [207], which can cause melting. However, faster picosecond lasers remove material via a mechanical stress-assisted lift-off mechanism resulting in steep edges and less residue, but may lead to microcracks and delamination [208]–[210]. Studies have shown that the edges of laser scribes decompose to PbI_2, forming a type-I heterojunction with surrounding MHP [211]–[213]. Using carbon-based electrodes [214] or TCOs [215], [216] may be a mitigation method. Alternatively, adding a diffusion barrier inside laser scribe line P2 (e.g., Al_2O_3, nanoparticles, polydimethylsiloxane (PDMS), carbon nitride [198], or CTL [217]) to separate the MHP and electrode is being considered.

Strain induced by differences in CTE – The variety of materials used in MHP cells and modules have a range of different CTEs and therefore, when the MHP layer is annealed at ~100°C and then cooled, the film is in a state of elevated stress. Encapsulation can also introduce stress in the cooled modules. Mitigations include replacing thermal annealing with longer processing steps at lower temperatures [218], but adding processing time may not be feasible in commercial production lines. Other authors have suggested additives to reduce tensile stress including octylammonium iodide (OAI) and phenethylammonium iodide (PEAI) [219].

3.3 Extrinsic degradation causes

Reactions with water vapour and oxygen – MHP layers are generally hydrophilic and degrade in the presence of water as the organic cations oxidise [220]. The degradation mechanisms related to oxygen are not fully understood but are enhanced by exposure to light, especially organic components in the MHP and CTL layers [221]–[224]. Mitigation strategies include encapsulation and the embedding of glass-glass modules to prevent water and O_2 from coming into contact with the device. The addition of lower dimensional MHP layers between the absorber and ETL [225], and other additives (e.g., TFPCBP [226]) can help reduce the effect of moisture. Some of the solutions for intrinsic degradation modes related to ion mobility are likely to help with the effects of water and O_2 reactivity.

Reverse voltage – MHPs are very sensitive to and can degrade by even low levels of reverse voltage (< -5 V), which causes band bending and ion crowding near the MHP-CTL interfaces [227], [228] and possibly leading to the oxidation of iodide [228]. Local shunts can form, especially when metal electrodes are used [227], [229], which can lead to local heating and further damage to the cell [230], [231]. Options for mitigating the bias sensitivity and degradation include using non-metal electrodes [231], blocking layers [232], TCO between HTL and metal electrodes [233], polymer HTLs [234]. Despite showing some improvements, none of the potential solutions have been shown to prevent damage to the cell from reverse bias conditions, yet.

3.4 Module-device-specific degradation modes

Module layout and embedment – MHP modules perform best if water and O_2 are not allowed to react with the layers of the device stack. In addition to glass-glass module designs, PO-based encapsulants are recommended rather than EVA, which requires higher lamination temperatures [235] and can produce acetic acid [236]–[238]. POEs also have lower WVTRs.

Potential-induced degradation – In string-connected modules, high PV system voltages (up to ± 1500 V, can build up between grounded module frames and solar cells under operation [239]. Several PID tests are performed on PSCs and MHP/Si tandem solar cells/minimodules, showing no degradation at positive voltages but much more pronounced degradation at

negative voltages and also at higher temperatures due to movement of Na^+ ions from the glass into the MHP layer, causing recombination centres [240]–[242]. Other ion movements are observed such as Pb^+, Cs^+, Br^- and I^- towards the encapsulant materials and Ag^+ ions from the back contact leading to the formation of AgI. The PID degradation can be mitigated by optimising the fabrication and deposition of MHP layers, resulting in low defect densities (i.e. I-rich synthesis conditions), using MHP compositions with high defect tolerance [243] and adding either additional barrier layer (e.g. PCBM between SnO_2 (HTL) and MHP) [244] or inert materials that occupy interstitials in the MHP structure to inhibit Na^+ penetration [240]. Other mitigation strategies could be used such as inducing recovery of MHP by applying positive bias during the night to drive Na^+ ions out of the active layer [245] or using suitable encapsulation material [241].

Testing and qualification - Accelerated indoor tests reproduce the standard 20 years of outdoor functioning in much shorter times, enabling reliable predictive analysis. The IEC 61215 series 2021 standards [6], [246]–[248] are developed to assess the reliability of PV modules. They contain accelerated ageing protocols, including climatic (e.g. DH, TC, HF, …), mechanical (e.g. mechanical loads and hail impact), and electrical (e.g. PID, wet and dry insulation) tests in addition to electrical and mechanical safety requirements as addressed in the IEC 61730:2023 [249]. Other tests can be tailored to cope with some technology specificities such as the International Summit on Organic PV stability protocols, as in the case of MHPs. Compliance with these standards is generally considered a minimum quality requirement and should be considered a prerequisite for MHP module commercialization.

4 CONCLUSION

It is recommended to review published reports on PV failures observed for the type of cell/module technologies being used in a PV project. In order to reduce the number of failures in large PV systems, the impact of the corresponding degradation modes should be verified by accelerated testing prior to their installation. For 2024, the main cell related degradation modes are PID, UVID, and humidity related corrosion for SHJ and TOPCon modules.

From the perspective of the module design glass breakage failure for bifacial glass/glass modules with thin glass got a high relevance in the field. The more power is achieved per module and in the module string, the more important the safety measures become, as the consequences of an imperfectly connected BPD can lead to a fire much more easily than before.

All these degradation/failure causes are known from former failure reports. However, due to new methods for passivation layer, metallization and thin glass, the reliability of the modules has to be reoptimized for these new manufacturing processes. Some of the reported degradation issues may already been solved from PV module manufacturers by the time this report is published. The most important standard IEC 61215 [6] does not cover the UVID, because the UV test included in the standard is too short and may not take recovery effects into account. Similarly, for PID effects in SHJ PV module types, it is still not clear how the PID test represents relevant conditions in the field, as the influence of recovery conditions in the application has not yet been tested. More research is needed to adapt the UVID and PID tests. For the humidity related corrosion of TOPCon and SHJ the main root cause (TOPCon: degradation of the front metal contacts, SHJ: Na related degradation of the a-Si-layer) is known. By optimizing the high-volume resistivity encapsulant with a low WVTR and low water uptake, the degradation speed can be mitigated. However, the relevance in the field is unknown and needs more research. Furthermore, glass breakage rates cannot be detected within the IEC 61215 mechanical load test, because for a brittle glass material much more than one test sample is needed to detect a failure rate of 10% and below. In particular when optimising the glass thickness closer to the application load, the according test must be much more precise. Therefore, we need extended standard tests for these types of failures for the current PV technologies, which is ongoing work.

Process instabilities that lead to unreliable cold solder joints in junction boxes must be monitored as an integral part of production control. As the correct function of the BPDs is very important for safety, we recommend checking the BPD function during the module production and performing a module string wise diode test during the construction phase of the PV system. If there are indications of probable cold solder joints in some of the junction boxes, the whole PV system should be checked for cold solder joints in the junction boxes. The risk of a fire within the service life of the PV system is high in this scenario.

On a positive note LeTID and cell crack degradation are still a possible degradation mode but their relevance practically vanished in the new PV module types based on TOPCon and SHJ cells, as well as multi-wire connection technology. As LeTID is reduced using thinner and thinner wafers, the effect may vanish even further as the wafer thickness continues to decrease with new technology steps. Glass/glass encapsulation is becoming increasingly popular. This trend can support humidity sensitive cell technologies like TOPCon which are less affected by humidity than in glass/backsheet BOMs. Thus, the shift to glass/glass modules protects cell technologies which are less moisture resistive. Furthermore, the chemical interaction and material variety are also reduced in glass/glass module designs compared to glass/backsheet modules.

For future PV technologies based on MHP-containing cells and modules, we relied only on published literature data to support our findings. Reliability data from commercial products were not available to the authors of this report. In the literature, nearly all types of degradation mechanisms, and therefore all kinds of tests are highly relevant. Ion migration is a dominant characteristic involved in many published degradation modes, such as chemical interface reactions, phase changes, reverse voltage instability, PID, and metastability of the electrical characteristic, such as IV curve hysteresis. In this way, mitigating ion migration in MHP containing solar cells might be a way to solve many degradation pathways at once.

Today's silicon-based module designs must withstand high absorber temperatures above 150°C and more during partial shading. Many researchers wrongly assume that MHP absorbers/solar cells only need to be stable up to 85°C. In fact, the number of cells per BPD, the reverse voltage characteristic of the cells and the cell efficiency determine the maximum cell temperature in the application profile. We would need new (and expensive) module designs allowing this low application temperature of 85°C in reality. Some types of degradation mechanisms for MHP solar cells, such as PID and hot spot tests, have not yet been tested for realistic scenarios in the literature. We recommend not losing focus on the corresponding tests for MHP-containing solar cells and modules. For commercial products, all known degradation pathways must be mitigated simultaneously, as all degradation pathways have a major impact on MHP-based PV modules.

REFERENCES

[1] M. Köntges *et al.*, “Review of Failures of Photovoltaic Modules,” Report IEA-PVPS T13-01:2014, 2014. [Online]. Available: http://iea-pvps.org/index.php?id=275 [Accessed 18-Sep-2014]

[2] M. Köntges *et al.*, “Assessment of Photovoltaic Module Failures in the Field,” IEA PVPS, 2017. [Online]. Available: http://www.iea-pvps.org/index.php?id=435

[3] M. Herz, G. Friesen, U. Jahn, M. Köntges, S. Lindig, and D. Moser, *Quantification of Technical Risks in PV Power Systems 2021, IEA-PVPS T13-23:2021*. IEA PVPS, 2021. [Online]. Available: https://iea-pvps.org/wp-content/uploads/2021/11/Report-IEA–PVPS-T13-23_2021-Quantification-of-Technical-Risks-in-PV-Power-Systems_final.pdf

[4] D. C. Jordan, T. J. Silverman, J. H. Wohlgemuth, S. R. Kurtz, and K. T. VanSant, “Photovoltaic failure and degradation modes,” *Prog. Photovoltaics Res. Appl.*, vol. 25, no. 4, pp. 318–326, Apr. 2017, doi: 10.1002/pip.2866.

[5] G. Friesen *et al.*, “Photovoltaic Failure Fact Sheets (PVFS),” Report IEA-PVPS T13-30:2024, 2025. [Online]. Available: https://iea-pvps.org/publications/?year_p=&task=67&order=DESC&keyword=&cpt=keytopics&keytopic=

[6] *Terrestrial photovoltaic (PV) modules - Design qualification and type approval, IEC 61215-Series-2021*. 2021.

[7] S. Hwang and Y. Kang, “Reliability study on the half-cutting PERC solar cell and module,” *Energy Reports*, vol. 10, pp. 678–685, 2023, doi: 10.1016/j.egyr.2023.07.023.

[8] F. Kaule, M. Pander, M. Turek, M. Grimm, E. Hofmueller, and S. Schoenfelder, “Mechanical damage of half-cell cutting technologies in solar cells and module laminates,” *AIP Conf. Proc.*, vol. 1999, no. February 2022, 2018, doi: 10.1063/1.5049252.

[9] F. Fertig, K. Krauß, and S. Rein, “Light-induced degradation of PECVD aluminium oxide passivated silicon solar cells,” *Phys. status solidi - Rapid Res. Lett.*, vol. 9, no. 1, pp. 41–46, Jan. 2015, doi: 10.1002/pssr.201409424.

[10] D. Chen *et al.*, “Investigating the degradation behaviours of n+-doped Poly-Si passivation layers: An outlook on long-term stability and accelerated recovery,” *Sol. Energy Mater. Sol. Cells*, vol. 236, no. May 2021, p. 111491, 2022, doi: 10.1016/j.solmat.2021.111491.

[11] D. Macdonald and L. J. Geerligs, “Recombination activity of interstitial iron and other transition metal point defects in p- and n-type crystalline silicon,” *Appl. Phys. Lett.*, vol. 85, no. 18, pp. 4061–4063, Nov. 2004, doi: 10.1063/1.1812833.

[12] J. Karas *et al.*, “Results from an international interlaboratory study on light- and elevated temperature-induced degradation in solar modules,” *Prog. Photovoltaics Res. Appl.*, vol. 30, no. 11, pp. 1255–1269, Nov. 2022, doi: 10.1002/pip.3573.

[13] D. Chen *et al.*, “Progress in the understanding of light- and elevated temperature-induced degradation in silicon solar cells: A review,” *Prog. Photovoltaics Res. Appl.*, vol. 29, no. 11, pp. 1180–1201, Nov. 2021, doi: 10.1002/pip.3362.

[14] R. Eberle, W. Kwapil, F. Schindler, M. C. Schubert, and S. W. Glunz, “Impact of the firing temperature profile on light induced degradation of multicrystalline silicon,” *Phys.*

status solidi – Rapid Res. Lett., vol. 10, no. 12, pp. 861–865, Dec. 2016, doi: 10.1002/pssr.201600272.

[15] C. E. Chan *et al.*, “Rapid Stabilization of High-Performance Multicrystalline P-type Silicon PERC Cells,” *IEEE J. Photovoltaics*, vol. 6, no. 6, pp. 1473–1479, Nov. 2016, doi: 10.1109/JPHOTOV.2016.2606704.

[16] D. Bredemeier, D. C. Walter, and J. Schmidt, “Possible Candidates for Impurities in mc-Si Wafers Responsible for Light-Induced Lifetime Degradation and Regeneration,” *Sol. RRL*, vol. 2, no. 1, Jan. 2018, doi: 10.1002/solr.201700159.

[17] F. T. Thome, C. Yilmaz, W. Kwapil, F. Schindler, and M. C. Schubert, “Why is gallium-doped silicon (sometimes) stable? Kinetics of light and elevated temperature induced degradation,” *Sol. Energy Mater. Sol. Cells*, vol. 275, p. 112986, Sep. 2024, doi: 10.1016/j.solmat.2024.112986.

[18] P. Gebhardt, U. Kräling, E. Fokuhl, I. Haedrich, and D. Philipp, “Reliability of Commercial TOPCon PV Modules - An Extensive Comparative Study,” *Prog. Photovoltaics Res. Appl.*, 2024, doi: 10.24406/publica-3553.

[19] C. Molto *et al.*, “Review of Potential-Induced Degradation in Bifacial Photovoltaic Modules,” *Energy Technol.*, vol. 11, no. 4, Apr. 2023, doi: 10.1002/ente.202200943.

[20] W. Luo *et al.*, “Elucidating potential-induced degradation in bifacial PERC silicon photovoltaic modules,” *Prog. Photovoltaics Res. Appl.*, vol. 26, no. 10, pp. 859–867, Oct. 2018, doi: 10.1002/pip.3028.

[21] K. Sporleder, V. Naumann, J. Bauer, D. Hevisov, M. Turek, and C. Hagendorf, “Time-Resolved Investigation of Transient Field Effect Passivation States during Potential-Induced Degradation and Recovery of Bifacial Silicon Solar Cells,” *Sol. RRL*, vol. 5, no. 7, Jul. 2021, doi: 10.1002/solr.202100140.

[22] P. Hacke *et al.*, “Evaluation of bifacial module technologies with combined-accelerated stress testing,” *Prog. Photovoltaics Res. Appl.*, vol. 31, no. 12, pp. 1270–1284, Dec. 2023, doi: 10.1002/pip.3636.

[23] P. Hacke *et al.*, “Polarization-Type Potential-Induced Degradation in Bifacial PERC Modules in the Field,” in *Proc. 41st EUPVSEC, in Press*, Vienna, Austria: WIP, 2024.

[24] T. Pu, H. Shen, K. H. Neoh, F. Ye, and Q. Tang, “Reduced power degradation in bifacial PERC modules by a rear silicon oxide additive layer,” *Int. J. Energy Res.*, vol. 45, no. 6, pp. 8659–8665, May 2021, doi: 10.1002/er.6402.

[25] P. Hacke, S. Spataru, B. Habersberger, and Y. Chen, “Field-representative evaluation of PID-polarization in TOPCon PV modules by accelerated stress testing,” *Prog. Photovoltaics Res. Appl.*, vol. 32, no. 5, pp. 346–355, May 2024, doi: 10.1002/pip.3774.

[26] *Photovoltaic (PV) modules - Test methods for the detection of potential-induced degradation - Part 1: Crystalline silicon, IEC 62804-1-2015*. VDE, 2015.

[27] *Photovoltaic (PV) modules - Test methods for the detection of potential-induced degradation - Part 1: Crystalline silicon, IEC 62804-1-2025*. VDE, 2025.

[28] *Terrestrial photovoltaic (PV) modules - Design qualification and type approval - Part 2: Test procedures, IEC 61215-2-2021*. 2021.

[29] W. Luo *et al.*, “Investigation of polysilicon passivated contact’s resilience to potential-induced degradation,” *Sol. Energy Mater. Sol. Cells*, vol. 195, pp. 168–173, Jun. 2019, doi: 10.1016/j.solmat.2019.02.038.

[30] W. Luo *et al.*, “Investigation of Potential-Induced Degradation in Bifacial n-PERL Modules,” *IEEE J. Photovoltaics*, vol. 10, no. 4, pp. 935–939, Jul. 2020, doi: 10.1109/JPHOTOV.2020.2981841.

[31] S. Yamaguchi, K. Nakamura, A. Masuda, and K. Ohdaira, “Rapid progression and subsequent saturation of polarization-type potential-induced degradation of n-type front-emitter crystalline-silicon photovoltaic modules,” *Jpn. J. Appl. Phys.*, vol. 57, no. 12, p. 122301, Dec. 2018, doi: 10.7567/JJAP.57.122301.

[32] B. M. Habersberger and P. Hacke, “Impact of illumination and encapsulant resistivity on polarization-type potential-induced degradation on n-PERT cells,” *Prog. Photovoltaics Res. Appl.*, vol. 30, no. 5, pp. 455–463, May 2022, doi: 10.1002/pip.3505.

[33] K. Ohdaira, M. Akitomi, Y. Chiba, and A. Masuda, “Potential-induced degradation of n-type front-emitter crystalline silicon photovoltaic modules — Comparison between indoor and outdoor test results,” *Sol. Energy Mater. Sol. Cells*, vol. 249, p. 112038, Jan. 2023, doi: 10.1016/j.solmat.2022.112038.

[34] K. A. Kim and P. T. Krein, “Photovoltaic hot spot analysis for cells with various reverse-bias characteristics through electrical and thermal simulation,” in *2013 IEEE 14th Workshop on Control and Modeling for Power Electronics (COMPEL)*, IEEE, Jun. 2013, pp. 1–8. doi: 10.1109/COMPEL.2013.6626399.

[35] R. Witteck, M. Siebert, S. Blankemeyer, H. Schulte-Huxel, and M. Köntges, “Three Bypass Diodes Architecture at the Limit,” *IEEE J. Photovoltaics*, vol. 10, no. 6, pp. 1828–1838, Nov. 2020, doi: 10.1109/jphotov.2020.3021348.

[36] C. Reichel *et al.*, “Design aspects in consideration of hotspot phenomena in high-performance photovoltaic modules featuring different silicon solar cell architectures,” *Sol. Energy Mater. Sol. Cells*, vol. 276, no. July, p. 113058, 2024, doi: 10.1016/j.solmat.2024.113058.

[37] Y. Jia *et al.*, “Diagnosing breakdown mechanisms in monocrystalline silicon solar cells via electroluminescence imaging,” *Sol. Energy*, vol. 225, pp. 463–470, Sep. 2021, doi: 10.1016/j.solener.2021.07.052.

[38] D. C. Jordan, T. J. Silverman, J. H. Wohlgemuth, S. R. Kurtz, and K. T. VanSant, “Photovoltaic failure and degradation modes,” *Prog. Photovoltaics Res. Appl.*, vol. 25, no. 4, pp. 318–326, Jan. 2017, doi: 10.1002/pip.2866.

[39] M. C. A. García, W. Herrmann, W. Böhmer, and B. Proisy, “Thermal and electrical effects caused by outdoor hot-spot testing in associations of photovoltaic cells,” *Prog. Photovoltaics Res. Appl.*, vol. 11, no. 5, pp. 293–307, 2003, doi: https://doi.org/10.1002/pip.490.

[40] K. A. Kim and P. T. Krein, “Hot spotting and second breakdown effects on reverse I-V characteristics for mono-crystalline Si Photovoltaics,” in *2013 IEEE Energy Conversion Congress and Exposition*, IEEE, Sep. 2013, pp. 1007–1014. doi: 10.1109/ECCE.2013.6646813.

[41] J. Appelbaum, A. Chait, and D. Thompson, “Parameter estimation and screening of solar cells,” *Prog. Photovoltaics Res. Appl.*, vol. 1, no. 2, pp. 93–106, Feb. 1993, doi: 10.1002/pip.4670010202.

[42] J. Hudson, L. Vasilyev, J. Schmidt, and G. Horner, “Economic impacts and approaches to address hot-spot defects in photovoltaic devices,” in *2010 35th IEEE Photovoltaic Specialists Conference*, IEEE, Jun. 2010, pp. 001706–001709. doi: 10.1109/PVSC.2010.5616102.

[43] R. G. Vieira, F. M. U. de Araújo, M. Dhimish, and M. I. S. Guerra, “A comprehensive review on bypass diode application on photovoltaic modules,” *Energies*, vol. 13, no. 10, p. 2472, 2020, doi: 10.3390/en13102472.

[44] H. Hanifi, J. Schneider, and J. Bagdahn, “Reduced shading effect on half-cell modules – Measurement and simulation,” in *31st European Photovoltaic Solar Energy Conference and Exhibition*, 2015, pp. 2529–2533.

[45] D. Götz, D. Hahn, R. Gottschalg, D. Dassler, S. Schindler, and H. Hanifi, “Evaluation of shading tolerance of PV modules with different module designs for mobile applications by simulation, indoor and outdoor measurements,” in *36th European Photovoltaic Solar Energy Conference and Exhibition*, 2019.

[46] N. Klasen, D. Weisser, T. Rößler, D. H. Neuhaus, and A. Kraft, “Performance of shingled solar modules under partial shading,” *Prog. Photovoltaics Res. Appl.*, vol. 30, no. 4, pp. 325–338, Apr. 2022, doi: 10.1002/pip.3486.

[47] H. Sträter and S. Riechelmann, “An approach for a shading resistance classification of PV modules,” in *8th World Conference on Photovoltaic Energy Conversion*, Milano, 2022, pp. 492–497.

[48] E. Özkalay, F. Valoti, M. Caccivio, A. Virtuani, G. Friesen, and C. Ballif, “The effect of partial shading on the reliability of photovoltaic modules in the built-environment,” *EPJ Photovoltaics*, vol. 15, p. 7, Feb. 2024, doi: 10.1051/epjpv/2024001.

[49] H. Chu, L. J. Koduvelikulathu, V. D. Mihailetchi, G. Galbiati, A. Halm, and R. Kopecek, “Soft Breakdown Behavior of Interdigitated-back-contact Silicon Solar Cells,” *Energy Procedia*, vol. 77, pp. 29–35, Aug. 2015, doi: 10.1016/j.egypro.2015.07.006.

[50] R. Müller *et al.*, “Analysis of n-type IBC solar cells with diffused boron emitter locally blocked by implanted phosphorus,” *Sol. Energy Mater. Sol. Cells*, vol. 142, pp. 54–59, Nov. 2015, doi: 10.1016/j.solmat.2015.05.046.

[51] S. Deng *et al.*, “Research on hot spot risk for high-efficiency solar module,” *Energy Procedia*, vol. 130, pp. 77–86, Sep. 2017, doi: 10.1016/j.egypro.2017.09.399.

[52] T. Geipel, M. Moeller, J. Walter, A. Kraft, and U. Eitner, “Intermetallic compounds in solar cell interconnections: Microstructure and growth kinetics,” *Sol. Energy Mater. Sol. Cells*, vol. 159, pp. 370–388, 2017, doi: https://doi.org/10.1016/j.solmat.2016.08.039.

[53] D. Phillip, H. Manuel, E. Fokuhl, and G. Mülhöfer, “Hot-spot endurance test—Modifications for bifacial photovoltaic modules,” in *35th European Photovoltaic Solar Energy Conference & Exhibition*, 2018.

[54] Y. Zhang, Y. Yu, F. Meng, and Z. Liu, “Experimental Investigation of the Shading and Mismatch Effects on the Performance of Bifacial Photovoltaic Modules,” *IEEE J. Photovoltaics*, vol. 10, no. 1, pp. 296–305, 2020, doi: 10.1109/JPHOTOV.2019.2949766.

[55] C. Xiao, P. Hacke, S. Johnston, D. B. Sulas-Kern, C.-S. Jiang, and M. Al-Jassim, “Failure analysis of field-failed bypass diodes,” *Prog. Photovoltaics Res. Appl.*, vol. 28, no. 9, pp. 909–918, Sep. 2020, doi: 10.1002/pip.3297.

[56] D. C. Jordan, N. Haegel, and T. M. Barnes, “Photovoltaics module reliability for the terawatt age,” *Prog. Energy*, vol. 4, no. 2, 2022, doi: 10.1088/2516-1083/ac6111.

[57] H. E. Yang, R. H. French, and L. S. Bruckman, *Durability and Reliability of Polymers and Other Materials in Photovoltaic Modules*. Elsevier, 2018. doi: 10.1016/C2016-0-01032-X.

[58] Y. Voronko, G. C. Eder, M. Knausz, G. Oreski, T. Koch, and K. A. Berger, “Correlation of the loss in photovoltaic module performance with the ageing behaviour of the backsheets used,” *Prog. Photovoltaics Res. Appl.*, vol. 23, no. 11, pp. 1501–1515, Nov. 2015, doi: 10.1002/pip.2580.

[59] G. Oreski *et al.*, “Properties and degradation behaviour of polyolefin encapsulants for photovoltaic modules,” *Prog. Photovoltaics Res. Appl.*, vol. 28, no. 12, pp. 1277–1288, Dec. 2020, doi: 10.1002/pip.3323.

[60] G. Oreski *et al.*, “Performance of PV modules using co-extruded backsheets based on polypropylene,” *Sol. Energy Mater. Sol. Cells*, vol. 223, p. 110976, 2021, doi: 10.1016/j.solmat.2021.110976.

[61] B. Brune *et al.*, “Quantifying the influence of encapsulant and backsheet composition on PV-power and electrical degradation,” *Prog. Photovoltaics Res. Appl.*, vol. 31, no. 7, pp. 716–728, 2023, doi: 10.1002/pip.3679.

[62] E. Bonekamp, Jeffrey and H. Zhang, “Polyolefin photovoltaic backsheet comprising a stabilized polypropylene layer,” 2017

[63] B. Adothu *et al.*, “Newly developed thermoplastic polyolefin encapsulant–A potential candidate for crystalline silicon photovoltaic modules encapsulation,” *Sol. Energy*, vol. 194, no. July, pp. 581–588, 2019, doi: 10.1016/j.solener.2019.11.018.

[64] G. Beaucarne *et al.*, “Low temperature solar cell encapsulation with novel silicone elastomer for building integrated PV,” in *8th World Conference on Photovoltaic Energy Conversion*, 2021, pp. 893–897.

[65] M. Halwachs *et al.*, “Statistical evaluation of PV system performance and failure data among different climate zones,” *Renew. Energy*, vol. 139, pp. 1040–1060, Aug. 2019, doi: 10.1016/j.renene.2019.02.135.

[66] M. Aghaei *et al.*, “Review of degradation and failure phenomena in photovoltaic modules,” *Renew. Sustain. Energy Rev.*, vol. 159, no. February, p. 112160, May 2022, doi: 10.1016/j.rser.2022.112160.

[67] “DuPont global PV reliability 2019 Field analysis.” [Online]. Available: https://www.dupont.com/news/20190618-dupont-issues-2019-pv-reliability-study.htm

[68] “DuPont global PV reliability 2020 Field analysis.” [Online]. Available: https://www.dupont.com/news/20200512-2020-global-pv-reliability-report.html

[69] G. C. Eder *et al.*, “Error analysis of aged modules with cracked polyamide backsheets,” *Sol. Energy Mater. Sol. Cells*, vol. 203, no. August, p. 110194, 2019, doi: 10.1016/j.solmat.2019.110194.

[70] Y. Voronko *et al.*, “Repair options for PV modules with cracked backsheets,” *Energy Sci. Eng.*, vol. 9, no. 9, pp. 1583–1595, Sep. 2021, doi: 10.1002/ese3.936.

[71] C. Buerhop-Lutz, O. Stroyuk, T. Pickel, T. Winkler, J. Hauch, and I. M. Peters, “PV modules and their backsheets - A case study of a Multi-MW PV power station,” *Sol. Energy Mater. Sol. Cells*, vol. 231, no. May, p. 111295, 2021, doi: 10.1016/j.solmat.2021.111295.

[72] C. Buerhop Lutz, L. Lüer, O. Stroyuk, J. Hauch, and I. M. Peters, “Dynamics of backsheet-driven insulation issues,” *Sol. Energy Mater. Sol. Cells*, vol. 257, no. April, p. 112398, Aug. 2023, doi: 10.1016/j.solmat.2023.112398.

[73] C. Buerhop, O. Stroyuk, J. Zöcklein, T. Pickel, J. Hauch, and I. M. Peters, “Wet leakage

resistance development of modules with various backsheet types," *Prog. Photovoltaics Res. Appl.*, vol. 30, no. 8, pp. 938–947, Aug. 2022, doi: 10.1002/pip.3481.

[74] M. Owen-Bellini *et al.*, "Advancing reliability assessments of photovoltaic modules and materials using combined-accelerated stress testing," *Prog. Photovoltaics Res. Appl.*, vol. 29, no. 1, pp. 64–82, Jan. 2021, doi: 10.1002/pip.3342.

[75] M. D. Kempe, T. Lockman, and J. Morse, "Development of Testing Methods to Predict Cracking in Photovoltaic Backsheets," *Conf. Rec. IEEE Photovolt. Spec. Conf.*, pp. 2411–2416, 2019, doi: 10.1109/PVSC40753.2019.8980818.

[76] T. T. Gernot Oreski, Ioannis Tsanakas, Arvid van der Heide, Gabriele Eder, "Performance and Reliability of Second Life PV," 2025. [Online]. Available: https://iea-pvps.org/publications/?year_p=&task=67&order=DESC&keyword=&cpt=keytopics&keytopic=

[77] J. Markert, S. Kotterer, D. E. Mansour, D. Philipp, and P. Gebhardt, "Advanced analysis of backsheet failures from 26 power plants," *EPJ Photovoltaics*, vol. 12, no. September, pp. 6–10, 2021, doi: 10.1051/epjpv/2021006.

[78] P. Lechner *et al.*, "Analysis of Fielded PV-Modules with Backsheet Issues," in *Proceedings of the 36th European Photovoltaic Solar Energy Conference and Exhibition*, Marseille, France, 2019, pp. 930–934.

[79] K.-A. Weiß, "Accelerated testing - combined stress vs. sequential stress testing methods and inclusion of specific load situations," 2025. [Online]. Available: https://iea-pvps.org/publications/?year_p=&task=67&order=DESC&keyword=&cpt=keytopics&keytopic=

[80] Y. Voronko, G. C. Eder, E. Reiser, M. Babin, and G. Oreski, "Development of Novel Frontsheets With Protective Coatings to Increase the Durability and Reliability of Glass-Free Lightweight PV Modules," *Prog. Photovoltaics Res. Appl.*, pp. 1823–1823, Nov. 2024, doi: 10.1002/pip.3871.

[81] H. Hu, S. Chen, O. Fu, M. Demko, and K. R. Choudhury, "Transparent Tedlar® Frontsheet for Lightweight PV Module Designs," in *2023 IEEE 50th Photovoltaic Specialists Conference (PVSC)*, IEEE, Jun. 2023, pp. 1–3. doi: 10.1109/PVSC48320.2023.10359631.

[82] G. Oreski *et al.*, "Investigation of the crack propensity of co-extruded polypropylene backsheet films for photovoltaic modules," *Sol. Energy Mater. Sol. Cells*, vol. 259, no. March, p. 112438, 2023, doi: 10.1016/j.solmat.2023.112438.

[83] S. Uličná, A. Sinha, D. C. Miller, B. M. Habersberger, L. T. Schelhas, and M. Owen-Bellini, "PV encapsulant formulations and stress test conditions influence dominant degradation mechanisms," *Sol. Energy Mater. Sol. Cells*, vol. 255, no. December 2022, p. 112319, Jun. 2023, doi: 10.1016/j.solmat.2023.112319.

[84] C. Barretta, E. Helfer, A. E. Macher, and G. Oreski, "What Are PVDF-Based Backsheets Made Of?," in *2022 IEEE 49th Photovoltaics Specialists Conference (PVSC)*, IEEE, Jun. 2022, pp. 0633–0636. doi: 10.1109/PVSC48317.2022.9938844.

[85] S. Uličná *et al.*, "A study of degradation mechanisms in PVDF-based photovoltaic backsheets," *Sci. Rep.*, vol. 12, no. 1, pp. 1–11, 2022, doi: 10.1038/s41598-022-18477-1.

[86] S. L. Moffitt *et al.*, "Microstructure changes during failure of PVDF-based photovoltaic backsheets," *Prog. Photovoltaics Res. Appl.*, vol. 31, no. 1, pp. 26–35, 2023, doi:

10.1002/pip.3605.

[87] S. Smith *et al.*, “Long-term durability of transparent backsheets for bifacial photovoltaics: An in-depth degradation analysis,” *Sol. Energy Mater. Sol. Cells*, vol. 256, p. 112309, Jul. 2023, doi: 10.1016/j.solmat.2023.112309.

[88] I. Bennett, E. Bende, M. J. A. A. Goris, and W. Eerenstein, “An Overview of Developments in Foil-Based Back-Contact Modules,” in *Conference Proceedings of 29th European Photovoltaic Solar Energy Conference and Exhibition*, Amsterdam, 2014. doi: 10.4229/EUPVSEC20142014-1AP.1.3.

[89] Y. Voronko, G. Eder, M. Edler, G. Oreski, and W. Muehleisen, “Analysis of the triggers for the yellowing of PV materials during artificial ageing,” in *9th European Weathering Symposium Natural and Artificial Ageing of Polymers*, Basel, 2019.

[90] C. Barretta, G. Oreski, S. Feldbacher, K. Resch-Fauster, and R. Pantani, “Comparison of Degradation Behavior of Newly Developed Encapsulation Materials for Photovoltaic Applications under Different Artificial Ageing Tests,” *Polymers (Basel).*, vol. 13, p. 271, 2021, doi: 10.3390/polym13020271.

[91] B. Adothu, P. Bhatt, S. Zele, J. Oderkerk, F. R. Costa, and S. Mallick, “Investigation of newly developed thermoplastic polyolefin encapsulant principle properties for the c-Si PV module application,” *Mater. Chem. Phys.*, vol. 243, no. January, p. 122660, 2020, doi: 10.1016/j.matchemphys.2020.122660.

[92] B. Lin, C. Zheng, Q. Zhu, and F. Xie, “A polyolefin encapsulant material designed for photovoltaic modules: from perspectives of peel strength and transmittance,” *J. Therm. Anal. Calorim.*, vol. 140, no. 5, pp. 2259–2265, Jun. 2020, doi: 10.1007/s10973-019-09006-w.

[93] J. H. Park and S.-H. Hwang, “A Polyolefin Elastomer Encapsulant Modified by an Ethylene–Propylene–Diene Terpolymer for Photovoltaic Applications,” *ACS Omega*, Jan. 2024, doi: 10.1021/acsomega.3c07969.

[94] J. H. Park and S. H. Hwang, “Construction and Characterization of Polyolefin Elastomer Blends with Chemically Modified Hydrocarbon Resin as a Photovoltaic Module Encapsulant,” *Polymers (Basel).*, vol. 14, no. 21, 2022, doi: 10.3390/polym14214620.

[95] N. T. Dintcheva, E. Morici, and C. Colletti, “Encapsulant Materials and Their Adoption in Photovoltaic Modules: A Brief Review,” *Sustainability*, vol. 15, no. 12, p. 9453, Jun. 2023, doi: 10.3390/su15129453.

[96] H. Hanifi *et al.*, “Loss analysis and optimization of PV module components and design to achieve higher energy yield and longer service life in desert regions,” *Appl. Energy*, vol. 280, no. September, p. 116028, Dec. 2020, doi: 10.1016/j.apenergy.2020.116028.

[97] K. Hara, Y. Chiba, and Y. Shirahige, “Durable polyolefin encapsulants in aged photovoltaic modules,” *J. Photochem. Photobiol. A Chem.*, vol. 431, no. February, p. 114015, 2022, doi: 10.1016/j.jphotochem.2022.114015.

[98] B. Adothu, F. R. Costa, and S. Mallick, “Damp heat resilient thermoplastic polyolefin encapsulant for photovoltaic module encapsulation,” *Sol. Energy Mater. Sol. Cells*, vol. 224, no. February, p. 111024, 2021, doi: 10.1016/j.solmat.2021.111024.

[99] G. Oreski *et al.*, “Polyethylene copolymers as solar cell encapsulants : A critical overview,” in *Conference Proceedings of 40th European Photovoltaic Solar Energy Conference and Exhibition*, Lisbon, 2023, p. 3AV.1.35.

[100] Z. Yang *et al.*, “Novel EPE co-extruded encapsulating films with UV down-conversion

power gain effect for highly efficient solar cells," *Sol. Energy Mater. Sol. Cells*, vol. 257, no. January, p. 112373, 2023, doi: 10.1016/j.solmat.2023.112373.

[101] M. Köntges, A. Morlier, G. Eder, E. Fleis, B. Kubicek, and J. Lin, "Review: Ultraviolet Fluorescence as Assessment Tool for Photovoltaic Modules," *IEEE J. Photovoltaics*, vol. 10, no. 2, pp. 616–633, 2020, doi: 10.1109/JPHOTOV.2019.2961781.

[102] G. Oreski *et al.*, "Motivation, benefits, and challenges for new photovoltaic material & module developments," *Prog. Energy*, vol. 4, no. 3, p. 032003, Jul. 2022, doi: 10.1088/2516-1083/ac6f3f.

[103] A. Borja Block *et al.*, "Colouring solutions for building integrated photovoltaic modules: A review," *Energy Build.*, vol. 314, no. April, p. 114253, 2024, doi: 10.1016/j.enbuild.2024.114253.

[104] A. J. Curran *et al.*, "Field studies of PERC and Al-BSF PV module performance loss using power and I-V timeseries," *Front. Energy Res.*, vol. 11, Jul. 2023, doi: 10.3389/fenrg.2023.1127775.

[105] R. Rüther, "Make PV modules as cheap as possible, but not cheaper," PV Magazine International. [Online]. Available: https://www.pv-magazine.com/2024/01/03/make-pv-modules-as-cheap-as-possible-but-not-cheaper/

[106] M. Braga, G. X. A. Pinto, A. M. Pires, A. H. Zamboni, L. R. Nascimento, and R. Rüther, "No Title," Universidade Federal de Santa Catarina, Florianópolis-SC, Brazil,. [Online]. Available: https://scorecard.pvel.com/mechanical-stress-sequence/

[107] F. O. Santos, C. Louter, and J. R. Correia, "Exploring thin glass strength test methodologies," *Challenging Glas. 6 Conf. Archit. Struct. Appl. Glas. CGC 2018 - Proc.*, no. May, 2018, doi: 10.7480/cgc.6.2192.

[108] C. Sillerud, D. Zirzow, and J. Crimmins, "Past , Current , and Future Issues in PV Reliability Testing," in *Proc. 53nd European Photovoltaic Solar Energy Conference, Seattle, WA*, 2023.

[109] K. Thiele, S. Müller-Braun, and J. Schneider, "Evaluation methods for surface compression stress measurements with unknown principle stress directions," *Glas. Struct. Eng.*, vol. 7, no. 2, pp. 121–137, Aug. 2022, doi: 10.1007/s40940-022-00184-y.

[110] J. Markert, F. Ensslen, T. Rist, E. Job, I. Hädrich, and D. Philipp, "Mechanical Stability of PV Modules," in *PV Symp.*, 2024, pp. 1–12.

[111] C. Kedir, "Solar Risk Assessment," Report: kWh analytics. [Online]. Available: https://www.kwhanalytics.com/solar-risk-assessment

[112] VDMA, "International Technology Roadmap for Photovoltaic (ITRPV) - 15th Edition," 2023.

[113] T. G. Allen, J. Bullock, X. Yang, A. Javey, and S. De Wolf, "Passivating contacts for crystalline silicon solar cells," *Nat. Energy*, vol. 4, no. 11, pp. 914–928, Sep. 2019, doi: 10.1038/s41560-019-0463-6.

[114] C. Peike *et al.*, "Origin of damp-heat induced cell degradation," *Sol. Energy Mater. Sol. Cells*, vol. 116, pp. 49–54, 2013, doi: 10.1016/j.solmat.2013.03.022.

[115] A. Kraft *et al.*, "Investigation of Acetic Acid Corrosion Impact on Printed Solar Cell Contacts," *IEEE J. Photovoltaics*, vol. 5, no. 3, pp. 736–743, May 2015, doi: 10.1109/JPHOTOV.2015.2395146.

[116] M. D. Kempe, G. J. Jorgensen, K. M. Terwilliger, T. J. McMahon, C. E. Kennedy, and

T. T. Borek, “Acetic acid production and glass transition concerns with ethylene-vinyl acetate used in photovoltaic devices,” *Sol. Energy Mater. Sol. Cells*, vol. 91, no. 4, pp. 315–329, 2007, doi: 10.1016/j.solmat.2006.10.009.

[117] E. A. Gaulding *et al.*, “Differences in Printed Contacts Lead to Susceptibility of Silicon Cells to Series Resistance Degradation,” *IEEE J. Photovoltaics*, vol. 12, no. 3, pp. 690–695, 2022, doi: 10.1109/JPHOTOV.2022.3150727.

[118] M. Liggett *et al.*, “Characterization of Field Exposed Photovoltaic Modules Featuring Signs of Contact Degradation,” in *2023 IEEE 50th Photovoltaic Specialists Conference (PVSC)*, IEEE, Jun. 2023, pp. 1–3. doi: 10.1109/PVSC48320.2023.10360087.

[119] O. K. Segbefia, N. Akhtar, and T. O. Sætre, “Moisture induced degradation in field-aged multicrystalline silicon photovoltaic modules,” *Sol. Energy Mater. Sol. Cells*, vol. 258, no. March, p. 112407, Aug. 2023, doi: 10.1016/j.solmat.2023.112407.

[120] T. H. Kim, N. C. Park, and D. H. Kim, “The effect of moisture on the degradation mechanism of multi-crystalline silicon photovoltaic module,” *Microelectron. Reliab.*, vol. 53, no. 9–11, pp. 1823–1827, 2013, doi: 10.1016/j.microrel.2013.07.047.

[121] A. J. Curran *et al.*, “Degradation of PERC and Al-BSF Cells with UV Cutoff and White Variations of EVA and POE Encapsulant,” *Conf. Rec. IEEE Photovolt. Spec. Conf.*, pp. 1510–1516, 2021, doi: 10.1109/PVSC43889.2021.9519110.

[122] N. Iqbal *et al.*, “Characterization of front contact degradation in monocrystalline and multicrystalline silicon photovoltaic modules following damp heat exposure,” *Sol. Energy Mater. Sol. Cells*, vol. 235, no. February 2021, p. 111468, 2022, doi: 10.1016/j.solmat.2021.111468.

[123] D. B. Sulas-Kern, H. Moutinho, T. Erion-Lorico, and S. Johnston, “Near-Busbar Degradation of Screen-Printed Metallization in Silicon Photovoltaic Modules,” *Conf. Rec. IEEE Photovolt. Spec. Conf.*, vol. 2022-June, pp. 200–203, 2022, doi: 10.1109/PVSC48317.2022.9938799.

[124] A. M. Jeffries, T. Nietzold, L. T. Schelhas, and M. I. Bertoni, “Corrosion of novel reactive silver ink and commercial silver-based metallizations in diluted acetic acid,” *Sol. Energy Mater. Sol. Cells*, vol. 223, no. July 2020, p. 110900, 2021, doi: 10.1016/j.solmat.2020.110900.

[125] N. Iqbal *et al.*, “Impact of acetic acid exposure on metal contact degradation of different crystalline silicon solar cell technologies,” *Sol. Energy Mater. Sol. Cells*, vol. 250, no. August 2022, p. 112089, 2023, doi: 10.1016/j.solmat.2022.112089.

[126] C. Sen *et al.*, “Accelerated damp-heat testing at the cell-level of bifacial silicon HJT, PERC and TOPCon solar cells using sodium chloride,” *Sol. Energy Mater. Sol. Cells*, vol. 262, no. September, p. 112554, 2023, doi: 10.1016/j.solmat.2023.112554.

[127] P. M. Sommeling, J. Liu, and J. M. Kroon, “Corrosion effects in bifacial crystalline silicon PV modules; interactions between metallization and encapsulation,” *Sol. Energy Mater. Sol. Cells*, vol. 256, no. October 2022, p. 112321, 2023, doi: 10.1016/j.solmat.2023.112321.

[128] C. Sen *et al.*, “Buyer aware: Three new failure modes in TOPCon modules absent from PERC technology,” *Sol. Energy Mater. Sol. Cells*, vol. 272, no. March, p. 112877, 2024, doi: 10.1016/j.solmat.2024.112877.

[129] X. Wu *et al.*, “Enhancing the reliability of TOPCon technology by laser-enhanced contact firing,” *Sol. Energy Mater. Sol. Cells*, vol. 271, no. March, p. 112846, 2024, doi:

10.1016/j.solmat.2024.112846.

[130] O. Arriaga Arruti, A. Virtuani, and C. Ballif, “Long-term performance and reliability of silicon heterojunction solar modules,” *Prog. Photovoltaics Res. Appl.*, vol. 31, no. 7, pp. 664–677, Jul. 2023, doi: 10.1002/pip.3688.

[131] D. C. Jordan, S. R. Kurtz, K. VanSant, and J. Newmiller, “Compendium of photovoltaic degradation rates,” *Prog. Photovoltaics Res. Appl.*, vol. 24, no. 7, pp. 978–989, Jul. 2016, doi: 10.1002/pip.2744.

[132] D. C. Jordan *et al.*, “Silicon heterojunction system field performance,” *IEEE J. Photovoltaics*, vol. 8, no. 1, pp. 177–182, 2018, doi: 10.1109/JPHOTOV.2017.2765680.

[133] N. Iqbal *et al.*, “Accelerate Cycles of Learning: Unencapsulated Silicon Photovoltaic Cells to Environmental Stressors,” in *2022 IEEE 49th Photovoltaics Specialists Conference (PVSC)*, IEEE, Jun. 2022, pp. 0668–0674. doi: 10.1109/PVSC48317.2022.9938492.

[134] O. Arriaga Arruti, L. Gnocchi, Q. Jeangros, C. Ballif, and A. Virtuani, “Potential-induced degradation in bifacial silicon heterojunction solar modules: Insights and mitigation strategies,” *Prog. Photovoltaics Res. Appl.*, vol. 32, no. 5, pp. 304–316, May 2024, doi: 10.1002/pip.3765.

[135] L. Gnocchi, O. A. Arruti, C. Ballif, and A. Virtuani, “A comprehensive physical model for the sensitivity of silicon heterojunction photovoltaic modules to water ingress,” *Cell Reports Phys. Sci.*, vol. 5, no. 1, p. 101751, Jan. 2024, doi: 10.1016/j.xcrp.2023.101751.

[136] J. H. Wohlgemuth, P. Hacke, N. Bosco, D. C. Miller, M. D. Kempe, and S. R. Kurtz, “Assessing the causes of encapsulant delamination in PV modules,” in *2016 IEEE 43rd Photovoltaic Specialists Conference (PVSC)*, IEEE, Jun. 2016, pp. 0248–0254. doi: 10.1109/PVSC.2016.7749589.

[137] M. Taguchi, J. Irikawa, M. Iwata, H. Kannou, Y. Murakami, and S. Okamoto, “Approaches to the long-term stability of silicon heterojunction modules,” in *Proceedings of 4th International Workshop on Silicon Heterojunction Solar Cells*, 2021.

[138] C. Sen *et al.*, “Four failure modes in silicon heterojunction glass-backsheet modules,” *Sol. Energy Mater. Sol. Cells*, vol. 257, no. December 2022, p. 112358, 2023, doi: 10.1016/j.solmat.2023.112358.

[139] X. Wu *et al.*, “Addressing sodium ion-related degradation in SHJ cells by the application of nano-scale barrier layers,” *Sol. Energy Mater. Sol. Cells*, vol. 264, no. September 2023, p. 112604, Jan. 2024, doi: 10.1016/j.solmat.2023.112604.

[140] A. Sinha, J. Jaubert, and T. Karin, “UV-Induced Degradation Susceptibility of Industrial N-Type Silicon High-Efficiency PV Mod-ules,” in *IEEE 52nd Photovoltaic Specialist Conference on IEEE 52nd Photovoltaic Specialist Conference, Seattle, WA, USA*, Seattle: Seattle, 2024, p. Poster E3-#108. [Online]. Available: https://www.kiwa.com/49edc2/globalassets/usa/pvel/resorces/pvsc-2024-poster_final-version_sinha.pdf

[141] P. Thome, Fabian T. Meßmer, S. Mack, E. Schnabel, W. Schindler, Florian Kwapil, and C. M. Schubert, “UV-Induced Degradation of Industrial PERC, TOPCon, and HJT Solar Cells - The Next Big Reliability Challenge?,” *Sol. RRL, Press*, 2024.

[142] A. Sinha *et al.*, “UV-induced degradation of high-efficiency silicon PV modules with different cell architectures,” *Prog. Photovoltaics Res. Appl.*, vol. 31, no. 1, pp. 36–51, 2023, doi: 10.1002/pip.3606.

[143] T. Kamioka, D. Takai, T. Tachibana, T. Kojima, and Y. Ohshita, “Plasma damage effect on ultraviolet-induced degradation of PECVD SiNx:H passivation,” in *2015 IEEE 42nd Photovoltaic Specialist Conference (PVSC)*, IEEE, Jun. 2015, pp. 1–3. doi: 10.1109/PVSC.2015.7356326.

[144] R. Witteck *et al.*, “UV-induced degradation of PERC solar modules with UV-transparent encapsulation materials,” *Prog. Photovoltaics Res. Appl.*, vol. 25, no. 6, 2017, doi: 10.1002/pip.2861.

[145] B. Veith-Wolf, R. Witteck, A. Morlier, H. Schulte-Huxel, M. R. Vogt, and J. Schmidt, “Spectra-dependent stability of the passivation quality of Al2O3/c-Si interfaces,” *IEEE J. Photovoltaics*, vol. 8, no. 1, pp. 96–102, 2018, doi: 10.1109/JPHOTOV.2017.2775147.

[146] D. C. Jordan *et al.*, “Photovoltaic fleet degradation insights,” *Prog. Photovoltaics Res. Appl.*, vol. 30, no. 10, pp. 1166–1175, 2022, doi: 10.1002/pip.3566.

[147] S. W. Johnston *et al.*, “Degradation-related defect level in weathered silicon heterojunction modules characterized by deep level transient spectroscopy,” *Sol. Energy Mater. Sol. Cells*, vol. 262, no. September, p. 112527, 2023, doi: 10.1016/j.solmat.2023.112527.

[148] S. Bernardini and M. I. Bertoni, “Insights into the Degradation of Amorphous Silicon Passivation Layer for Heterojunction Solar Cells,” *Phys. Status Solidi Appl. Mater. Sci.*, vol. 216, no. 4, pp. 1–6, 2019, doi: 10.1002/pssa.201800705.

[149] S. Manzoor and M. Bertoni, “Degradation of Surface Recombination Velocity at a-Si/c-Si interface under light and temperature,” *Conf. Rec. IEEE Photovolt. Spec. Conf.*, pp. 1286–1288, 2021, doi: 10.1109/PVSC43889.2021.9518982.

[150] H. Ye *et al.*, “Short Wavelength Photons Destroying Si–H Bonds and Its Influence on High-Efficiency Silicon Solar Cells and Modules,” *Sol. RRL*, vol. 7, no. 15, Aug. 2023, doi: 10.1002/solr.202300334.

[151] M. M. Rasmussen, “Ultraviolet-Induced Degradationof PERC and TOPCon Architectures: Design of a Rapid Screening Process and Investigation of Degradation Signatures,” Case Western Reserve University, 2024. doi: http://orcid.org/0000-0001-5895-5051.

[152] “Best Research-Cell Efficiency Chart,” National Renewable Energy Laboratory. [Online]. Available: https://www.nrel.gov/pv/cell-efficiency.html

[153] A. Kojima, K. Teshima, Y. Shirai, and T. Miyasaka, “Organometal halide perovskites as visible-light sensitizers for photovoltaic cells,” *J. Am. Chem. Soc.*, vol. 131, no. 17, pp. 6050–6051, 2009, doi: 10.1021/ja809598r.

[154] G. E. Eperon, S. D. Stranks, C. Menelaou, M. B. Johnston, L. M. Herz, and H. J. Snaith, “Formamidinium lead trihalide: A broadly tunable perovskite for efficient planar heterojunction solar cells,” *Energy Environ. Sci.*, vol. 7, no. 3, pp. 982–988, 2014, doi: 10.1039/c3ee43822h.

[155] S. Baumann *et al.*, “Stability and reliability of perovskite containing solar cells and modules: degradation mechanisms and mitigation strategies,” *Energy Environ. Sci.*, vol. 17, no. 20, pp. 7566–7599, 2024, doi: 10.1039/D4EE01898B.

[156] R. I. Dawood, A. J. Forty, and M. R. Tubbs, “The photodecomposition of lead iodide,” *Proc. Roy. Soc. A*, vol. 284, pp. 272–288, 1964, doi: 10.1098/rspa.1965.0063.

[157] A. Donakowski *et al.*, “Improving Photostability of Cesium-Doped Formamidinium Lead Triiodide Perovskite,” *ACS Energy Lett.*, vol. 6, no. 2, pp. 574–580, 2021, doi:

10.1021/acsenergylett.0c02339.

[158] B. Roose, K. Dey, Y. H. Chiang, R. H. Friend, and S. D. Stranks, “Critical Assessment of the Use of Excess Lead Iodide in Lead Halide Perovskite Solar Cells,” *J. Phys. Chem. Lett.*, vol. 11, no. 16, pp. 6505–6512, 2020, doi: 10.1021/acs.jpclett.0c01820.

[159] G. Tumen-Ulzii *et al.*, “Detrimental Effect of Unreacted PbI2 on the Long-Term Stability of Perovskite Solar Cells,” *Adv. Mater.*, vol. 32, no. 16, p. 1905035, 2020, doi: 10.1002/adma.201905035.

[160] S. Macpherson *et al.*, “Local nanoscale phase impurities are degradation sites in halide perovskites,” *Nature*, vol. 607, no. 7918, pp. 294–300, 2022, doi: 10.1038/s41586-022-04872-1.

[161] L. T. Schelhas *et al.*, “Insights into operational stability and processing of halide perovskite active layers,” *Energy Environ. Sci.*, vol. 12, no. 4, pp. 1341–1348, 2019, doi: 10.1039/c8ee03051k.

[162] Y. Chen *et al.*, “Strain engineering and epitaxial stabilization of halide perovskites,” *Nature*, vol. 577, p. 209, 2020, doi: 10.1038/s41586-019-1868-x.

[163] A. Y. Alsalloum *et al.*, “22.8%-Efficient single-crystal mixed-cation inverted perovskite solar cells with a near-optimal bandgap,” *Energy Environ. Sci*, vol. 14, pp. 2263–2268, 2021, doi: 10.1039/d0ee03839c.

[164] B. Philippe *et al.*, “Chemical Distribution of Multiple Cation (Rb+,Cs+,MA+, and FA+) Perovskite Materials by Photoelectron Spectroscopy,” *Chem. Mater*, vol. 29, pp. 3589–3596, 2017, doi: 10.1021/acs.chemmater.7b00126.

[165] G. Y. Kim, A. Senocrate, T. Y. Yang, G. Gregori, M. Grätzel, and J. Maier, “Large tunable photoeffect on ion conduction in halide perovskites and implications for photodecomposition,” *Nat. Mater.*, vol. 17, no. 5, pp. 445–449, 2018, doi: 10.1038/s41563-018-0038-0.

[166] W. J. Yin, T. Shi, and Y. Yan, “Unusual defect physics in CH3NH3PbI3 perovskite solar cell absorber,” *Appl. Phys. Lett.*, vol. 104, no. 6, p. 063903, 2014, doi: 10.1063/1.4864778.

[167] B. Chen, M. Yang, S. Priya, and K. Zhu, “Origin of J-V Hysteresis in Perovskite Solar Cells,” *J. Phys. Chem. Lett.*, vol. 7, no. 5, pp. 905–917, 2016, doi: 10.1021/acs.jpclett.6b00215.

[168] H. Lee *et al.*, “Direct experimental evidence of halide ionic migration under bias in CH3NH3PbI3-xClx-based perovskite solar cells using GD-OES analysis,” *ACS Energy Lett.*, vol. 2, no. 4, pp. 943–949, 2017, doi: 10.1021/acsenergylett.7b00150.

[169] D. A. Jacobs *et al.*, “The two faces of capacitance: New interpretations for electrical impedance measurements of perovskite solar cells and their relation to hysteresis,” *J. Appl. Phys.*, vol. 124, no. 22, p. 225702, 2018, doi: 10.1063/1.5063259.

[170] C. C. Boyd, R. Cheacharoen, T. Leijtens, and M. D. McGehee, “Understanding Degradation Mechanisms and Improving Stability of Perovskite Photovoltaics,” *Chem. Rev.*, vol. 119, no. 5, pp. 3418–3451, 2019, doi: 10.1021/acs.chemrev.8b00336.

[171] S. P. Dunfield *et al.*, “From Defects to Degradation: A Mechanistic Understanding of Degradation in Perovskite Solar Cell Devices and Modules,” *Adv. Energy Mater.*, vol. 10, no. 26, pp. 1–35, 2020, doi: 10.1002/aenm.201904054.

[172] Y. Zhong *et al.*, “Inhibition of Ion Migration for Highly Efficient and Stable Perovskite

Solar Cells," *Adv. Mater.*, vol. 35, p. 2302552, 2023, doi: 10.1002/adma.202302552.

[173] S. Tan *et al.*, "Steric Impediment of Ion Migration Contributes to Improved Operational Stability of Perovskite Solar Cells," *Adv. Mater.*, vol. 32, p. 1906995, 2020, doi: 10.1002/adma.201906995.

[174] A. D. Jodlowski *et al.*, "Large guanidinium cation mixed with methylammonium in lead iodide perovskites for 19% efficient solar cells," *Nat. Energy*, vol. 2, pp. 972–979, 2017, doi: 10.1038/s41560-017-0054-3.

[175] P. Liu *et al.*, "Lattice-Matching Structurally-Stable 1D@3D Perovskites toward Highly Efficient and Stable Solar Cells," *Adv. Energy Mater.*, vol. 10, p. 1903654, 2020, doi: 10.1002/aenm.201903654.

[176] Z. Huang *et al.*, "Suppressed Ion Migration in Reduced-Dimensional Perovskites Improves Operating Stability," *ACS Energy Lett.*, vol. 4, p. 1521−1527, 2019, doi: 10.1021/acsenergylett.9b00892.

[177] W. Fan *et al.*, "Grain Boundary Perfection Enabled by Pyridinic Nitrogen Doped Graphdiyne in Hybrid Perovskite," *Adv. Funct. Mater.*, vol. 31, p. 2104633, 2021, doi: 10.1002/adfm.202104633.

[178] J. Yang *et al.*, "High-Performance Perovskite Solar Cells with Excellent Humidity and Thermo-Stability via Fluorinated Perylenediimide," *Adv. Energy Mater.*, vol. 9, p. 1900198, 2019, doi: 10.1002/aenm.201900198.

[179] S. Bai *et al.*, "Planar perovskite solar cells with long-term stability using ionic liquid additives," *Nature*, vol. 571, p. 245, 2019, doi: 10.1038/s41586-019-1357-2.

[180] Y. Ma *et al.*, "Suppressing Ion Migration across Perovskite Grain Boundaries by Polymer Additives," *Adv. Funct. Mater.*, vol. 31, p. 2006802, 2021, doi: 10.1002/adfm.202006802.

[181] H. Wang *et al.*, "Potassium Salt Coordination Induced Ion Migration Inhibition and Defect Passivation for High-Efficiency Perovskite Solar Cells," *J. Phys. Chem. Lett*, vol. 13, p. 8573−8579, 2022, doi: 10.1021/acs.jpclett.2c02414.

[182] J. Cao *et al.*, "Interstitial Occupancy by Extrinsic Alkali Cations in Perovskites and Its Impact on Ion Migration," *Adv. Mater*, vol. 30, p. 1707350, 2018, doi: 10.1002/adma.201707350.

[183] Y. Yang *et al.*, "A thermotropic liquid crystal enables efficient and stable perovskite solar modules," *Nat. Energy*, vol. 9, pp. 316–323, 2024, doi: 10.1038/s41560-023-01444-z.

[184] F. Cheng *et al.*, "85 °C/85%-Stable n-i-p Perovskite Photovoltaics with NiO x Hole Transport Layers Promoted By Perovskite Quantum Dots," *Adv. Sci.*, vol. 9, p. 2201573, 2022, doi: 10.1002/advs.202201573.

[185] Q. Tu *et al.*, "Out-of-Plane Mechanical Properties of 2D Hybrid Organic-Inorganic Perovskites by Nanoindentation," *ACS Appl. Mater. Interfaces*, vol. 10, no. 26, pp. 22167–22173, 2018, doi: 10.1021/acsami.8b05138.

[186] S. Baumann, A. Raugewitz, F. Haase, T. Wietler, R. Peibst, and M. Köntges, "Perovskite/silicon tandem solar cells with front side metallization applied prior to top cell fabrication enabling high curing temperatures," in *2023 IEEE 50th Photovoltaic Specialists Conference (PVSC)*, 2023. doi: 10.1109/PVSC48320.2023.10359983.

[187] T. Leijtens, G. E. Eperon, S. Pathak, A. Abate, M. M. Lee, and H. J. Snaith, "Overcoming ultraviolet light instability of sensitized TiO2 with meso-superstructured organometal tri-

halide perovskite solar cells," *Nat. Commun.*, vol. 4, p. 2885, 2013, doi: 10.1038/ncomms3885.

[188] B. Roose *et al.*, "Mesoporous SnO2 electron selective contact enables UV-stable perovskite solar cells," *Nano Energy*, vol. 30, no. October, pp. 517–522, 2016, doi: 10.1016/j.nanoen.2016.10.055.

[189] S. Zhang *et al.*, "Conjugated Self-Assembled Monolayer as Stable Hole-Selective Contact for Inverted Perovskite Solar Cells," *ACS Mater. Au*, vol. 4, pp. 1976–1983, 2022, doi: 10.1021/acsmaterialslett.2c00799.

[190] P. Jiang, L. Hu, L. Sun, Z. Li, H. Han, and Y. Zhou, "On the interface reactions and stability of nonfullerene organic solar cells," *Chem. Sci.*, vol. 13, no. 17, pp. 4714–4739, 2022, doi: 10.1039/d1sc07269b.

[191] A. Das Mahapatra and J.-W. Lee, "Metal oxide charge transporting layers for stable high-performance perovskite solar cells," *Cryst EngComm*, vol. 24, p. 7229, 2022, doi: 10.1039/d2ce00825d.

[192] B. Roose, Q. Wang, and A. Abate, "The Role of Charge Selective Contacts in Perovskite Solar Cell Stability," *Adv. Energy Mater*, vol. 9, p. 1803140, 2019, doi: 10.1002/aenm.201803140.

[193] I. Gueye *et al.*, "Analysis of Iodide Transport on Methyl Ammonium Lead Iodide Perovskite Solar Cell Structure Through Operando Hard X-ray Photoelectron Spectroscopy," *Chem. Mater*, vol. 35, 2023, doi: 10.1021/acs.chemmater.2c03162.

[194] N. N. Udalova *et al.*, "New Aspects of Copper Electrode Metamorphosis in Perovskite Solar Cells," *J. Phys. Chem. C*, vol. 2020, pp. 24601–24607, 2020, doi: 10.1021/acs.jpcc.0c06608.

[195] T. Chen *et al.*, "Efficient Perovskite Solar Cells with Titanium Cathode Interlayer," *Sol. RRL*, vol. 2, p. 1800167, 2018, doi: 10.1002/solr.201800167.

[196] M. Liu, Z. Chen, Y. Yang, H.-L. Yip, and Y. Cao, "Reduced open-circuit voltage loss for highly efficient low-bandgap perovskite solar cells via suppression of silver diffusion," *J. Mater. Chem. A*, vol. 7, p. 17324, 2019, doi: 10.1039/c9ta04366g.

[197] H. Lee and C. Lee, "Analysis of Ion-Diffusion-Induced Interface Degradation in Inverted Perovskite Solar Cells via Restoration of the Ag Electrode," *Adv. Energy Mater.*, vol. 8, p. 1702197, 2018, doi: 10.1002/aenm.201702197.

[198] E. Bi *et al.*, "Efficient Perovskite Solar Cell Modules with High Stability Enabled by Iodide Diffusion Barriers," *Joule*, vol. 3, no. 11, pp. 2748–2760, Nov. 2019, doi: 10.1016/j.joule.2019.07.030.

[199] J. A. Christians *et al.*, "Tailored interfaces of unencapsulated perovskite solar cells for >1,000 hour operational stability," *Nat. Energy*, vol. 3, no. 1, pp. 68–74, 2018, doi: 10.1038/s41560-017-0067-y.

[200] E. M. Sanehira *et al.*, "Influence of Electrode Interfaces on the Stability of Perovskite Solar Cells: Reduced Degradation Using MoO x /Al for Hole Collection," *ACS Energy Lett.*, vol. 1, pp. 38–45, 2016, doi: 10.1021/acsenergylett.6b00013.

[201] I. Jeon *et al.*, "Carbon nanotubes to outperform metal electrodes in perovskite solar cells via dopant engineering and hole-selectivity enhancement," *J. Mater. Chem. A*, vol. 8, pp. 11141–11147, 2020, doi: 10.1039/d0ta03692g.

[202] B. Nath, P. C. Ramamurthy, G. Hegde, and D. Roy Mahapatra, "Role of electrodes on

perovskite solar cells performance: A review," *ISSS J. Micro Smart Syst.*, vol. 11, no. 1, pp. 61–79, 2022, doi: 10.1007/s41683-021-00089-y.

[203] H. Zhang, K. Song, L. Zhu, and Q. Meng, "Back-interface regulation for carbon-based perovskite solar cells," *Carbon N. Y.*, vol. 168, pp. 372–391, Oct. 2020, doi: 10.1016/J.CARBON.2020.06.065.

[204] Y. J. Noh, J. G. Kim, S. S. Kim, H. K. Kim, and S. I. Na, "Efficient semi-transparent perovskite solar cells with a novel indium zinc tin oxide top electrode grown by linear facing target sputtering," *J. Power Sources*, vol. 437, p. 226894, Oct. 2019, doi: 10.1016/J.JPOWSOUR.2019.226894.

[205] S. Yoon *et al.*, "Highly Efficient and Reliable Semitransparent Perovskite Solar Cells via Top Electrode Engineering," *Adv. Funct. Mater.*, vol. 32, p. 2111760, 2022, doi: 10.1002/adfm.202111760.

[206] A. Rousse *et al.*, "Non-thermal melting in semiconductors measured at femtosecond resolution," *Nature*, vol. 410, no. 6824, pp. 65–67, 2001, doi: 10.1038/35065045.

[207] K. Sokolowski-Tinten *et al.*, "Transient states of matter during short pulse laser ablation," *Phys. Rev. Lett.*, vol. 81, no. 1, pp. 224–227, 1998, doi: 10.1103/PhysRevLett.81.224.

[208] F. Jamaatisomarin, R. Chen, S. Hosseini-Zavareh, and S. Lei, "Laser Scribing of Photovoltaic Solar Thin Films: A Review," *J. Manuf. Mater. Process.*, vol. 7, no. 3, p. 94, 2023, doi: 10.3390/jmmp7030094.

[209] L. Bayer *et al.*, "Morphology and topography of perovskite solar cell films ablated and scribed with short and ultrashort laser pulses," *Appl. Surf. Sci.*, vol. 416, pp. 112–117, 2017, doi: 10.1016/j.apsusc.2017.04.058.

[210] C. Schultz *et al.*, "Ablation mechanisms of nanosecond and picosecond laser scribing for metal halide perovskite module interconnection – An experimental and numerical analysis," *Sol. Energy*, vol. 198, no. January, pp. 410–418, 2020, doi: 10.1016/j.solener.2020.01.074.

[211] F. U. Kosasih, L. Rakocevic, T. Aernouts, J. Poortmans, and C. Ducati, "Electron Microscopy Characterization of P3 Lines and Laser Scribing-Induced Perovskite Decomposition in Perovskite Solar Modules," *ACS Appl. Mater. Interfaces*, vol. 11, no. 49, pp. 45646–45655, 2019, doi: 10.1021/acsami.9b15520.

[212] J. Zhao *et al.*, "Nonthermal laser ablation of high-efficiency semitransparent and aesthetic perovskite solar cells," *Nanophotonics*, vol. 11, no. 5, pp. 987–993, 2022, doi: 10.1515/nanoph-2021-0683.

[213] N. N. Udalova, A. S. Tutantsev, Q. Chen, A. Kraskov, E. A. Goodilin, and A. B. Tarasov, "New Features of Photochemical Decomposition of Hybrid Lead Halide Perovskites by Laser Irradiation," *ACS Appl. Mater. Interfaces*, vol. 12, no. 11, pp. 12755–12762, 2020, doi: 10.1021/acsami.9b21689.

[214] Y. Hu *et al.*, "Stable Large-Area (10 × 10 cm2) Printable Mesoscopic Perovskite Module Exceeding 10% Efficiency," *Sol. RRL*, vol. 1, no. 2, p. 1600019, 2017, doi: 10.1002/solr.201600019.

[215] B. Q. Lin, C. P. Huang, K. Y. Tian, P. H. Lee, W. F. Su, and L. Xu, "Laser Patterning Technology Based on Nanosecond Pulsed Laser for Manufacturing Bifacial Perovskite Solar Modules," *Int. J. Precis. Eng. Manuf. - Green Technol.*, vol. 10, no. 1, pp. 123–139, 2023, doi: 10.1007/s40684-022-00421-3.

[216] B. Chen *et al.*, "Bifacial all-perovskite tandem solar cells," *Sci. Adv.*, vol. 8, no.

November, pp. 1–12, 2022, doi: 10.1126/sciadv.add0377.

[217] S. Hong *et al.*, “A series connection architecture for large-area organic photovoltaic modules with a 7.5% module efficiency,” *Nat. Commun.*, vol. 7, pp. 3–8, 2016, doi: 10.1038/ncomms10279.

[218] M. Dailey, Y. Li, and A. D. Printz, “Residual Film Stresses in Perovskite Solar Cells: Origins, Effects, and Mitigation Strategies,” *ACS Omega*, vol. 6, p. 30214−30223, 2021, doi: 10.1021/acsomega.1c04814.

[219] H. Wang *et al.*, “Interfacial Residual Stress Relaxation in Perovskite Solar Cells with Improved Stability,” *Adv. Mater*, vol. 31, p. 904408, 2019, doi: 10.1002/adma.201904408.

[220] L. Duan and A. Uddin, “Defects and stability of perovskite solar cells: A critical analysis,” *Mater. Chem. Front.*, vol. 6, no. 4, pp. 400–417, 2022, doi: 10.1039/d1qm01250a.

[221] S. Mazumdar, Y. Zhao, and X. Zhang, “Stability of Perovskite Solar Cells: Degradation Mechanisms and Remedies,” *Front. Electron.*, vol. 2, p. 712785, 2021, doi: 10.3389/felec.2021.712785.

[222] F. M. Rombach, S. A. Haque, and T. J. Macdonald, “Lessons learned from spiro-OMeTAD and PTAA in perovskite solar cells,” *Energy Environ. Sci*, vol. 14, pp. 5161–5190, 2021, doi: 10.1039/d1ee02095a.

[223] C.-T. Lin *et al.*, “Passivation against oxygen and light induced degradation by the PCBM electron transport layer in planar perovskite solar cells,” *Sustain. Energy Fuels*, vol. 2, pp. 1686–1692, 2018, doi: 10.1039/c8se00095f.

[224] J. A. Mikroyannidis, A. N. Kabanakis, S. S. Sharma, and G. D. Sharma, “A Simple and Effective Modifi cation of PCBM for Use as an Electron Acceptor in Efficient Bulk Heterojunction Solar Cells,” *Adv. Funct. Mater.*, vol. 21, pp. 746–755, 2011, doi: 10.1002/adfm.201001807.

[225] Z. Zhu *et al.*, “Interaction of Organic Cation with Water Molecule in Perovskite MAPbI3: From Dynamic Orientational Disorder to Hydrogen Bonding,” *Chem. Mater.*, vol. 28, no. 20, pp. 7385–7393, 2016, doi: 10.1021/acs.chemmater.6b02883.

[226] L. Shi *et al.*, “Accelerated Lifetime Testing of Organic−Inorganic Perovskite Solar Cells Encapsulated by Polyisobutylene,” *ACS Appl. Mater. Interfaces*, vol. 9, p. 25073−25081, 2017, doi: 10.1021/acsami.7b07625.

[227] A. R. Bowring, L. Bertoluzzi, B. C. O’Regan, and M. D. McGehee, “Reverse Bias Behavior of Halide Perovskite Solar Cells,” *Adv. Energy Mater.*, vol. 8, no. 8, p. 1702365, 2018, doi: 10.1002/aenm.201702365.

[228] L. Bertoluzzi *et al.*, “Incorporating Electrochemical Halide Oxidation into Drift-Diffusion Models to Explain Performance Losses in Perovskite Solar Cells under Prolonged Reverse Bias,” *Adv. Energy Mater.*, vol. 11, no. 10, p. 2002614, Mar. 2021, doi: 10.1002/aenm.202002614.

[229] R. A. Z. Razera *et al.*, “Instability of p-i-n perovskite solar cells under reverse bias,” *J. Mater. Chem. A*, vol. 8, no. 1, pp. 242–250, 2020, doi: 10.1039/c9ta12032g.

[230] S. Johnston *et al.*, “Thin-Film Module Reverse-Bias Breakdown Sites Identified by Thermal Imaging,” in *2018 IEEE 7th World Conference on Photovoltaic Energy Conversion, WCPEC 2018 - A Joint Conference of 45th IEEE PVSC, 28th PVSEC and 34th EU PVSEC*, 2018, pp. 1897–1901. doi: 10.1109/PVSC.2018.8547766.

[231] D. Bogachuk *et al.*, “Perovskite Photovoltaic Devices with Carbon-Based Electrodes Withstanding Reverse-Bias Voltages up to –9 V and Surpassing IEC 61215:2016 International Standard,” *Sol. RRL*, vol. 6, no. 3, p. 2100527, Mar. 2022, doi: 10.1002/solr.202100527.

[232] Z. Ni *et al.*, “Evolution of defects during the degradation of metal halide perovskite solar cells under reverse bias and illumination,” *Nat. Energy*, vol. 7, no. 1, pp. 65–73, Dec. 2021, doi: 10.1038/s41560-021-00949-9.

[233] C. Jiang *et al.*, “Double Layer Composite Electrode Strategy for Efficient Perovskite Solar Cells with Excellent Reverse-Bias Stability,” *Nano-Micro Lett.*, vol. 15, no. 1, p. 12, 2023, doi: 10.1007/s40820-022-00985-4.

[234] F. Jiang *et al.*, “Architecture Optimization Dramatically Improves Reverse Bias Stability in Perovskite Solar Cells: A Role of Polymer Hole Transport Layers,” 2023, doi: 10.48550/arXiv.2308.08084.

[235] C. Peike, C. Peike, I. Hädrich, K. Weiß, I. Dürr, and F. Ise, “Overview of PV module encapsulation materials,” *Pvi*, vol. 22, no. November 2015, pp. 85–92, 2013.

[236] R. Cheacharoen *et al.*, “Encapsulating perovskite solar cells to withstand damp heat and thermal cycling,” *Sustain. Energy Fuels*, vol. 2, no. 11, pp. 2398–2406, 2018, doi: 10.1039/c8se00250a.

[237] Y. Wang *et al.*, “Encapsulation and Stability Testing of Perovskite Solar Cells for Real Life Applications,” *ACS Mater. Au*, vol. 2, pp. 215–236, 2022, doi: 10.1021/acsmaterialsau.1c00045.

[238] F. Toniolo *et al.*, “Efficient and reliable encapsulation for perovskite/silicon tandem solar modules,” *Nanoscale*, vol. 15, no. 42, pp. 16984–16991, 2023, doi: 10.1039/d2nr06873g.

[239] A. Virtuani, E. Annigoni, and C. Ballif, “One - type - fits - all - systems : Strategies for preventing potential - induced degradation in crystalline silicon solar photovoltaic modules,” *Prog Phptovolt Res Appl*, vol. 27, no. May 2018, pp. 13–21, 2019, doi: 10.1002/pip.3066.

[240] L. Nakka, W. Luo, A. G. Aberle, and F. Lin, “Study of Potential-Induced Degradation in Glass-Encapsulated Perovskite Solar Cells under Different Stress Conditions,” *Sol. RRL*, vol. 7, p. 2300100, 2023, doi: 10.1002/solr.202300100.

[241] L. Xu *et al.*, “Potential-induced degradation in perovskite/silicon tandem photovoltaic modules,” *Cell Reports Phys. Sci.*, vol. 3, no. 9, p. 101026, Sep. 2022, doi: 10.1016/j.xcrp.2022.101026.

[242] J. Carolus *et al.*, “Potential-Induced Degradation and Recovery of Perovskite Solar Cells,” *Sol. RRL*, vol. 3, no. 10, p. 1900226, 2019, doi: 10.1002/solr.201900226.

[243] M. A. Islam *et al.*, “Potential-Induced Performance Degradation (PID) Applied on a Perovskite Solar Cell: Exploring Its Effect on Cell Performance Through Numerical Simulation,” *J. Electron. Mater.*, vol. 52, pp. 3205–3218, May 2023, doi: 10.1007/s11664-023-10284-2.

[244] Z. Purohit *et al.*, “Impact of Potential-Induced Degradation on Different Architecture-Based Perovskite Solar Cells,” *Sol. RRL*, vol. 5, no. 9, p. 2100349, Sep. 2021, doi: 10.1002/solr.202100349.

[245] K. Brecl, M. Jošt, M. Bokalič, J. Ekar, J. Kovač, and M. Topič, “Are Perovskite Solar Cell Potential-Induced Degradation Proof?,” *Sol. RRL*, vol. 6, no. 2, p. 2100815, Feb. 2022,

doi: 10.1002/solr.202100815.

[246] D. Zhang, D. Li, Y. Hu, A. Mei, and H. Han, “Degradation pathways in perovskite solar cells and how to meet international standards,” *Commun. Mater.*, vol. 3, p. 58, 2022, doi: 10.1038/s43246-022-00281-z.

[247] A. Mei *et al.*, “Stabilizing Perovskite Solar Cells to IEC61215:2016 Standards with over 9,000-h Operational Tracking,” *Joule*, vol. 4, no. 12, pp. 2646–2660, 2020, doi: 10.1016/j.joule.2020.09.010.

[248] L. Duan *et al.*, “Stability challenges for the commercialization of perovskite–silicon tandem solar cells,” *Nat. Rev. Mater.*, vol. 8, no. 4, pp. 261–281, 2023, doi: 10.1038/s41578-022-00521-1.

[249] *Photovoltaic (PV) module safety qualification, IEC 61730-Series-2023*, 3.0. VDE, 2023.

Technology Collaboration Programme
by iea

ISBN 978-3-907281-71-0